

**Technical Report**

**GASEOUS DISPERSION INTO STRATIFIED  
BUILDING WAKES**

by

**B. T. Yang and R. N. Meroney**

Prepared for

**U. S. Atomic Energy Commission  
Contract AT (11-1)- 2053  
Fallout Studies Branch  
Division of Biology and Medicine  
Atomic Energy Commission**

**Fluid Dynamics and Diffusion Laboratory  
College of Engineering  
Colorado State University  
Fort Collins, Colorado 80521**

August 1970

CER70-71BTY-RNM-8



U18401 0077392

## ABSTRACT

### GASEOUS DISPERSION INTO STRATIFIED BUILDING WAKES

The dispersion of gases in the atmospheric boundary layer released from an elevated source may be predicted by numerous semi-empirical formulas; however, very little information is available to describe the dispersion within the cavity-wake region downwind of a leaking structure. This study reports the results of the first wind tunnel phase of a joint field and wind tunnel program to evaluate the wind tunnel as a site analysis tool for nuclear safety investigations. A series of diffusion measurements are tabulated for a simple cubical structure placed at different orientations in a stratified shear layer.

## TABLE OF CONTENTS

<u>Chapter</u>	<u>Page</u>
LIST OF FIGURES . . . . .	v
LIST OF SYMBOLS . . . . .	ix
I INTRODUCTION . . . . .	1
1.1 General Review . . . . .	1
1.2 Flow Fields Near a Cube . . . . .	4
II MODELING CRITERIA . . . . .	8
2.1 Geometric Similarity . . . . .	9
2.2 Kinematic Similarity . . . . .	9
2.3 Dynamic Similarity . . . . .	9
2.3.1 Duplication of $Re$ and $Ri$ . . . . .	9
2.3.2 Duplication of $Pr$ and $Sc$ . . . . .	12
2.3.3 Scaling factor of local concentration . . . . .	13
2.3.4 Effect of exit ratio $V_S/U$ . . . . .	14
2.3.5 Duplication of boundary and upwind conditions . . . . .	14
III EXPERIMENTAL FACILITIES AND APPARATUS . . . . .	15
3.1 Wind Tunnel. . . . .	15
3.2 Velocity and Temperature Measurements . . . . .	15
3.3 Smoke Visualization . . . . .	15
3.4 Radioactive Tracer Gas Kr-85 and its Detection . . . . .	16
3.5 Description of the Model . . . . .	17
IV EXPERIMENTAL PROCEDURE . . . . .	18
V COUNTING STATISTICS . . . . .	21
VI EXPERIMENTAL RESULTS AND DISCUSSION . . . . .	23
6.1 Governing Equations . . . . .	23
6.2 Ground-Level Concentration . . . . .	26
6.2.1 Building orientation $\theta = 0^\circ$ (i.e. a release on a downwind face) . . . . .	27
6.2.2 Building orientation $\theta = 180^\circ$ (upwind face release) . . . . .	27
6.2.3 Building orientation $\theta = 45^\circ$ $90^\circ, 135^\circ$ . . . . .	27
6.2.4 Comparison of the ground level concentration results with a typical prediction expression . . . . .	27
6.3 Dynamics and Kinematics of Plume Behavior . . . . .	29
6.3.1 Near building and cavity region dispersion . . . . .	29

TABLE OF CONTENTS - Continued

<u>Chapter</u>		<u>Page</u>
	6.3.2 Near-wake region behavior . . . . .	30
	6.3.3 Far-wake region behavior . . . . .	31
	6.3.4 Stratification effect on plume dispersion . . . . .	31
	6.3.5 Characteristic length scales of plume dispersion . . . . .	31
	6.3.6 Diffusion isopleths . . . . .	33
6.4	Comparison . . . . .	35
	6.4.1 Comparison to previous model studies . . .	35
	6.4.2 Correlation of wind tunnel measurements for meandering behaviors . . . . .	37
	6.4.3 Comparison to a similar previous field study . . . . .	38
VII	CONCLUSIONS . . . . .	40
	BIBLIOGRAPHY . . . . .	42
	APPENDIX I TABLE . . . . .	45
	APPENDIX II FIGURES . . . . .	60
	APPENDIX III SUPPLEMENTAL FIGURES . . . . .	101

## LIST OF FIGURES

<u>Figure</u>		<u>Page</u>
1	Flow fields about a cube . . . . .	61
2	Velocity profiles . . . . .	62
3	Background temperature and velocity profiles . . . . .	63
4	Richardson number profile . . . . .	64
5	Wind Tunnel . . . . .	65
6	The G-M Tube and the glass jacket . . . . .	66
7	The gas planchet . . . . .	67
8	Krypton-85 calibration arrangement . . . . .	67
9	Sketch of the model. . . . .	68
10	Lighting system . . . . .	69
11	Gas release system . . . . .	70
12	Detection system . . . . .	71
(13 to 36) Smoke pictures		
13	$\theta = 0^\circ, (90^\circ) (180^\circ)$ , Top exit port, Neutral stratification . . . . .	72
14	$\theta = 0^\circ$ , Middle exit port, Neutral stratification . . . . .	72
15	$\theta = 0^\circ$ , Bottom exit port, Neutral stratification . . . . .	73
16	$\theta = 45^\circ (135^\circ)$ , Top exit port, Neutral stratification . . . . .	73
17	$\theta = 45^\circ$ , Middle exit port, Neutral stratification . . . . .	74
18	$\theta = 45^\circ$ , Bottom exit port, Neutral stratification . . . . .	74
19	$\theta = 90^\circ$ , Middle exit port, Neutral stratification . . . . .	75
20	$\theta = 90^\circ$ , Bottom exit port, Neutral stratification . . . . .	75

LIST OF FIGURES - Continued

<u>Figure</u>		<u>Page</u>
21	$\theta = 135^{\circ}$ , Middle exit port, Neutral stratification . . . . .	76
22	$\theta = 135^{\circ}$ , Bottom exit port, Neutral stratification . . . . .	76
23	$\theta = 180^{\circ}$ , Middle exit port, Neutral stratification . . . . .	77
24	$\theta = 180^{\circ}$ , Bottom exit port, Neutral stratification . . . . .	77
25	$\theta = 0^{\circ}$ , ( $90^{\circ}$ ) ( $180^{\circ}$ ), Top exit port, Inversion stratification . . . . .	78
26	$\theta = 0^{\circ}$ , Middle exit port, Inversion stratification . . . . .	78
27	$\theta = 0^{\circ}$ , Bottom exit port, Inversion stratification . . . . .	79
28	$\theta = 45^{\circ}$ ( $135^{\circ}$ ), Top exit port, Inversion stratification . . . . .	79
29	$\theta = 45^{\circ}$ , Middle exit port, Inversion stratification . . . . .	80
30	$\theta = 45^{\circ}$ , Bottom exit port, Inversion stratification . . . . .	80
31	$\theta = 90^{\circ}$ , Middle exit port, Inversion stratification . . . . .	81
32	$\theta = 90^{\circ}$ , Bottom exit port, Inversion stratification . . . . .	81
33	$\theta = 135^{\circ}$ , Middle exit port, Inversion stratification . . . . .	82
34	$\theta = 135^{\circ}$ , Bottom exit port, Inversion stratification . . . . .	82
35	$\theta = 180^{\circ}$ , Middle exit port, Inversion stratification . . . . .	83
36	$\theta = 180^{\circ}$ , Bottom exit port, Inversion stratification . . . . .	83

LIST OF FIGURES - Continued

<u>Figure</u>		<u>Page</u>
37	Ground concentration $\theta = 0^\circ$ . . . . .	84
38	Ground concentration $\theta = 180^\circ$ . . . . .	85
39	Ground concentration $\theta = 45^\circ, 90^\circ, 135^\circ$ . . . . .	86
40	Comparison of ground concentration with Pasquill's categories . . . . .	87
41	Characteristic plume height $\lambda_z$ . . . . .	88
42	Characteristic plume width $\lambda_y$ . . . . .	89
43	$\lambda_y/\lambda_z$ . . . . .	90
44	Iso-pleths (a) for $\theta = 0^\circ, (180^\circ) (90^\circ)$ , Top exit port, neutral and inversion stratification. . . . .	91
45	Iso-pleths (b) for $\theta = 0^\circ$ , Middle exit port, neutral and inversion stratification . . . . .	92
46	Iso-pleths (c) for $\theta = 0^\circ$ , Bottom exit port, neutral and inversion stratification . . . . .	93
47	Iso-pleths (d) for $\theta = 45^\circ (135^\circ)$ , Top exit port, inversion stratification . . . . .	94
48	Iso-pleths (e) for $\theta = 45^\circ$ , Middle and bottom exit ports, inversion stratification . . . . .	95
49	Iso-pleths (f) for $\theta = 90^\circ$ , Middle and bottom exit ports, neutral stratification . . . . .	96
50	Iso-pleths (g) for $\theta = 135^\circ$ , Middle exit ports, inversion stratification . . . . .	97
51	Iso-pleths (h) for $\theta = 180^\circ$ , Middle exit port, neutral and inversion stratifications. . . . .	98
52	Iso-pleths (i) for $\theta = 180^\circ$ , Bottom exit port neutral and inversion stratifications . . . . .	99
53	Iso-pleth from the leak of a shell (by Halitsky) . . . . .	100
54	Iso-pleth from the leak of a shall (by Halitsky) . . . . .	100

LIST OF FIGURES - Continued

<u>Figure</u>		<u>Page</u>
A1	Temperature profiles for $x = 2^m$ and $x = -2^m$ at $y = 0$ . . . . .	102
A2	Temperature profiles for $y = 8^{cm}$ , $16^{cm}$ and $24^{cm}$ at $x = 1/2^m$ . . . . .	105

## LIST OF SYMBOLS

### Symbol

$C_p$	specific heat at constant pressure
$C_v$	specific heat at constant volume
D	characteristic length
D	molecular mass diffusivity
$D_\beta$	initial distribution factor
e	base of natural logarithm (2.718...)
Fr	Froude number
$F_t$	heat source or sink per unit mass
g	gravitational acceleration
K	K-factor (non-dimensional form for local concentration)
k	thermal conductivity
l	side length of the model cube (15 cm)
p	pressure
P	probability
Pr	Prandtl number
Q	source strength
Re	Reynolds number
Ri	Richardson number
s	proportional coefficient
Sc	Schmidt number
t	time
T	temperature
$T_*$	"friction" temperature
U	mean free stream velocity
u	mean local velocity

LIST OF SYMBOLS - Continued

Symbol

$u_*$	"friction" velocity
$V_s$	exit velocity of effluent
$x$	longitudinal axis
$y$	transverse axis
$z$	vertical axis

Greek letters

$\gamma$	specific weight
$\delta_{ij}$	Kronecker Delta
$\epsilon$	eddy diffusivity
$\theta$	building orientation (i.e. $\theta = 0^\circ$ indicates a downwind face release)
$\lambda_y$	characteristic plume width
$\lambda_z$	characteristic plume height
$\mu$	dynamic viscosity
$\nu$	kinematic viscosity
$\omega$	vorticity
$\sigma_y$	transverse plume standard deviation
$\sigma_z$	vertical plume standard deviation
$\pi$	3.1415...
$\rho$	density
$\tau$	time
$\tau_0$	shearing stress at wall
$\chi$	local concentration

LIST OF SYMBOLS - Continued

Symbol

Subscripts

o            subscript for reference quantities

Superscripts

\*            superscript for non-dimensional variables

## Chapter I

### INTRODUCTION

Nuclear power reactors are generally enclosed within a containment vessel to prevent the harmful release of solid contaminants or radioactive gases into the adjacent atmosphere. In the event of a power excursion, the containment vessel may conceivably be ruptured or cracked; thus, because of the leakage of the vessel, radioactive gases may escape and cause serious contamination downwind of the reactor complex.

Many continuous point-source formulas have been derived under the assumption that the flow field has homogeneous isotropic turbulence and straight mean streamlines parallel to the ground. The application of these formulas are considered to be extremely conservative in estimating the local concentration in a highly non-homogeneous and non-isotropic turbulence region with curved mean streamlines, as in the cavity-wake region. In this study extensive measurements of concentration data are reported in the hope of contributing experimental information to define actual dispersion behavior.

#### 1.1 General Review

Because of the complexities of diffusion in turbulent cavity-wake region, including such factors as the diffusivity distribution, terrain roughness, thermal stability, etc., the dispersion patterns could hardly be predicted by an analytic method.

For turbulent diffusion phenomena in the lower atmosphere, Sutton's equations have been widely used to estimate concentration distributions for a point source, but the application of his equations

is restricted because of many ideal assumptions. Also, they are not sensitive to atmospheric stratification situations. In an attempt to improve sensitivity to real conditions Pasquill-Gifford's semi-empirical formulas have become popular. A set of transverse and vertical standard deviations of the dispersion are plotted as functions of downwind distance. A "Stability Category", which classifies six different kinds of possible atmospheric stratifications, relates the various plume dispersions to different meteorological conditions. The primary drawback of this method is its insensitivity to the effects of terrain roughness.

Because of strong turbulent mixing motions, adverse pressure gradients, and highly non-stationary fluctuations in the cavity-wake region, both Sutton's and Pasquill-Gifford's methods fail to predict the dispersion of gases in the vicinity of a building.

In an earlier study, problems related to gas dispersion were investigated by Sherlock and Stalker (1940). In the interest of public health they attempted to determine appropriate locations for building ventilators to prevent the inhalation of gases released from nearby short stacks. Other investigators have attempted to specify the proper exit momentum to avoid downwash when short stacks are used. It is known that for a non-streamlined structure, a stack with a momentum ratio of  $V_s/U \leq 1$  will result in a plume downwash. When the exit momentum is less than the inertial momentum of the main stream the plume can not penetrate the cavity; hence, the effluent will enter the low-pressure back-flow region (cavity) and cause serious contamination in the vicinity of the building.

Meroney and Cermak (1968;1969) have investigated the different  $V_s/U$  ratios and critical values of  $V_s/U$  for different building shapes.

Davies and Moore (1964) used both a wind tunnel and a water tunnel to simulate gaseous plume behavior as disturbed by building wakes. The modeled experimental results were confirmed by a limited number of full scale tests. Comparison between the model study and field test indicates no substantial inconsistency.

Martin (1965) investigated airborne dispersion influenced by both buildings and terrain. The study included observations for a full scale field test and a model survey in a wind tunnel. He found the correlation was very satisfactory in terms of smoke visualization and mean concentration data.

Hinds (1967), in a large scale field survey, studied the gaseous emission from a short stack into a building wake. The data reported were from a test grid which consisted of three arcs at 30, 50, and 100 meters from the center of a  $24^m \times 34^m \times 11^m$  building. Two conclusions were obtained by investigating the time history of concentration. First it was found that Csanady's (1967) assumption, which states that the time distribution of concentration for different averaging times is akin to a Poisson distribution, is not applicable. Based on Hinds field data, the variances of the distribution curves are shown such smaller than mean values. The second is that the peak to mean ratios in wakes are greater than those for point source plumes and comparable to those observed on the ground near an elevated release.

In the recent years as a result of the extensive development of nuclear power plants, contamination caused by leaks from a containment

vessel has become a matter of great practical concern. Halitsky (1963) was the first to use a wind tunnel facility to simulate the gas leakage phenomenon. He measured the mean concentration in the cavity behind the proposed EBR - II containment structure. The measurements did not extend farther than  $X/D = 5$  downwind, in which  $D$  is the characteristic length defined by the diameter of the cylindrical structure.

Dickson, Start, and Markee (1967) compared the results from a full scale diffusion investigation of the EBR - II Nuclear Reactor complex with those from Halitsky's earlier study. They confirmed the validity of a properly planned model study if meteorological turbulence information is correctly defined.

Despite the several model and field programs sited above, understanding of gaseous dispersion near a building is still essentially crude, especially regarding the effects due to various meteorological stratifications.

This study is the first wind tunnel phase of a joint field-wind tunnel program which evaluates the wind tunnel as a site analysis tool for nuclear safety investigations. A series of diffusion measurements are reported for a simple, isolated, cubical structure placed at different orientations in a stratified shear layer. The co-operating full scale program is the responsibility of the Air Resource Laboratory Group at the National Reactor Test Station, Idaho Falls, Idaho.

## 1.2 Flow Fields Near a Cube

Aerodynamic turbulence, produced when a flow is interrupted by an obstruction, in contrast to atmospheric turbulence, is completely

mechanical; it is a result of the action of shearing forces between layers of air and the inertial forces as air is accelerated along curved streamlines. Atmospheric turbulence, primarily a result of thermal influence, is relatively uniform over a site. The aerodynamic turbulence varies markedly around an obstruction and decreases rapidly with distance.

The description of flow field near a building because of the aerodynamic effects has been described by J. Halitsky by using smoke visualization. His general arrangement of the flow fields (Figure 1) has been accepted as a reasonable description. In the background flow, the fluid follows the mean streamlines which are essentially parallel to the ground surface. Near the cubic structure, streamlines diverge and curve and gradually return to the horizontal flow as the aerodynamic turbulence decays at some distance downstream. The significant effects of the cube on the background flow are essentially the aerodynamically distorted velocity fields and pressure fields. The displacement zone\* has been defined as the region in which either velocity distortion is greater than 5% or pressure distortion is greater than 10% of the background flow field. Due to the high adverse pressure gradients near the cube, the kinetic energy of the fluid is dissipated because of greater surface friction.

As kinetic energy is dissipated along the ground surface, the fluid particle is not able to surmount the "pressure hill." Therefore, the thickness of the boundary layer increases rapidly and the fluid

---

\* In some books the displacement zone is defined simply as the region where the fluid changes direction because of the presence of an obstruction in a flow field.

particles eventually detach from the boundary layer and flow into the free stream, i.e., separation. The same phenomenon appears in front of the structure.

In the cavity region, the fluid motions are characterized by a great loss of momentum, large eddy motion, low pressure, and strong turbulent mixing. The flow directions in the cavity region have been investigated by P. L. Mantle (1966) with flexible wool tufts and smoke pictures. The toroidal circulation that develops in the cavity region indicates the possibility of serious accumulation of contaminants which are released into the trapped area. According to Mantle, the cavity region behind a cube may extend approximately to two times the cube length when the cube side is normal to the flow and three times the cube length when the cube is installed with the diagonal parallel to the flow. Outside the cavity region, the mean streamlines become gradually parallel to the ground surface and show appreciable amounts of velocity defect\* as the result of diffusion of the vorticities generated by the cube.

The wake region is actually the interaction of the classical wake\*\* and the turbulent boundary layer. The region is a long parabolic envelope surrounding the cavity and extends in the downstream direction from the point of separation. The lateral pressure

---

\* The difference between the local mean velocity without being distorted by the cube and the mean velocity after the distortion.

\*\* According to G. K. Batchelor, the term "wake" is applied to the whole region of non-zero vorticity on the downstream side of a body in an otherwise uniform stream of fluid.

difference is negligible. At the beginning of the wake region the shape of the 3-dimensional wake may be affected by orientations of the cube. Whereas, in farther downstream, the mean velocity profiles are very similar, as first mentioned by H. Schlichting, (1930).

## Chapter II

## MODELING CRITERIA

In simulating a prototype flow system in a model study with a different scale length the limitations of geometric, kinematic, and dynamic similarity should be recognized. In some circumstances, strict adherence to all three similarity laws cannot be achieved at the same time so compromises must be made to attain the best approximation. Some of these compromises follow.

In a fixed reference frame, the equation of motion reads

$$\frac{\partial u_i}{\partial t} + u_j \frac{\partial u_i}{\partial x_j} = -\frac{1}{\rho} \frac{\partial p}{\partial x_i} - \frac{\Delta \gamma}{\gamma} g \delta_{i3} + \nu \frac{\partial^2 u_i}{\partial x_j \partial x_j} - \frac{\partial (\overline{u_i' u_j'})}{\partial x_j}, \quad (1)$$

in which  $i, j = 1, 2, 3$ . The variables in the equation can be expressed in dimensionless form by using scaling factors as follows,

$$u_i^* = \frac{u_i}{U}, \quad p^* = \frac{p}{\rho U^2}, \quad t^* = \frac{tU}{L}, \quad x_i^* = \frac{x_i}{L}, \quad \rho^* = \frac{\rho}{\rho_0}, \quad g^* = \frac{g}{g_0},$$

$$v^* = \frac{\nu}{\nu_0}, \quad \gamma^* = \frac{\gamma}{\gamma_0}, \quad \overline{u_i' u_j'}^* = \frac{\overline{u_i' u_j'}}{U^2}$$

so that the dimensionless expression of equation (1) becomes,

$$\frac{\partial u_i^*}{\partial t^*} + u_j^* \frac{\partial u_i^*}{\partial x_j^*} = -\frac{1}{\rho^*} \frac{\partial p^*}{\partial x_i^*} - \frac{1}{Fr^2} \frac{\Delta \gamma^*}{\gamma^*} g^* \delta_{i3}$$

$$+ \frac{1}{Re} \frac{\partial^2 u_i^*}{\partial x_j^* \partial x_j^*} - \frac{\partial (\overline{u_i' u_j'}^*)}{\partial x_j^*} \quad (2)$$

in which the Froude number  $Fr = \left( \frac{U^2}{g_0 L (\Delta \gamma_0 / \gamma_0)} \right)^{1/2}$ , and the

Reynolds number  $Re = \frac{UL}{\nu_0}$  .

## 2.1 Geometric Similarity

Geometric similarity represents the requirement of similar boundary restraints to fluid movement. Geometric similarity is easily realized by an undistorted scaled model.

The model used in this study was constructed with a linear scale of 1/50 to a cubical structure proposed for a full scale study at the National Reactor Test Station, Idaho.

## 2.2 Kinematic Similarity

The law of kinematic similarity requires the same patterns of streamlines for model and prototype flow fields. In Figure 1, the flow fields distorted by the presence of a cube are shown. Main streamlines near the cube are essentially affected by the size of the cavity which varies with different orientations as cited by Mantle (1966). For each specific orientation the length of the cavity region is almost invariant when  $Re$  exceeds a critical value (according to Golden, 1961,  $Re_{critical} = 11,000$ ), so that the basic pattern of the streamlines is the same when turbulent separation occurs.

## 2.3 Dynamic Similarity

2.3.1 Duplication of  $Re$  and  $Ri$  - The law of dynamic similarity requires that the force vectors at the equivalent points for model and prototype are parallel and have identical ratios.

The Reynolds number  $Re$  is defined by the ratio  $Re = UL/\nu_0 = \rho U^2/\mu_0(U/L)$ . It may also be interpreted as a ratio of a reference inertial force to a reference viscous shear force. When the flow is over sharp-edged geometry, mean flow patterns are independent of the Reynolds numbers if the Reynolds number exceeds a lower limit which is independent of the geometric form. In such instances a value of  $10^3$  for the ratio of

$$\frac{(Re)_{\text{prototype}}}{(Re)_{\text{model}}}$$

may not introduce significant error in the modeled mean flow patterns. However, considerable caution must be exercised in comparing turbulence statistics in such a model with prototype turbulence. In the gaseous dispersion near buildings, Golden (1961) found that for flow about a cube, for Reynolds numbers above 11,000, there was no significant change in concentration distribution.

Froude number,  $Fr$ , is interpreted as the ratio of reference inertial force to reference buoyancy force produced by the difference in specific weights. In meteorological applications for small vertical distance, the difference of specific weight can be expressed by the temperature difference. A gradient Richardson number (or atmospheric Froude number is defined as

$$Ri = \frac{g}{T_0} \frac{\left(\frac{dT}{dz}\right)}{\left(\frac{du}{dz}\right)^2} .$$

Examining the physical interpretations of Richardson number, we can see

$$\begin{aligned}
 Ri &= \frac{\text{buoyancy force}}{\text{inertial force}} \\
 &= \frac{\text{restoring force in a unit mass of air parcel}}{\text{inertial force in a unit mass of air parcel}} \\
 &= \frac{\text{rate of consumption of turbulent energy by buoyancy force}}{\text{rate of production of turbulent energy by the mean wind shear.}}
 \end{aligned}$$

Evidently, we may conclude:

$$\begin{aligned}
 Ri &< \quad \text{unstable stratification} \\
 Ri &= 0 \quad \text{neutral stratification} \\
 Ri &> \quad \text{stable stratification}
 \end{aligned}$$

From the last physical interpretation, in the unstable stratification case, the turbulent intensities are enhanced; hence in the stable stratification case, the turbulent intensities are suppressed.

In calculating the gradient Richardson number, the difficulty of finding the exact values of  $(dT/dz)$  and  $(du/dz)$  always arises. By using the universal logarithmic profiles to define both mean velocity and temperature distribution, Plate and Lin (1968) calculated the gradient Richardson number from

$$\frac{u}{u_*} = \frac{1}{k} \ln z + A ,$$

and

$$\frac{T}{T_*} = \frac{1}{k} \ln z + B ;$$

hence

$$\begin{aligned}
 Ri &= \frac{T_*}{T_0} \frac{gk}{u_*} z \\
 &= C \frac{z}{T_0} \quad \text{in which} \quad C = \frac{T_* g k}{u_*} .
 \end{aligned}$$

Figure 2 shows the velocity profiles. Figure 3 shows the background

temperature and velocity profiles in a log-linear scale. Figure 4 displays the variation  $Ri$  with the above definition.

Mentioned previously, the Richardson number relates closely to flow field turbulent intensities. It is apparent from a Lagrangian description of a turbulent diffusion process that local turbulent intensities directly affect turbulent diffusion rates. Since the primary interest in this model study is the gaseous dispersion behavior in stratified flow, the Richardson number should be the same in both the model and prototype.

2.3.2 Duplication of Pr and Sc - Thermal similtude is governed by the energy equation

$$\frac{\partial T}{\partial t} + u_j \frac{\partial T}{\partial x_j} = \frac{1}{\rho C_v} \frac{\partial}{\partial x_j} \left( k \frac{\partial T}{\partial x_j} \right) + F_T \quad .$$

With the previous scaling factors and the following ones:

$$C_v^* = \frac{C_v}{C_{v0}}, \quad k^* = \frac{k}{k_0}, \quad T^* = \frac{T}{\Delta T_0}$$

(neglecting  $F_T$  term), the non-dimensional form for the energy equation reads

$$\frac{\partial T^*}{\partial t^*} + u_j^* \frac{\partial T^*}{\partial x_j^*} = \gamma \frac{1}{Pr} \frac{1}{Re} \frac{\partial}{\partial x_j^*} \left( k^* \frac{\partial T^*}{\partial x_j^*} \right) \quad ,$$

$j = 1, 2, 3$  . In the above equation there are two new dimensionless parameters, namely Prandtl's number,  $Pr = \frac{C_{p0} \mu_0}{k_0}$  , and the specific heat ratio  $\gamma$  . If the fluids in both model and prototype are all air, there is no difficulty in presenting the same  $Pr$  and  $\gamma$  .

For the diffusion problem, based on the same criteria with additional scaling factors,

$$D^* = \frac{D}{D_0} ,$$

and

$$\chi^* = \frac{\chi}{\chi_0} ,$$

the diffusion equation becomes (if no chemical reaction occurs)

$$\frac{\partial \chi^*}{\partial t^*} + u_j^* \frac{\partial \chi^*}{\partial x_j^*} = \frac{1}{Re} \frac{1}{Sc} \frac{\partial}{\partial x^*} (D^* \frac{\partial \chi^*}{\partial x_j^*})$$

in which  $Sc = \frac{v_0}{D_0}$  .

A new dimensionless parameter, Schmidt number  $Sc$  , appears in the diffusion equation. Like the Reynolds number, the Schmidt number is important only when the diffusion process is carried out in laminar flow, i.e., the diffusivity  $D$  relates to physical properties of the mixture species. In the turbulent transport, because of the mixing motion, the dispersion of matter no longer depends on  $D$  ; however, for turbulent mass dispersion similitude, duplication of the Schmidt number is not important.

### 2.3.3 Scaling factor of local concentration - The scaling factor

$\chi_0$

$$\chi_0 = \frac{Q}{UL^2}$$

is used in general diffusion problems where,  $Q$  is the source strength or as the sample (mass or  $\mu\mu$  curies) released from the source per unit of time.

In this study, the dispersion is essentially influenced by the mechanical turbulence (i.e., the building wake). The projected area of the structure normal to the main stream  $A$  is used to replace the  $L^2$  term. Thus, the conventional dimensionless  $K$  factor is defined

as

$$K = \frac{\chi AU}{Q} .$$

For every release situation, the  $K$  field is a function of spatial coordinates and is always determined by empirical formulae based on experimental observations. A higher  $K$  value implies a higher probability for the effluent to enter the local region.

2.3.4 Effect of exit ratio  $V_s/U$  - Another important factor in gaseous dispersion simulation is the  $V_s/U$  ratio when short stacks or leakage holes are used. The  $V_s/U$  ratio determines the initial plume trajectory, i.e., the degree to which the plume penetrates the low-pressured cavity region. It has been shown (see "Recommended Guide for the Prediction of the Dispersion of Airborne Effluents," ASME, 1968) that a  $V_s/U$  ratio of 1 is marginal with respect to the short stack downwash for a non-streamlined structure. For a leakage problem, the ratio  $V_s/U$  approaches zero. In this experiment, in order to insure a detectable local concentration level at downwind distance of  $x/\ell = 30$  and yet maintain safe radioactive handling conditions,  $V_s/U$  was set equal to 1/4. Based on  $V_s/U = 1/4 \ll 1$ , the same concentration distribution pattern as that from  $V_s/U \rightarrow 0$  may be reasonably expected.

2.3.5 Duplication of boundary and upwind conditions - Besides the requirement that all dimensionless parameters are equivalent in the complete simulation study, the boundary conditions and upwind flow conditions must be the same. Such conditions include the roughness, temperature, and gas absorbing properties of the ground, and the upwind velocity and Richardson number profiles.

## Chapter III

## EXPERIMENTAL FACILITIES AND APPARATUS

## 3.1 Wind Tunnel

The meteorological wind tunnel (Figure 5) at the Fluid Dynamics and Diffusion Laboratory, Colorado State University, was specifically designed to simulate atmospheric shear flows. A 25 m long test section provides a well-developed turbulent boundary layer for different degrees of thermal stratification and surface roughness. The pressure gradient along the test section can be controlled by an adjustable height ceiling. A 15 m long portion of the test section consists of an aluminum plate that can be cooled\* or heated to temperatures between  $-8^{\circ}\text{C}$  and  $180^{\circ}\text{C}$ . The air temperature in the free-stream can be maintained at values from  $5^{\circ}\text{C}$  to  $90^{\circ}\text{C}$ . The air speed can be regulated to values from -2 to 35m/sec.

## 3.2 Velocity and Temperature Measurements

A pitot-static tube was used to measure both vertical and horizontal mean wind profiles; the out-put signal (velocity head) was analyzed by a Transonic model A, Type 120 electronic pressure meter. The mean temperature of the air flow was measured with a copper-constantan thermocouple referenced to an OMEGA-CJ cold junction compensator. The output was determined by a sensitive millivolt potentiometer.

## 3.3 Smoke Visualization

Smoke was generated by bubbling compressed air through a container of titanium-tetrachloride located outside the wind tunnel and transported

---

\* For stable stratification, the plate was maintained at a temperature of  $0^{\circ}\text{C}$ .

through the tunnel wall by means of a tube terminating at the release holes. A visible record was obtained by means of photographs taken with a speed-graphic camera using polaroid film.

### 3.4 Radioactive Tracer Gas Kr-85 and its Detection

Krypton-85 is a radioactive noble gas produced by nuclear fission. With the atomic number 36, atomic mass unit 85, and the maximum energy of 0.67 Mev., Kr-85 has been widely used as an effective tracer gas in recent years because of its long half life (10.3 years) and its pure beta-emitting property.

Like other radio-isotopes, Kr-85, which is a Beta-emitter, ionizes the gas molecules as it passes through them. With these ionization properties, the Geiger-Mueller counter (Figure 6) is thus designed to detect the radiation. (See Chaudhry and Meroney, "Turbulent Diffusion in a Stably Stratified Shear Layer," 1969). The counter tube consists of two electrodes, a fine metal wire, the anode, surrounded by a hollow conducting cylinder, the cathode. The two electrodes are enclosed in a glass envelope containing gas at low pressure. When the ionizing radiation penetrates the G-M detector, the electrons released from the ionized gas molecules moves quickly toward the anode. Because of the high electrical potential (about 1,000 volts) near the anode wire, the electrons gain very high kinetic energy and produce a large number of secondary electrons by multiple collisions with other molecules. At the same time, the positive cloud moves toward the cathode cylinder. By using the pulse forming resistor and proper out-put circuits, one can count up to 100 picro-curie.

In the experiment the sample gas was calibrated by flushing it through a special thin mylar covered planchet (Figure 7) at a very low speed. A sensitive end window G-M counter (Figure 8) was used to compare the concentration of the sample gas with a thalium-204 standard source. Corrections for geometry, backscattering, and absorption were also made. The source strengths are 3.51  $\mu\text{ci/cc}$  and 3.72  $\mu\text{ci/cc}$ .

Eight halogen-quenched, stainless-steel, thin walled G-M tubes (Tracerlab type 1108) were used to study the concentration of the sampled gases. The flow rates of flushing the sampled gases through the eight G-M tubes were controlled by eight flowmeters (Fischer and Porter Co., Model 10 A 103 multiple tube panel). The output signals of the concentration were obtained from counts per minute by three sets of scalers (Nuclear - Chicago Corp., Model 192A "Ultrascaler")

### 3.5 Description of the Model

A 15 cm x 15 cm plexiglass model (Figure 9) was constructed under the consideration that the degree of blockage of 0.75% presented by the model would not affect the simulating flow due to the contraction of the side walls of the tunnel (the ratio of projected model area to the area of the 2 m x 2 m wind tunnel cross-section should not exceed 1 to 2%). In order to simulate potential release positions, there are three exit ports--top, middle, and bottom--built as shown in Figure 9. The exit gas temperatures were monitored by the three copper-constantan thermocouples installed at each exit; the fine screens inside the exit holes are provided to eliminate the jet effects and to insure a uniform flow. The screens could be removed when the smoke ( $\text{TiCl}_4$ ) used for visualization was passing.

## Chapter IV

## EXPERIMENTAL PROCEDURE

The procedures for the experiment were as follows:

(1) The model was installed 7 m from the beginning of the aluminum plate, whose temperature can be controlled as mentioned in section 3.1. The 7 m distance was adequate for establishing fully developed thermal stratified flow. (2) A pitot-static tube and a copper-constantan thermocouple were mounted in the free-stream to monitor the wind speed and temperature. (3) The barometer was checked and the corresponding air density was formed correspondently. Then the wind tunnel was started, and the free stream velocity adjusted from a reading of the Transonic electronic pressure meter. The free stream velocity used throughout this experiment was  $2^m$ /sec. (4) In the smoke visualization process, a qualitative study of the dispersion behavior and flow fields observation were held. A simple lighting system (Figure 10) was used to illuminate the smoke plume, this system also eliminated reflections from the tunnel walls. The exit speed of the smoke generated by passing moist air through  $TiCl_4$  was controlled to provide an optimum value for photographing, but was not allowed to exceed  $U$ . Whenever the dispersion of the smoke plume trajectories was observed to be relatively steady a picture was taken and checked for suitable visibility. A long exposure time was used since the mean trajectory was essentially the data of interest. (5) Velocity and temperature measurement - The pitot-static tube mounted on a carriage was connected to the pressure transducer by means of vinyl tubing. The carriage could be moved both vertically and laterally by remote control. An x-y plotter was used to plot the velocity profiles

from the out-put of the pressure transducer. Temperature data were collected point by point by using a set of thermocouples with a compensator and potentiometer, also mentioned in 3.2. (6) Gaseous concentration measurement - A flowmeter (Fischer and Porter Co., Model 10 A 103) was used to control the flow rate at 2350 cc/min\* (exit velocity = 0.5 m/sec). The tracer release system is shown schematically in Figure 11. The Kr-85 mixture was passed through the gas regulator into a simple tubular heat exchanger\*\* to condition the temperatures of exit gases to the values of temperature of release height.

Samples were drawn from the wind tunnel through a rack\*\*\* of eight sampling tubes 3/32 inch in diameter which were mounted on the remote-controlled carriage.

The rack could be moved vertically and transversally to take data in different positions. Samples were drawn by a vacuum pump and flushed through the eight G-M tubes for two minutes, the electronic valves (solenoid) were closed and each individual sample concentration counted the scaler. Figure 12 shows schematically the detection system. In order to shorten the counting period, three sets of

---

\* This is done to insure the exit momentum relatively small so the plume cannot penetrate the cavity region.

\*\* This was a 12" copper coil, with 3/16 inch I.D., hung downstream. The height is adjustable with different release positions and temperatures.

\*\*\* In the vertical concentration measurement, the distance between each probe was 2 cm, in the transverse concentrations measurement, the distance was 4 cm due to the much wider spread.

scalers were used. Each G-M tube scaler pair was carefully chosen, according to the operating voltage\*. Each tube constants\*\* were precalibrated with its associated scaler.

---

\* A defined voltage from which a small deviation of voltage would not affect the counting rate to an appreciable amount.

\*\* The equivalent concentration to each count.

## Chapter V

### COUNTING STATISTICS

A nuclear scaler was used to monitor the G-M apparatus while measuring sample concentrations. Different counts may be observed for the same gas sample. This is ordinarily due to the random nature of the nuclear disintegration phenomena.

A Poisson distribution model which satisfies the following three conditions was proposed to treat the random process of radioactive emission. (1) The probability that exactly one disintegration will occur in a small time interval  $\Delta t$  is approximately equal to  $s\Delta t$ , i.e.,

$$p \{\text{one disintegration at } \Delta t\} = s\Delta t + o(\Delta t)$$

in which  $s$  is a proportional constant, and  $o(\Delta t)$  indicates the small order terms. (2) The probability of more or less than one disintegration in  $\Delta t$  is small compared to the probability of exactly one disintegration, i.e.,

$$p \{\text{other than one disintegration at } \Delta t\} = o(\Delta t)$$

(3) The number of disintegrations in non-overlapping time intervals is independent.

The quantity  $s$  can be interpreted as the mean rate of disintegrations per unit time. In a Poisson distribution, the probability  $p_n$  for disintegrations during the time interval  $t$  from a constant radioactive source to be  $n$  is

$$p_n = \frac{(st)^n e^{-st}}{n!}$$

(assuming that the half life of the sample gas is long compared with the counting time that it can be treated as a constant radioactivity).

Suppose the G-M tube can produce  $m$  counts for each disintegration\* then utilizing the same argument, one can show that the probability of observing  $N$  counts per unit time is

$$P_n = \frac{(sm)^N e^{-sm}}{N!}$$

$$= \frac{R^N e^{-R}}{N!}$$

in which  $R = sm$ , indicates average counts per unit time. With a normal distribution approximation (see E. Parzen, 1967), the probability that the counts per unit time fall within a standard deviation  $\sigma$  of the mean count value  $R$  is

$$p \{N - \sigma < x < N + \sigma\}$$

$$= p \{N - \sigma < x < N + \sigma\}$$

$$= 68.3\%.$$

Therefore, it is reasonable to assume that scaler outputs monitored during an experiment measurement fall within the range  $N \pm \sqrt{N}$ . For example, if the observed counts per minute is 100, then one is 68% confidence that the mean value will fall between 110 and 90, (i.e., 68% of the time if 100 is the true mean). All the concentration profiles have been interpreted and smoothed out in terms of these limitations.

---

\* counting yield (usually  $m < 1$ ).

## Chapter VI

## EXPERIMENTAL RESULTS AND DISCUSSION

Since the conventional point-source diffusion equation cannot be used for predicting diffusion near buildings, it is necessary to calculate gaseous concentration on the basis of experimental data. It is convenient to report dilution results in terms of a non-dimensional factor independent of the model to prototype scale.

Section 6.1 discusses alternative data presentation formulations as suggested from the physics of the source release process in the near vicinity of buildings.

## 6.1 Governing Equations

For a general turbulent diffusion problem, a set of simultaneous equations (i.e., equation of continuity, equation of motion, equation of energy, equation of diffusion) must be solved along with proper boundary conditions and initial conditions.

The equation of turbulent diffusion reads (using Reynold's averaging process)

$$\frac{\partial \chi}{\partial t} + u_j \frac{\partial \chi}{\partial x_j} = \frac{\partial}{\partial x_j} \left( D_j \frac{\partial \chi}{\partial x_j} - \overline{u_i' \chi'} \right)$$

in which  $i, j = 1, 2, 3$ . According to Boussinesq, the correlation term  $\overline{u_i' \chi'}$  can be replaced by introducing an eddy diffusivity  $\epsilon_j$  as

$$\overline{u_i' \chi'} = - \epsilon_j \frac{\partial \chi}{\partial x_i} \quad \text{in which}$$

$i, j = 1, 2, 3$ . Generally, the molecular diffusivity  $D_j$  is at least three orders of magnitude smaller than the eddy diffusivity and can be neglected. The final form for the turbulent diffusion equation becomes

$$\frac{\partial \chi}{\partial t} + u_j \frac{\partial \chi}{\partial x_j} = \frac{\partial}{\partial x_j} \left( \epsilon_j \frac{\partial \chi}{\partial x_j} \right)$$

in which  $i, j = 1, 2, 3$ .

Boundary conditions for the above equations are as follows:

(using a conventional meteorological coordinate system)

(1)

$$\frac{\partial \chi}{\partial z} = 0 \quad \text{when } z = 0$$

(2)

$$\chi \rightarrow 0 \quad \text{when } \begin{array}{l} x \rightarrow \infty \\ y \rightarrow \infty \\ z \rightarrow \infty \end{array}$$

(3)

$$\int_0^{\infty} \int_{-\infty}^{\infty} \int_{-\infty}^{\infty} \chi \, dx \, dy \, dz = \int_0^t Q \, dt$$

in which  $t$  is total release time,  $Q$  is the source strength defined as,

$$Q = x_s V_s A_s, \quad \text{and}$$

$x_s, V_s, A_s$  indicate the source concentration, exit speed and exit area.

The unsteady character of the entrainment of gases into the cavity and the subsequent re-injection into the down-wind wake suggests the character of mass species conservation at any section may be time dependent, or

$$\int_0^{\infty} \int_{-\infty}^{\infty} \chi u \, dy \, dz \neq \text{constant}.$$

Intuitively one knows, for short periods of release, the trapped effluent occupies an important portion of the total amount released, i.e.,

$$\int_0^{\infty} \int_{-\infty}^{\infty} \chi u \, dy \, dz \Big|_{\substack{x \gg 0 \\ t \text{ small}}} < Q .$$

For a long period of release, the problem can be treated as a continuous volume or plane source with a constant amount of effluent flowing into the wake region. Hence, the gas passing into the wake region from the cavity will obey a simple steady conservation law; however, the individual fluid particles which enters the wake together may not have begun their travels from the building leak at the same instant.

A volume source assumption was suggested by Fuquay in 1960, (Slade, 1968). With the argument that any material escaping from a building disperses rapidly into a uniformly distributed volume, he defined an initial distribution factor  $D_{\beta}$  as an equivalent volume of the source, i.e.,

$$D_{\beta} = c A U \quad \text{in which } 1/2 \leq c \leq 2$$

and  $c$  is a proportional constant depending on building geometry and orientation. Hence, one expects

$$\frac{Q}{\chi_{\text{total}}} = D_{\beta} + \frac{Q}{\chi_{\text{gaussian}}}$$

The real dispersion patterns behind a building show a special characteristic behavior and cannot be estimated by the superposition as cited above. For instance, much wider transverse spreads compared to vertical ones are observed. In addition, the vertical concentration distributions show a negative exponential form in the wake region.

As also observed by Halitsky (1963), the real concentration in the cavity region is not uniformly distributed.

Barry (1964) reviewed building effects in relation to airborne pollutant dispersion. His summary of wind tunnel experiments suggest a  $c =$  value varying from 0.5 to 0.67. He also recommended a  $k$  formulation discussed in section 2.3.3.

A dimensional form for isopleths construction, which was used by Hilsemier and Gifford (1962) and frequently utilized for flow fields independent of source configuration, is

$$\frac{\chi U}{Q} [L^2] .$$

The formulation is of course dependent upon the scale of experiments. Data presented in this study is to the scale of 1:50 for the prototype model. Data from these experiments have been correlated in terms of both  $K$  and  $\chi U/Q$ .

## 6.2 Ground-Level Concentration

The health physicist is primarily interested in the probable environment of the average citizen; hence, the distribution of ground level concentration has been a conventional measure of probable health hazard. In fact, for low velocity releases, near building faces, the ground level concentration will also be the maximum concentration. Figure 13 through 36 show the smoke picture near the cubical structure. Figures 37, 38 and 39 display the ground level concentrations for different building orientations (i.e., different angles between the release sites and the flow directions) and for neutral and inversion stratification.

6.2.1 Building orientation theta = 0° (i.e., a release on a downwind face) - The slopes of ground concentration versus distance are determined by a linear regression of all the mean values on the mean concentration over the three release ports. The values at  $x = 1/2$  m ( $x/l \sim 3.3$ ) are not used in the regression process because of the random scattering due to the greater mechanical turbulence.

6.2.2 Building orientation theta = 180° (upwind face release) - Two approximately parallel lines are observed with almost the same slopes as that of theta = 0°. The magnitudes of concentration for the upwind face release, however, are slightly greater than those for the downwind release. Part of the effluent follows the outer cavity streamlines and enters directly into the far downwind wake region. When  $\theta = 0^\circ$ , all the effluent must pass through the strongly turbulent mixing process in the cavity region before entering the wake region.

6.2.3 Building orientation theta = 45°, 90°, 135° - The ground level concentrations for  $\theta = 45^\circ$ ,  $90^\circ$ , and  $135^\circ$  are plotted in Figure 39. The concentration data plotted were measured directly downwind of the center of the cubical structure. Since the release position is not symmetric with respect to the flow, the concentrations shown may not be the maximum values of the transverse profiles.

When theta = 45°, extremely high concentrations are measured at  $x/l \sim 3.3$ . This is because of the significant extension of the cavity length when the cube is oriented with the diagonal parallel to the flow direction as mentioned in section 1.2.

6.2.4 Comparison of the ground level concentration results with a typical prediction expression - A conventional first estimation of

ground level concentration from a ground level release source has been compared with wind tunnel data in Figure 40.

The prediction formula as developed for reflected normal distribution may be expressed as

$$x_{\text{ground}} = \frac{Q}{\pi \sigma_y \sigma_z U}$$

so,

$$K = \frac{x_{\text{ground}} UA}{Q} = \frac{A}{\pi \sigma_y \sigma_z} .$$

Different sets of  $\sigma_y$  and  $\sigma_z$  are chosen from Pasquill's diffusion categories for different classes of meteorological stability conditions A, D, E, and F. These classifications are related to various potential stratification conditions and (i.e., turbulent conditions) are defined as follows

- A - Extremely unstable
- B - Moderately unstable
- C - Slightly unstable
- D - Neutral
- E - Slightly stable
- F - Moderately stable.

These sets of classifications have not been firmly related to specific Richardson number or Monin Obukhov stability ranges. However, Pasquill and Meade have associated the standard deviations of bivariate excursions with the diffusion categories.

The rough estimates using  $\sigma_y$  and  $\sigma_z$  from Pasquill's empirical stability categories exhibit significantly steeper slopes than those from the measurements. This results initially in a conservative estimate of mean concentrations, however, farther downwind the concentration level may be under-estimated by one order of magnitude.

Other investigators have suggested that wind tunnel data must be corrected downwind for lack of large scales of eddies which exist in the atmosphere. A detailed discussion is given in section 6.4. This discussion shows that taking into consideration the large eddy effect results only in a displacement of the concentration distribution with no adjustment for dispersion rate.

### 6.3 Dynamics and Kinematics of Plume Behavior

The mechanism of gaseous dispersion is a combination of two flow phenomena, the general convective motions transport effluent into downwind areas, while the turbulent mixing motions cause vertical and transverse diffusion.

Therefore, dispersion is related very closely to the associated flow fields. The following paragraphs discuss the flow field sectors and their associated dispersion patterns.

6.3.1 Near building and cavity region dispersion - At the beginning of the wake region, mechanical turbulence generated by the structure plays a dominant role. This was also discussed in section 6.1. Strong turbulent mixing tends to smooth out the effects of different release ports. Smoke pictures (Figures 13 to 36) show that after approximately three scale lengths downwind the smoke patterns for different release ports, structure orientations, and stratification have almost the same type of distribution, i.e., the densest smoke is near the ground surface. This agrees with the quantitative concentration measurements subsequently discussed in the latter sections.

In each vertical concentration profile (see Appendix), higher concentrations are always at ground level. This can be appreciated when

one notes that streamlines move downward after passing the structure. Thus part of effluent follows the main convective motion and is transported into the near ground region. Part of effluent is carried by toroidal motion in the cavity.

At the downwind end of the cavity, the effluent is brought to the surface at a stagnation position where streamlines divide into both upwind and downwind. The higher turbulent amplification in this region tends to exhale much of the effluent from cavity into the wake region. The downwind space between  $x/l = 3$  and  $x/l = 5$  may be visualized as a transition region between the cavity and wake dominated flow region.

A remark may be made for the case  $\theta = 135^\circ$ , that is, the release ports are on the upwind face which is  $45^\circ$  with the flow direction. Because of a thin boundary layer, a significant convection-dominant phenomenon is observed in smoke pictures (Figures 21 and 22). A small change of exit momentum may cause different distribution patterns at the beginning of wake region; greater exit momentum may cause more skew transverse distribution in the downwind.

6.3.2 Near-wake region behavior - Farther downwind ( $x > 5l$ ), higher concentrations remain at ground level (see Figures 44 to 52). This is due to the reflection effect at the ground ( $\partial\chi/\partial z = 0$ ). This effect can be visualized by considering an image volume or plane source at the beginning of the wake region in a symmetrical position on the negative side of the ground plane.

Similar patterns for vertical concentration distribution are found in the downwind wake region regardless of release ports or building orientation. Wake structure is apparently independent of building orientations if the difference between projected areas normal to the

flow is not very great. Since similar distributions are observed at the beginning stage of the wake region, similar distributions farther downwind are naturally to be expected.

6.3.3 Far-wake region behavior - Intuitively, one would expect that beyond some distance downwind, the wake effects will decrease to such an extent that flow field is no longer dependent on the origin of perturbation introduced by the presence of a building. At such a region, (evidently  $x$  is at least greater than  $30l$ ), the dispersion rate should asymptotically approach that for a general continuous source release (in a open field). Unfortunately, neither this experiment nor those which preceded it in the field (in the field test done by Dickson, Start and Markee, Jr., the data were measured to 600 meters, i.e., approximate 23 scale length  $D$ ) clearly delineates a far wake region behavior.

6.3.4 Stratification effect on plume dispersion - In the previous discussion, equivalent stratification conditions are assumed throughout. For different thermally stratified flow, dispersion patterns can vary significantly. For instance, in the farther downwind region, the consistently higher ground level concentrations for the inversion case are due to the suppressions of the turbulent mixing. On the other hand, small turbulent intensities cause smaller dispersion rates in both vertical and transverse directions. For  $x < 5l$ , the dispersion effects of different stratification conditions is not significant because of the dominant mechanical turbulence produced by the building.

6.3.5 Characteristic length scales of plume dispersion - The characteristic dispersion length in this study was chosen to be the length between a maximum concentration and half-maximum concentration. Thus,  $\lambda_y$  and  $\lambda_z$  stand, respectively, for "characteristic plume

width" and "characteristic plume height". For a normal distribution,  $\lambda_y$  and  $\lambda_z$  are linearly proportional to the standard deviations  $\sigma_y$  and  $\sigma_z$  and have equivalent physical interpretations.

Figure 41 plots  $\lambda_z/\ell$  vs. distance for  $\theta = 0^\circ$  and  $180^\circ$ . For the downwind face release, higher  $\lambda_z$  values are observed for inversion stratification. This may be due to the dominance of the convective transport motion. Dispersion patterns at the beginning of the wake region can be considered to be "frozen"\* and transported downwind along main streamlines. In a neutral stratification the effluent continuously diffuses in the vertical direction because of strong undamped turbulent motions.

For an upwind face release, two different phenomena are observed. First, average  $\lambda_z$ 's are smaller than those for downwind face release. This may occur because part of the effluent flows directly into the wake region at approximately the same heights of their original release positions ( $0 \sim .5\ell$ ). Whereas, for  $\theta = 0^\circ$  (downwind face release), most effluent enters the toroidal cavity region before entering the wake region. In the mixing process, some effluent may be carried downwind at a higher location than those of the original release port. Second, in a manner similar to that suggested for  $\theta = 0^\circ$  releases, inversion stratification will inhibit vertical dispersions; hence, a frozen concentration pattern will be transported downwind. For a neutral stratification case, part of the effluent diffuses into greater height than that of the

---

\* In the inversion condition, turbulent mixing in vertical direction is impeded. Each air parcel tends to stay in the same temperature (density) layer because the vertical motion must be against the hydrostatic force.

release ports. This explains the higher  $\lambda_z$  values in neutral cases; hence the character of  $\lambda_z$ -distribution is governed by the initial concentration profiles immediately downwind of the cavity.

Figure 42 plots characteristic plume width  $\lambda_y$  vs. distance. Since stable stratification does not tend to inhibit lateral motions. Thus  $\lambda_y$  continues to increase with downwind distance.

The ratios  $\lambda_y/\lambda_z$  are used as indications for the gross physical behavior of the leakage plumes. As displayed by Figure 43, obviously, the transverse dispersion rates are much larger than vertical ones.

6.3.6 Diffusion isopleths - In Figures 44 through 52 the isopleths (equi-concentration contours) are plotted for various building orientations and stratification conditions. A table which lists the equivalent dimensional figures  $\chi U/Q [L^2]$  against the K-factor is also presented. Concentration data are listed in Appendix I.

Figure 44 presents the comparison for  $\theta = 0^\circ$  ( $90^\circ$ ,  $180^\circ$ ) at the top release port for both neutral and inversion stratification (compare Figures 13 and 25). Isopleths in the inversion case show somewhat concave downward shapes. However, in the neutral case, isopleths tend to be concave upward. Smaller transverse spreads in the inversion case are also observed.

Figure 45 also displays similar comparisons to those in Figure 44 with the addition of data for the middle exit port (compare Figures 14 and 26).

Figure 46, like the previous cases, displays isopleths in both stratifications for the bottom exit port (compare Figures 15 and 27).

Comparing Figures 44, 45, and 46, one can find a basically similar dispersion pattern for all the cases: the gaseous plumes do not tend

to go upward and the blunt shapes at the downwind ends of the transverse isopleths indicate the well-mixed phenomena.

Figure 47 shows the isopleth distribution for  $\theta = 45^\circ$  ( $135^\circ$ ) for the inversion stratification at the top exit port release (compare Figure 28). Comparing the result to Figure 44, one can find that if a reference area  $A = \ell^2$ , is still used for calculating K-factors, the isopleth patterns do not vary much for  $x/\ell > 15$ . The K-factors defined with  $A = \sqrt{2} \ell^2$  are also listed in the figure. The same isopleth distributions, using the same reference areas ( $A = \ell^2$ ), can be explained by the fact that the wake structure in the region farther downwind is independent of the original shape of the building. A more significant difference can be observed at the  $x/\ell < 10$  region.

Figure 48 presents the comparison of the isopleth distribution for different exit ports (bottom and middle) at  $\theta = 45^\circ$  in the inversion stratification (compare Figures 29 and 30). One finds that there is not any significant difference between the two sets of isopleth patterns.

Figure 49 presents the same comparison as in the previous case for  $\theta = 90^\circ$  in neutral stratification (compare Figures 19 and 20). The effect of release port location does not appear significant.

Figure 50 presents only the isopleths at the center plane ( $y = 0$ ) for both middle and bottom exit ports at  $\theta = 135^\circ$ , inversion stratification (compare Figures 33 and 34). (Notice the release port is not on the center plane).

Figure 51 presents the isopleths at  $\theta = 180^\circ$ , middle exit ports, for both neutral and inversion stratification conditions (compare Figures 23 and 35). The convective motion dominance is very significant in the inversion case.

Figure 52 presents the isopleths at  $\theta = 180^\circ$ , bottom exit port, for both neutral and inversion conditions (compare Figures 24 and 36). Basically the isopleth patterns found in Figure 51 are similar to those in Figure 52. As cited before, in the far downwind region, the isopleths are independent of the exit ports (relaxation effects).

## 6.4 Comparison

6.4.1 Comparison to previous model studies - A previous model study concerning the gaseous dispersion from leaks in a building was performed by Halitsky in 1963. He was interested in gaseous dispersion in the cavity region; hence, his concentration measurements are limited to  $x/D \leq 5$ . The data reported in this study cover the downwind region from  $x/l \approx 3$  to 30.

The K-factor distributions are not necessarily dominated by original building shapes (if shapes of buildings are of a simple geometry, for instance, a truncated cylinder with approximately the same height and diameter, a cube, a rectanguloid, etc.); hence some correlation may be expected between this study and Halitsky's.

Figures 44 through 52 demonstrate the isopleths from the present study. The tendency for the main plume to go downward and to cause the maximum concentration on the ground level is significant. Figures 53 and 54 display the isopleth distributions, about a model reactor shell, published by Halitsky. The patterns of these isopleths, which tend to flatten, but not expand in the longitudinal center plane, are similar. Both studies also present a decrease in the rate of transverse speed for  $x/l > 4$ .

A universal dispersion behavior is noticed for these leakage problems; i.e., the main plume tends to go downward beyond the cavity

region and transverse dispersion rates are much greater than the vertical ones.

A coarse estimation of the average K-factor at the end of the cavity, as mentioned by Halitsky, can be made through the following arguments. At the end of a cavity region, the average concentration for the entire section is approximately equal to the source strength divided by the total volume flow, i.e.,

$$\chi_{ave} = \frac{Q}{A_1 V_1} ,$$

in which  $A_1$  , a wake area at the end of the cavity region, is assumed to be twice the characteristic area, i.e.,  $A_1 = 2A$ , and  $V_1$  , the average velocity of this entire section (varying from 0 to the free stream velocity), is assumed to be half the value of the free stream velocity, i.e.,  $V_1 = 1/2 U$ . The average concentration thus reads:

$$\chi_{ave} = \frac{Q}{2A \cdot (U/2)} = \frac{Q}{AU}$$

$$K_{ave} = \frac{\chi_{ave} AU}{Q} = 1 .$$

For a cubical structure, the cavity length extends from  $2\ell$  to  $3.5\ell$ , varying with the building orientations, as cited in section 1.2.

For the nearest station of concentration measurements,  $3.3\ell$ , the approximate average K-factors are found to be 1.20 to 1.13 by using the above arguments. (The comparison made is from Figures 47 and 48, since only when  $\theta = 45^\circ$  may the cavity extend to  $x/\ell = 3.3$ ).

6.4.2 Correlation of wind tunnel measurements for meandering behaviors - It is known that average maximum concentrations of gaseous dispersion in the atmosphere tend to decrease with increasing sampling time. Since the motion of air flow in lower atmosphere is limited in the vertical direction by the presence of the ground, the magnitude of eddy size in the transverse direction may be much greater than that in the vertical direction. Thus, the meandering behavior or gustiness effect because of the large scale of eddy in the atmosphere causes a greater transverse dispersion. Since the larger eddy motion cannot be produced in the wind tunnel, some adjustments must be made for field application.

This phenomenon, often known as the gustiness effect, was first considered by Inoue (Hino, 1968). He reported that a smoke cloud width increases at a rate proportional to the  $1/2$  power of the observation time. Ogura (1959) developed a mathematical model which suggested a  $-1/2$  power variation of the maximum concentration with time. Hino (1967) performed a large scale study for a time range from ten minutes to five hours. The study which involved releasing tracer materials from high stacks of thermal electric power stations also gives support to the  $-1/2$  power law. Hino also found that atmospheric instability has only small effect on the exponent of the power law, i.e.,  $\chi \sim \tau^{-1/2}$ . The applicable range of the  $-1/2$  law is greater for unstable than for neutral stratification.

An alternative  $-1/5$  power law was proposed by Nonhebel. Hino (1968) suggested, however, that the applicable time range for this law

is less than ten minutes. Other exponents for the peak to mean concentration ratio from -0.65 to -0.35 depending on meteorological condition, have been recommended by the ASMC Committee on Air Pollution Control. Hinds (1967) measured the peak to mean concentration ratios in a building wake region. Data indicated the  $-1/2$  law can also be used satisfactorily to predict the dispersion in the wake flow.

When a gustiness effect is considered, the average concentration  $\chi_t$  (with a release period  $\tau_t$ ) can be expressed as a function of reference concentration  $\chi_0$  (with a reference release period  $\tau_0$ ), i.e.,

$$\chi_t = \chi_0 \left( \frac{\tau_t}{\tau_0} \right)^{-1/2} .$$

Adjustment of various measurements of concentrations for the effects of different averaging time will apparently only shift the absolute magnitudes of ground concentrations vs. distance linearly.

6.4.3 Comparison to a similar previous field study - As cited in section 2.1, Dickson, Start and Markee, Jr., (1967) observed a -0.6 value for the average maximum concentrations vs. downwind distance in a wake region. The slopes of -0.59 to -0.68 observed in different orientation angles are close to -0.6. These slopes, which are much flatter than those of dispersion in an open field, may be considered to be a characteristic of dispersion in a wake region.

The extent of the -0.6 slope region for the modeled flow in the downstream direction may be greater than that which will be observed for the prototype flow. If the large scale eddies, which are typical of atmospheric turbulence, are absent, the wake turbulence will be permitted to dominate the dispersion process over a greater distance. This has been discussed in detail in Section 6.4.2

## Chapter VII

## CONCLUSIONS

Gaseous dispersion from leaks in a cubical structure is a practical engineering problem. From an experimental approach, this study has led to the following conclusions.

1. Dispersion patterns differ in regions with and without the presence of a structure. The ground-level concentration variation with longitudinal distance in the wake region show much flatter slopes ( $\sim -0.6 \sim -0.7$ ) than those in open fields ( $\sim -1.3 \sim -1.7$ ).
2. For a specific building orientation, dispersions are similar for different release ports (from the top, middle, and bottom of the building height). Strong turbulent mixing motions are believed to smooth out any effects from the origin of release.
3. Aerodynamic effects due to building orientations ( $0^\circ$ ,  $45^\circ$ ,  $90^\circ$ ,  $135^\circ$ ,  $180^\circ$ ) cause a slightly different concentration distribution in the cavity and near wake region. This difference depends on the portion of effluent which is initially carried downwind by convective motions.
4. Farther downwind the dispersion will be independent of the original building shapes, ( $x/l \geq 5$ ).
5. Mechanical turbulence dominates the dispersion behavior in the  $x/l \leq 5$  region. The stratification becomes more important farther downwind.
6. Inversion stratification ( $Ri|_{z=l} = 0.15$ ) causes higher ground concentration (about 8%) than those in neutral stratification.

7. Inversion stratification causes smaller transverse spreads and "freezes" the plume growth in the vertical direction.
8. The plume growth in the transverse direction is much greater than (about 3 - 5 times) that in the vertical direction for both neutral and stabilized stratified shear flows.
9. Because of the dispersion characteristics in the wake flow linear superposition is not applicable to predict the real dispersion behavior.

## BIBLIOGRAPHY

- Barry, P. J., "Estimation of Downwind Concentration of Airborne Effluents Discharged in the Neighborhood of Buildings". Talk presented to Advisory Committee on the Safety of Particle Accelerators of the Atomic Energy Control Board. Atomic Energy of Canada Limited, Chalk River, Ontario. Sept. 1963.
- Cermak, J. E., Sandborn, V. A., Plate, E. J., Binder, G. H., Chuang, H., Meroney, R. N. and Ito, S., "Simulation of Atmospheric Motion by Wind Tunnel Flows". FDDL Report CER66JEC-VAS-EJP-GJB-HC-RNM-SI17, Colorado State University. May 1966.
- Chaudhry, F. H., and Meroney, R. N., "Turbulent Diffusion in a Stably Stratified Shear Layer", Technical Report C-0423-J, Colorado State University, 1969.
- Csanady, G. T., "Concentration Fluctuation in Turbulent Diffusion," J. of Atmospheric Science, vol. 24, Jan. 1967, pp. 21-28.
- Davis, P. O. A. L. and Moore, P. L., "Experiments on the Behavior of Effluent Emitted from Stacks at or Near the Roof Level of Tall Reactor Buildings," International Journal of Air and Water Pollution, vol. 8, pp. 515-533 (1964).
- Dickson, C. R., Start, G. E., and Markee, E. H., Jr., "Aerodynamic Effects of the EBR-II Containment Vessel Complex on Effluent Concentration," USAEC Meteorological Information Meeting, September 11-14, 1967, pp. 87-104.
- Golden, J., "Scale Model Technique" M.S. Thesis, New York University, Dept. of Meteor. and Ocean, (1961).
- Halitsky, Golden, Halpern, and Wu, "Wind Tunnel Tests of Gas Diffusion from a Leak in the Shell of a Nuclear Power Reactor and from a Nearby Stack," Geoph. Sci. Laboratory Report No. 63-2, New York University, (1963).
- Halitsky, J., "Gas Diffusion Near Buildings," Geophysical Sci. Lab., Report No. 63-3, New York University (1963).
- Halitsky, J., "Gas Diffusion Near Buildings," Meteorology and Atomic Energy, pp. 221-231, (1968).
- Hinds, W. T., "On the Variation of Concentration in Plumes and Building Wakes," USAEC Meteor. Information Meeting, September 11-14, 1967, pp. 105-131.
- Hino, M., "Computer Experiment on Smoke Diffusion over a Complicated Topograph," Atmospheric Environment, Vol. 2, 1968, pp. 543-558.

- Hino, M., "Maximum Ground Level Concentration and Sampling Time," Atmospheric Environment Pergamon Press, Vol. 2, 1968, pp. 149-165.
- Inoue, E., "On the Turbulent Diffusion in the Atmosphere," I. Journal of Meteorological Society of Japan, No. 28, p. 219, 1950.
- Lapp, R. E., and Andrews, H. L., Nuclear Radiation Physics, Prentice Hall, Inc., (1964)
- Mantle, P. L., "A New Type of Roughened Heat Transfer Surface Selected by Flow Visualization Techniques," International Heat Transfer Conference, Vol. 1, 1966, pp. 45-55.
- Martin, J. E., "The Correlation of Wind Tunnel and Field Measurements of Gas Diffusion Using Krypton-85 as a Tracer," Ph.D. Thesis, MMpp 272, University of Michigan (1965).
- Meroney, R. N., Cermak, J. E., and Chaudhry, F. H., "Wind Tunnel Model Study of Shoreham Nuclear Power Station Unit 1, Long Island Lighting Company," Progress Report No. 1 & 2, FDDL Report CER68-69RNM-JEC-FHC-1, Colorado State University, July 1968.
- Monroe, R. H., Jr., and Mei, C. C., "The Shape of Two-Dimensional Turbulent Wakes in Density-Stratified Fluids," Hydrodynamics Laboratory Report No. 110. Civil Engineering, School of Engineering, M.I.T., June 1968.
- Ogura, Y., "Diffusion from a Continuous Source in Relation to a Finite Observation Interval," Adv. Geophysics, Vol. 6, 1959, pp. 149-159.
- Panofsky, H. A., "Air Pollution Meteorology," American Scientist 57, 2, 1969, pp. 269-285.
- Parzen, E., Modern Probability Theory and Its Applications, John Wiley and Sons, Inc., (1967).
- Pasquill, F., Atmospheric Diffusion, D. Van Nostrand Co., London (1962).
- Pasquill, F., "The Estimation of the Dispersion of Wind-borne Material," Meteor. Mag., 90, 1963, p. 33.
- Plate, E. J., and Lin, C. W., "Investigations of the Thermally Stratified Boundary Layer," Fluid Mechanics Paper No. 5, Colorado State University, 1966.
- Rouse, H., "Use of the Low-Velocity Air Tunnel in Hydraulic Research," Proceedings of the Third Hydraulics Conference, University of Iowa Studied in Engineering, Bulletin 31, 1947, p. 121.
- Schlichting, H., Boundary Layer Theory, McGraw-Hill, New York. 6th edition, 1966.

- Sherlock, R. H. and Stalker, E. A., "The Control of Gases in the Wake of Smokestacks," Mechanical Engineering, Vol. 62, No. 6, pp. 455-458, June (1940).
- Singer, I. A. and Smith, M. E., "The Relation of Gustiness to other Meteorological Parameters," Journal of Meteorology, Vol. 10. April 1953, P. 121.
- Singer, I. A., Imai, Kazuhiko and Roman Gonzalez Del Campo, "Peak to Mean Pollutant Concentration Ratios for Various Terrain and Vegetation Cover," Journal APCA, Vol. 13, #1, p. 40, (1963).
- Slade, D. H., editor, Meteorology and Atomic Energy, U. S. Atomic Energy Commission, Division of Technical Information, 1968.
- Smith, M., editor, Recommended Guide for the Prediction of the Dispersion of Airborne Effluents, ASME, 1968.
- Sutton, O. G., "The Theoretical Distribution of Airborne Pollution from Factory Chimneys," Quar. J. R. Meteor. Soc. 73, 1947, p. 426.
- Sutton, O. G., Micrometeorology, McGraw-Hill Book Co., Inc., New York (1953).

**APPENDIX I**

**TABLES**

Table of Measured Concentration Profiles

Orientation $\theta^\circ$	Vertical or Transverse	Neutral or Stable Stratification	Top, Middle or Bottom Release Port
0	V	N	T.M.B.
	V	S	T.M.B.
	H	N	T.M.B.
	H	S	T.M.B.
45	V	N	-----
	V	S	T.M.B.
	H	N	-----
	H	S	T.M.B.
90	V	N	M.B.
	V	S	M.B.
	H	N	M.B.
	H	S	---
135	V	N	---
	V	S	M.B.
	H	N	---
	H	S	---
180	V	N	M.B.
	V	S	M.B.
	H	N	---
	H	S	M.B.

TABLE OF K FACTORS IN VERTICAL PROFILE

NEUTRAL THETA=0 TOP						NEUTRAL THETA=0 MID					
Z (CM)	K-FACTOR		K-FACTOR			Z (CM)	K-FACTOR		K-FACTOR		
	X=.5M	X=1M	X=2 M	X=3 M	X=4 M		X=.5M	X=1M	X=2 M	X=3 M	X=4 M
0.000	1.434	.631	.493	.344	.241	0.000	.861	.585	.482	.298	.252
2.000	1.163	.538	.464	.261	.184	2.000	.794	.481	.436	.264	.219
4.000	1.020	.408	.348	.225	.147	4.000	.700	.471	.383	.203	.196
6.000	1.222	.444	.376	.218	.188	6.000	.741	.501	.391	.222	.161
8.000	1.193	.396	.226	.193	.132	8.000	.652	.434	.294	.172	.153
10.000	2.010	.257	.283	.156	.152	10.000	.669	.456	.287	.166	.150
12.000	1.039	.311	.199	.157	.116	12.000	.582	.294	.183	.124	.193
14.000	1.244	.499	.185	.112	.113	14.000	.872	.313	.243	.174	.167
16.000	1.015	.256	.157	.063	.102	16.000	.744	.265	.185	.134	.199
18.000	.792	.155	.100	.050	.063	18.000	.491	.207	.141	.087	.187
20.000	.723	.125	.134	.095	.071	20.000	.322	.071	.130	.073	.184
22.000	.356	.069	.094	.087	.063	22.000	.208	.107	.137	.062	.157
24.000	.220	.044	.057	.056	.050	24.000	.108	.047	.121	.053	.157
26.000	.011	.014	.026	.029	.026	26.000	.007	.030	.023	.018	0.100
28.000	0.000	0.000	.055	.022	.028	28.000	.013	.010	.034	.043	0.100
30.000	0.000	0.000	.038	0.000	0.000	30.000	0.000	0.000	.030	.019	0.100
32.000	0.000	0.000	.025	0.000	0.000	32.000	0.000	0.000	0.000	0.000	0.100
34.000	0.000	0.000	0.000	0.000	0.000	34.000	0.000	0.000	0.000	0.000	0.100
36.000	0.000	0.000	0.000	0.000	0.000	36.000	0.000	0.000	0.000	0.000	0.100
38.000	0.000	0.000	0.000	0.000	0.000	38.000	0.000	0.000	0.000	0.000	0.100
40.000	0.000	0.100	0.000	0.000	0.000	40.000	0.000	0.000	0.000	0.000	0.100

NEUTRAL THETA=0 BUT						NEUTRAL THETA=180 MID					
Z (CM)	K-FACTOR		K-FACTOR			Z (CM)	K-FACTOR		K-FACTOR		
	X=.5M	X=1M	X=2 M	X=3 M	X=4 M		X=.5M	X=1M	X=2 M	X=3 M	X=4 M
0.000	1.285	.631	.402	.264	.218	0.000	1.044	.631	.493	.413	.229
2.000	1.253	.510	.338	.187	.148	2.000	.923	.494	.435	.349	.186
4.000	1.024	.407	.278	.169	.153	4.000	.634	.311	.322	.223	.165
6.000	.932	.496	.257	.173	.168	6.000	.610	.432	.409	.227	.143
8.000	.742	.374	.204	.155	.148	8.000	.436	.273	.289	.194	.116
10.000	.977	.386	.172	.114	.122	10.000	.404	.270	.214	.208	.199
12.000	.523	.222	.132	.110	.070	12.000	.137	.178	.194	.174	.104
14.000	.497	.199	.184	.088	.092	14.000	.098	.231	.162	.152	.121
16.000	.349	.161	.109	.078	.089	16.000	.069	.170	.102	.079	.148
18.000	.195	.091	.090	.065	.063	18.000	0.000	.118	.095	.065	.160
20.000	.243	.133	.081	.059	.067	20.000	0.000	.081	.115	.104	.163
22.000	.084	.085	.064	.056	.068	22.000	0.000	.080	.055	.115	.168
24.000	.051	.037	.048	.051	.041	24.000	0.000	.042	.071	.062	.141
26.000	0.000	0.000	.017	.018	.031	26.000	0.000	.021	.031	.020	.131
28.000	0.000	.020	.034	.032	.026	28.000	0.000	0.000	.035	.062	.131
30.000	0.000	0.000	.022	0.000	0.000	30.000	0.000	0.000	0.000	.021	.118
32.000	0.000	0.000	0.000	0.000	0.000	32.000	0.000	0.000	0.000	.026	0.100
34.000	0.000	0.000	0.000	0.000	0.000	34.000	0.000	0.000	0.000	.017	0.100
36.000	0.000	0.000	0.000	0.000	0.000	36.000	0.000	0.000	0.000	.037	0.100
38.000	0.000	0.000	0.000	0.000	0.000	38.000	0.000	0.000	0.000	0.000	0.100
40.000	0.000	0.100	0.000	0.000	0.000	40.000	0.000	0.000	0.000	0.000	0.100

TABLE OF K FACTORS IN VERTICAL PROFILE

NEUTRAL THETA=180				BOT				NEUTRAL THETA=90				MID						
NEUTRAL		THETA=180		BOT		NEUTRAL		THETA=90		MID		NEUTRAL		THETA=90		MID		
Z (CM)	X=0.5M	X=1M	X=2 M	K-FACTOR X=2 M	X=3 "	X=4 M	Z (CM)	X=0.5M	X=1M	K-FACTOR X=2 M	X=3 M	X=4 M	Z (CM)	X=0.5M	X=1M	K-FACTOR X=2 M	X=3 M	X=4 M
0.000	.918	.624	.459	.390	.341	.241	0.000	1.400	.826	.574	.298	.075						
2.000	.866	.614	.400	.344	.304	.204	2.000	1.381	.692	.504	.232	.043						
4.000	.850	.651	.335	.254	.158	.158	4.000	1.208	.583	.482	.195	.022						
6.000	.830	.628	.309	.209	.146	.146	6.000	1.448	.586	.483	.170	.017						
8.000	.804	.603	.341	.210	.187	.187	8.000	1.128	.483	.311	.148	.016						
10.000	.774	.574	.226	.244	.133	.133	10.000	1.094	.467	.390	.148	.011						
12.000	.749	.549	.209	.197	.093	.093	12.000	.677	.265	.244	.107	.012						
14.000	.721	.521	.185	.235	.102	.102	14.000	.588	.264	.225	.095	.016						
16.000	.695	.495	.112	.142	.045	.045	16.000	.388	.208	.138	.073	.021						
18.000	.669	.469	.105	.085	.046	.046	18.000	.293	.170	.077	.048	.083						
20.000	.641	.441	.072	.104	.041	.041	20.000	.262	.084	.118	.083	.083						
22.000	.621	.421	.044	.087	.123	.076	22.000	.130	.095	.079	.057	.090						
24.000	.601	.401	.032	.054	.114	.076	24.000	.058	.049	.106	.039	.066						
26.000	.580	.380	.019	.019	.000	.012	26.000	0.000	0.000	0.000	0.000	0.000						
28.000	.560	.360	.041	.041	.103	.021	28.000	0.000	0.000	0.000	0.000	0.000						
30.000	.540	.340	0.000	0.000	0.000	0.000	30.000	0.000	0.000	0.000	0.000	0.000						
32.000	.520	.320	0.000	0.000	0.000	0.000	32.000	0.000	0.000	0.000	0.000	0.000						
34.000	.500	.300	0.000	0.000	0.000	0.000	34.000	0.000	0.000	0.000	0.000	0.000						
36.000	.480	.280	0.000	0.000	0.000	0.000	36.000	0.000	0.000	0.000	0.000	0.000						
38.000	.460	.260	0.000	0.000	0.000	0.000	38.000	0.000	0.000	0.000	0.000	0.000						
40.000	.440	.240	0.000	0.000	0.000	0.000	40.000	0.000	0.000	0.000	0.000	0.000						

NEUTRAL THETA=90				TOP							
NEUTRAL		THETA=90		INVERSION THETA=000		TOP					
Z (CM)	X=0.5M	X=1M	K-FACTOR X=2 M	X=3 M	X=4 M	Z (CM)	X=0.5M	X=1M	K-FACTOR X=2 M	X=3 M	X=4 M
0.000	1.836	.918	.574	.321	.252	0.000	.746	.918	.574	.470	.167
2.000	1.674	.814	.462	.304	.145	2.000	.781	.889	.549	.518	.163
4.000	1.272	.565	.379	.227	.154	4.000	.824	.732	.507	.507	.135
6.000	1.250	.436	.355	.231	.167	6.000	1.028	.899	.484	.629	.138
8.000	.986	.481	.374	.213	.134	8.000	1.160	.877	.485	.556	.112
10.000	.798	.432	.326	.194	.147	10.000	1.304	.928	.388	.564	.177
12.000	.559	.340	.173	.120	.130	12.000	.991	.837	.314	.503	.133
14.000	.464	.302	.176	.152	.137	14.000	1.156	.590	.349	.480	.156
16.000	.319	.194	.104	.138	.138	16.000	.461	.533	.249	.485	.102
18.000	.197	.108	.045	.100	.092	18.000	.630	.544	.227	.297	.158
20.000	.156	.162	.097	.090	.055	20.000	.580	.377	.221	.413	.113
22.000	.085	.111	.085	.061	.055	22.000	.276	.266	.215	.384	.110
24.000	.046	.045	.040	.067	.092	24.000	.124	.187	.193	.221	.153
26.000	0.000	0.000	0.000	0.000	0.000	26.000	0.000	.041	.088	.183	.153
28.000	0.000	0.000	0.000	0.000	0.000	28.000	0.000	.013	.103	.198	.164
30.000	0.000	0.000	0.000	0.000	0.000	30.000	0.000	0.000	.056	.108	.108
32.000	0.000	0.000	0.000	0.000	0.000	32.000	0.000	0.000	.039	.044	.044
34.000	0.000	0.000	0.000	0.000	0.000	34.000	0.000	0.000	.039	.076	.124
36.000	0.000	0.000	0.000	0.000	0.000	36.000	0.000	0.000	0.000	0.000	.091
38.000	0.000	0.000	0.000	0.000	0.000	38.000	0.000	0.000	0.000	0.000	.054
40.000	0.000	0.000	0.000	0.000	0.000	40.000	0.000	0.000	0.000	0.000	0.000

TABLE OF K FACTORS IN VERTICAL PROFILE

INVERSION THETA=000						INVERSION THETA=000					
Z (CM)	MID					Z (CM)	BOT				
	X=.5M	X=1M	K-FACTOR				X=.5M	X=1M	K-FACTOR		
			X=2 M	X=3 M	X=4 M			X=2 M	X=3 M	X=4 M	
0.000	1.147	.711	.631	.470	.367	0.000	1.377	1.170	.631	.516	.402
2.000	1.172	.734	.626	.484	.357	2.000	1.334	.804	.570	.518	.444
4.000	.976	.544	.505	.352	.243	4.000	.964	.638	.430	.424	.333
6.000	1.036	.422	.604	.357	.211	6.000	.887	.487	.425	.402	.307
8.000	1.041	.547	.501	.360	.216	8.000	.101	.386	.406	.378	.290
10.000	1.014	.557	.464	.305	.163	10.000	.558	.373	.368	.298	.243
12.000	.689	.435	.361	.297	.152	12.000	.396	.194	.167	.169	.168
14.000	.703	.337	.370	.308	.275	14.000	.356	.178	.297	.234	.223
16.000	0.000	.317	.312	.233	.188	16.000	.234	.151	.239	.203	.212
18.000	.319	.257	.244	.214	.143	18.000	.167	.069	.139	.175	.145
20.000	.320	.203	.264	.193	.164	20.000	.130	.096	.140	.152	.137
22.000	.158	.150	.214	.170	.198	22.000	.058	.067	.120	.138	.127
24.000	.060	.097	.143	.154	.166	24.000	.742	.038	.042	.126	.112
26.000	0.000	.055	.070	.098	.072	26.000	0.000	.016	.047	.041	.154
28.000	.024	.037	.087	.070	.114	28.000	0.000	.014	.040	.055	.194
30.000	0.000	0.000	.018	.092	.048	30.000	0.000	0.000	0.000	.027	.144
32.000	0.000	0.000	0.000	.011	.059	32.000	0.000	0.000	0.000	0.000	.121
34.000	0.000	0.000	0.000	.020	.046	34.000	0.000	0.000	0.000	0.000	0.100
36.000	0.000	0.000	0.000	0.000	0.000	36.000	0.000	0.000	0.000	0.000	0.100
38.000	0.000	0.000	0.000	0.000	0.000	38.000	0.000	0.000	0.000	0.000	0.100
40.000	0.000	0.000	0.000	0.000	0.000	40.000	0.000	0.000	0.000	0.000	0.100

INVERSION THETA=180						INVERSION THETA=180					
Z (CM)	MID					Z (CM)	BOT				
	X=.5M	X=1M	K-FACTOR				X=.5M	X=1M	K-FACTOR		
			X=2 M	X=3 M	X=4 M			X=2 M	X=3 M	X=4 M	
0.000	1.377	.641	.711	.631	.482	0.000	1.859	1.170	.861	.620	.459
2.000	1.179	.890	.639	.429	.446	2.000	1.521	1.193	.684	.446	.451
4.000	.884	.661	.452	.311	.284	4.000	1.126	.703	.534	.341	.332
6.000	.706	.451	.366	.316	.337	6.000	.950	.579	.535	.318	.258
8.000	.621	.387	.342	.250	.269	8.000	.797	.413	.462	.253	.227
10.000	.471	.301	.329	.194	.263	10.000	.526	.349	.358	.232	.208
12.000	.222	.181	.147	.130	.164	12.000	.303	.176	.228	.133	.104
14.000	.194	.190	.190	.142	.134	14.000	.243	.212	.250	.147	.105
16.000	.176	.153	.145	.110	.118	16.000	.199	.154	.176	.109	.102
18.000	.118	.105	.106	.065	.107	18.000	.147	.110	.095	.086	.155
20.000	.092	.084	.094	.108	.167	20.000	.103	.067	.118	.088	.189
22.000	.124	.084	.100	.122	.171	22.000	.184	.111	.127	.091	.194
24.000	.047	.045	.080	.101	.123	24.000	.051	.029	.086	.083	.181
26.000	.009	0.000	.024	.044	0.000	26.000	0.000	0.000	.039	.026	0.100
28.000	.015	0.000	.018	.078	0.000	28.000	0.000	0.000	.043	.047	0.100
30.000	0.000	0.000	.013	.048	0.000	30.000	0.000	0.000	.023	.033	0.100
32.000	0.000	0.000	0.000	.031	0.000	32.000	0.000	0.000	0.000	.011	0.100
34.000	0.000	0.000	0.000	.029	0.000	34.000	0.000	0.000	0.000	.020	0.100
36.000	0.000	0.000	0.000	0.000	0.000	36.000	0.000	0.000	0.000	0.000	0.100
38.000	0.000	0.000	0.000	0.000	0.000	38.000	0.000	0.000	0.000	0.000	0.100
40.000	0.000	0.000	0.000	0.000	0.000	40.000	0.000	0.000	0.000	0.000	0.100

TABLE OF K FACTORS IN VERTICAL PROFILE

INVERSION THETA=5				BOT				INVERSION THETA=45				MID					
Z (CM)	X=5M	X=1M	K-FACTOR X=2 M	X=3 M	X=4 M	Z (CM)	X=5M	X=1M	K-FACTOR X=2 M	X=3 M	X=4 M	Z (CM)	X=5M	X=1M	K-FACTOR X=2 M	X=3 M	X=4 M
0.000	4.282	1.411	.711	.551	.528	0.000	1.721	1.406	.603	.585	.482	0.000	1.721	1.406	.603	.585	.482
2.000	3.135	1.182	.584	.471	.506	2.000	1.753	1.424	.724	.483	.401	4.000	1.587	1.424	.724	.483	.401
4.000	2.048	.842	.474	.382	.392	4.000	1.484	1.096	.873	.356	.368	6.000	1.484	1.096	.873	.356	.368
6.000	1.213	.608	.497	.375	.324	6.000	1.302	.863	.434	.288	.286	8.000	1.302	.863	.434	.288	.286
8.000	.995	.642	.380	.290	.324	8.000	1.127	.652	.408	.223	.288	10.000	1.127	.652	.408	.223	.288
10.000	.788	.471	.383	.257	.273	10.000	.598	.612	.278	.141	.303	12.000	.598	.612	.278	.141	.303
12.000	.442	.266	.202	.191	.178	12.000	.464	.464	.381	.179	.191	14.000	.464	.464	.381	.179	.191
14.000	.390	.258	.193	.147	.189	14.000	.212	.485	.241	.166	.136	16.000	.212	.485	.241	.166	.136
16.000	.242	.178	.150	.143	.194	16.000	.132	.339	.219	.091	.128	18.000	.132	.339	.219	.091	.128
18.000	.114	.125	.096	.114	.106	18.000	.047	.178	.123	.076	.122	20.000	.047	.178	.123	.076	.122
20.000	.104	.084	.084	.077	.105	20.000	.029	.106	.062	.062	.101	22.000	.029	.106	.062	.062	.101
22.000	.049	.026	.066	.072	.092	22.000	.009	.039	.042	.064	.081	24.000	.009	.039	.042	.064	.081
24.000	.014	.027	.043	.059	.083	24.000	0.000	0.000	0.000	0.000	0.000	26.000	0.000	0.000	0.000	0.000	0.000
26.000	0.000	0.000	0.000	0.000	0.000	26.000	0.000	0.000	0.000	0.000	0.000	28.000	0.000	0.000	0.000	0.000	0.000
28.000	0.000	0.000	0.000	0.000	0.000	28.000	0.000	0.000	0.000	0.000	0.000	30.000	0.000	0.000	0.000	0.000	0.000
30.000	0.000	0.000	0.000	0.000	0.000	30.000	0.000	0.000	0.000	0.000	0.000	32.000	0.000	0.000	0.000	0.000	0.000
32.000	0.000	0.000	0.000	0.000	0.000	32.000	0.000	0.000	0.000	0.000	0.000	34.000	0.000	0.000	0.000	0.000	0.000
34.000	0.000	0.000	0.000	0.000	0.000	34.000	0.000	0.000	0.000	0.000	0.000	36.000	0.000	0.000	0.000	0.000	0.000
36.000	0.000	0.000	0.000	0.000	0.000	36.000	0.000	0.000	0.000	0.000	0.000	38.000	0.000	0.000	0.000	0.000	0.000
38.000	0.000	0.000	0.000	0.000	0.000	38.000	0.000	0.000	0.000	0.000	0.000	40.000	0.000	0.000	0.000	0.000	0.000
40.000	0.000	0.000	0.000	0.000	0.000	40.000	0.000	0.000	0.000	0.000	0.000						

INVERSION THETA=135				BOT				INVERSION THETA=135 (45)				TOP					
Z (CM)	X=5M	X=1M	K-FACTOR X=2 M	X=3 M	X=4 M	Z (CM)	X=5M	X=1M	K-FACTOR X=2 M	X=3 M	X=4 M	Z (CM)	X=5M	X=1M	K-FACTOR X=2 M	X=3 M	X=4 M
0.000	1.033	1.429	.803	.402	.275	0.000	2.295	.918	.585	.367	.498	0.000	2.295	.918	.585	.367	.498
2.000	.815	1.404	.706	.366	.254	2.000	2.032	.839	.479	.245	.245	4.000	1.465	.839	.479	.245	.245
4.000	.577	1.193	.566	.305	.211	4.000	1.366	.716	.363	.243	.286	6.000	1.366	.716	.363	.243	.286
6.000	.511	1.113	.584	.260	.176	6.000	1.141	.617	.391	.280	.191	8.000	1.141	.617	.391	.280	.191
8.000	.342	.787	.466	.212	.129	8.000	1.010	.550	.293	.243	.163	10.000	1.010	.550	.293	.243	.163
10.000	.284	.643	.394	.174	.149	10.000	.707	.395	.240	.240	.192	12.000	.707	.395	.240	.240	.192
12.000	.165	.436	.252	.138	.107	12.000	.613	.312	.207	.149	.114	14.000	.613	.312	.207	.149	.114
14.000	.149	.396	.256	.138	.114	14.000	.494	.210	.168	.124	.100	16.000	.494	.210	.168	.124	.100
16.000	.097	.157	.204	.099	.100	16.000	.291	.116	.099	.087	.080	18.000	.291	.116	.099	.087	.080
18.000	.051	.076	.136	.070	.074	18.000	.175	.067	.134	.068	.047	20.000	.175	.067	.134	.068	.047
20.000	.038	.151	.090	.063	.071	20.000	.074	.046	.085	.082	.078	22.000	.074	.046	.085	.082	.078
22.000	.018	.083	.065	.048	.063	22.000	.040	.025	.082	.082	.062	24.000	.040	.025	.082	.082	.062
24.000	0.000	0.000	0.000	0.000	.025	24.000	0.000	0.000	0.000	0.000	0.000	26.000	0.000	0.000	0.000	0.000	0.000
26.000	0.000	0.000	0.000	0.000	.037	26.000	0.000	0.000	0.000	0.000	0.000	28.000	0.000	0.000	0.000	0.000	0.000
28.000	0.000	0.000	0.000	0.000	.026	28.000	0.000	0.000	0.000	0.000	0.000	30.000	0.000	0.000	0.000	0.000	0.000
30.000	0.000	0.000	0.000	0.000	.022	30.000	0.000	0.000	0.000	0.000	0.000	32.000	0.000	0.000	0.000	0.000	0.000
32.000	0.000	0.000	0.000	0.000	0.000	32.000	0.000	0.000	0.000	0.000	0.000	34.000	0.000	0.000	0.000	0.000	0.000
34.000	0.000	0.000	0.000	0.000	0.000	34.000	0.000	0.000	0.000	0.000	0.000	36.000	0.000	0.000	0.000	0.000	0.000
36.000	0.000	0.000	0.000	0.000	0.000	36.000	0.000	0.000	0.000	0.000	0.000	38.000	0.000	0.000	0.000	0.000	0.000
38.000	0.000	0.000	0.000	0.000	0.000	38.000	0.000	0.000	0.000	0.000	0.000	40.000	0.000	0.000	0.000	0.000	0.000
40.000	0.000	0.000	0.000	0.000	0.000	40.000	0.000	0.000	0.000	0.000	0.000						

## INVERSION THETA=135 MID

Z (CM)	K-FACTOR				
	x=.5M	x=1 M	x=2 M	x=3 M	x=4 M
0.000	1.170	1.262	.746	.402	.298
2.000	1.064	1.176	.599	.345	.245
4.000	.805	.830	.451	.282	.172
6.000	.657	.770	.466	.219	.214
8.000	.439	.564	.359	.167	.169
10.000	.374	.498	.348	.151	.179
12.000	.190	.287	.196	.102	.106
14.000	.199	.323	.219	.092	.129
16.000	.128	.208	.149	.071	.110
18.000	.082	.111	.092	.054	.080
20.000	.043	.072	.101	.072	.073
22.000	.011	.043	.088	.040	.083
24.000	.009	.027	.070	.026	.075
26.000	0.000	0.000	0.000	0.000	.028
28.000	0.000	0.000	0.000	0.000	0.000
30.000	0.000	0.000	0.000	0.000	.026
32.000	0.000	0.000	0.000	0.000	0.000
34.000	0.000	0.000	0.000	0.000	0.000
36.000	0.000	0.000	0.000	0.000	0.000
38.000	0.000	0.000	0.000	0.000	0.000
40.000	0.000	0.000	0.000	0.000	0.000

(Continued)

TABLE OF K FACTORS IN HORIZONTAL PROFILE

THETA=0°(90) NEUTRAL TOP.						THETA=0 NEUTRAL MID.					
Y (CM)	K-FACTOR					Y (CM)	K-FACTOR				
	X=.5M	X=1M	X=2 M	X=3 M	X=4 M		X=.5M	X=1M	X=2 M	X=3 M	X=4 M
-64.000	0.000	0.000	0.000	0.000	0.000	-64.000	0.000	0.000	0.000	0.000	0.000
-60.000	0.000	0.000	0.000	0.000	0.000	-60.000	0.000	0.000	0.000	0.000	0.000
-56.000	0.000	0.000	0.000	0.000	0.000	-56.000	0.000	0.000	0.000	0.000	0.000
-52.000	0.000	0.000	0.000	0.000	.011	-52.000	0.000	0.000	0.000	0.000	0.000
-48.000	0.000	0.000	0.000	0.000	.051	-48.000	0.000	0.000	0.000	.022	0.000
-44.000	0.000	0.000	.024	.051	.054	-44.000	0.000	.033	.029	.040	.028
-40.000	0.000	0.000	.028	.109	.085	-40.000	0.000	.029	.059	.048	.047
-36.000	0.000	0.000	.063	.154	.118	-36.000	.032	.048	.081	.087	.056
-32.000	.070	.122	.176	.174	.146	-32.000	.054	.145	.146	.128	.071
-28.000	.297	.238	.239	.235	.164	-28.000	.158	.191	.260	.200	.133
-24.000	.239	.318	.301	.270	.214	-24.000	.238	.303	.282	.159	.139
-20.000	.300	.320	.319	.227	.159	-20.000	.317	.325	.321	.169	.153
-16.000	.343	.481	.414	.317	.218	-16.000	.559	.511	.353	.230	.231
-12.000	.600	.433	.355	.293	.215	-12.000	.608	.512	.341	.225	.190
-8.000	.822	.577	.415	.281	.225	-8.000	.739	.557	.426	.241	.242
-4.000	.824	.614	.465	.287	.205	-4.000	.834	.539	.402	.255	.233
0.000	1.141	.514	.383	.249	.201	0.000	.491	.473	.327	.188	.190
4.000	1.476	.612	.453	.343	.223	4.000	.838	.552	.438	.269	.229
8.000	1.356	.634	.427	.260	.218	8.000	.600	.599	.394	.249	.177
12.000	1.195	.464	.389	.240	.193	12.000	.479	.460	.400	.211	.176
16.000	1.053	.432	.445	.271	.209	16.000	.423	.507	.374	.283	.227
20.000	.712	.333	.332	.265	.184	20.000	.299	.363	.343	.243	.225
24.000	.543	.270	.343	.245	.225	24.000	.224	.396	.390	.275	.222
28.000	.218	.163	.245	.229	.204	28.000	.132	.294	.323	.245	.223
32.000	.054	.026	.093	.109	.119	32.000	.017	.078	.250	.197	.131
36.000	.024	.009	.054	.154	.107	36.000	.021	.076	.335	.215	.211
40.000	0.000	0.000	.028	.091	.091	40.000	0.000	.034	.129	.159	.197
44.000	0.000	0.000	.012	.061	.056	44.000	0.000	0.000	.079	.108	.151
48.000	0.000	0.000	0.000	.046	.061	48.000	0.000	0.000	.069	.067	.115
52.000	0.000	0.000	0.000	0.000	.020	52.000	0.000	0.000	.035	.072	.091
56.000	0.000	0.000	0.000	0.000	0.000	56.000	0.000	0.000	.033	.032	.074
60.000	0.000	0.000	0.000	0.000	0.000	60.000	0.000	0.000	.017	.016	.047

TABLE OF K FACTORS IN HORIZONTAL PROFILE

THETA=0 NEUTRAL BOT.						THETA=90 NEUTRAL MID.					
Y (CM)	K-FACTOR					Y (CM)	K-FACTOR				
	X=.5M	X=1M	X=2 M	X=3 M	X=4 M		X=.5M	X=1M	X=2 M	X=3 M	X=4 M
-64.000	0.000	0.000	0.000	0.000	0.000	-64.000	0.000	0.000	0.000	0.000	0.000
-60.000	0.000	0.000	0.000	0.000	0.000	-60.000	0.000	0.000	0.000	0.000	0.000
-56.000	0.000	0.000	0.000	0.000	0.000	-56.000	0.000	0.000	0.000	0.000	0.000
-52.000	0.000	0.000	0.000	0.000	0.000	-52.000	0.000	0.000	0.000	0.000	0.000
-48.000	0.000	0.000	0.000	0.000	0.000	-48.000	0.000	0.000	0.000	0.000	.042
-44.000	0.000	.029	.041	.065	.039	-44.000	0.000	0.000	.022	.062	.064
-40.000	.026	.042	.085	.083	.063	-40.000	0.000	0.000	.056	.085	.069
-36.000	.057	.106	.126	.132	.085	-36.000	.047	.057	.085	.130	.121
-32.000	.143	.227	.198	.167	.136	-32.000	.061	.122	.158	.163	.101
-28.000	.367	.412	.294	.196	.199	-28.000	.117	.201	.291	.194	.147
-24.000	.087	.511	.326	.220	.194	-24.000	.188	.285	.322	.253	.174
-20.000	.786	.501	.328	.220	.175	-20.000	.256	.344	.283	.209	.128
-16.000	1.244	.660	.412	.255	.205	-16.000	.495	.530	.366	.281	.148
-12.000	1.197	.652	.368	.234	.183	-12.000	.516	.480	.390	.263	.182
-8.000	1.234	.664	.385	.234	.190	-8.000	.799	.570	.466	.294	.173
-4.000	1.152	.624	.392	.253	.185	-4.000	.987	.695	.406	.256	.211
0.000	.887	.483	.316	.171	.151	0.000	1.238	.608	.434	.248	.149
4.000	.979	.540	.345	.225	.193	4.000	1.395	.740	.476	.271	.218
8.000	.987	.502	.329	.206	.204	8.000	1.438	.790	.528	.251	.200
12.000	.820	.434	.302	.199	.187	12.000	1.239	.680	.491	.261	.177
16.000	.796	.507	.339	.190	.205	16.000	1.136	.758	.578	.288	.231
20.000	.588	.449	.328	.210	.175	20.000	.749	.618	.507	.288	.229
24.000	.515	.497	.344	.224	.199	24.000	.605	.564	.508	.259	.263
28.000	.333	.395	.335	.238	.212	28.000	.268	.433	.468	.294	.260
32.000	.044	.109	.218	.180	.139	32.000	.682	.088	.197	.208	.156
36.000	0.000	.140	.162	.186	.152	36.000	.416	.047	.179	.225	.194
40.000	.006	.084	.119	.177	.164	40.000	.488	0.000	.086	.167	.165
44.000	0.000	.016	.077	.115	.117	44.000	0.000	0.000	.026	.110	.106
48.000	0.000	0.000	.041	.097	.137	48.000	0.000	0.000	0.000	.109	.093
52.000	0.000	0.000	.014	.062	.117	52.000	0.000	0.000	0.000	.062	.055
56.000	0.000	0.000	0.000	.063	.092	56.000	0.000	0.000	0.000	.043	.057
60.000	0.000	0.000	0.000	.024	.057	60.000	0.000	0.000	0.000	.015	.029

THETA=90      NEUTRAL BOT.

Y (CM)	K-FACTOR				
	X=.5M	X=1 M	X=2 M	X=3 M	X=4 M
-64.000	0.000	0.000	0.000	0.000	0.000
-60.000	0.000	0.000	0.000	0.000	0.000
-56.000	0.000	0.000	0.000	0.000	0.000
-52.000	0.000	0.000	0.000	0.000	0.000
-48.000	0.000	0.000	0.000	0.000	0.000
-44.000	0.000	0.000	.008	.048	.054
-40.000	0.000	0.000	.050	.073	.061
-36.000	.055	.047	.084	.101	.089
-32.000	.068	.102	.165	.146	.118
-28.000	.177	.268	.222	.174	.164
-24.000	.200	.252	.272	.183	.166
-20.000	.310	.297	.310	.177	.118
-16.000	.448	.425	.332	.247	.173
-12.000	.566	.454	.336	.219	.147
-8.000	.786	.550	.367	.268	.140
-4.000	.919	.579	.371	.292	.164
0.000	1.246	.551	.322	.192	.140
4.000	1.758	.685	.429	.176	.239
8.000	1.221	.794	.440	.197	.197
12.000	1.836	.735	.415	.194	.171
16.000	1.950	.902	.501	.271	.231
20.000	1.510	.764	.496	.295	.206
24.000	.906	.776	.580	.321	.230
28.000	.558	.576	.511	.313	.256
32.000	.011	.148	.299	.251	.180
36.000	.012	.057	.242	.230	.191
40.000	0.000	.030	.170	.163	.202
44.000	0.000	0.000	.100	.110	.127
48.000	0.000	0.000	.038	.112	.096
52.000	0.000	0.000	0.000	.061	.061
56.000	0.000	0.000	0.000	.037	.061
60.000	0.000	0.000	0.000	.019	.049

(Continued)

TABLE OF K FACTORS IN HORIZONTAL PROFILE

THETA=0.(180) INVERSION, TOP.						THETA=0 INVERSION, MID.					
Y (CM)	K-FACTOR					Y (CM)	K-FACTOR				
	X=.5M	X=1M	X=2 M	X=3 M	X=4 M		X=.5M	X=1M	X=2 M	X=3 M	X=4 M
-20.000	.667	.534	.332	.216	.157	-20.000	.934	.621	.350	.166	.178
-16.000	.724	.908	.501	.290	.215	-16.000	1.119	.697	.452	.312	.197
-12.000	.734	.710	.499	.370	.241	-12.000	1.064	.711	.507	.362	.219
-8.000	.511	.647	.502	.340	.255	-8.000	.825	.608	.549	.365	.229
-4.000	.498	.644	.552	.396	.322	-4.000	.707	.726	.638	.390	.328
0.000	.311	.511	.502	.404	.314	0.000	.512	.526	.590	.407	.322
4.000	.259	.445	.461	.497	.382	4.000	.366	.522	.575	.452	.344
8.000	.192	.308	.555	.427	.342	8.000	.283	.399	.579	.424	.370
12.000	.046	.155	.209	.190	.233	12.000	.073	.223	.228	.257	.235
16.000	.027	.131	.182	.188	.200	16.000	.031	.169	.212	.298	.266
20.000	.019	.060	.130	.177	.199	20.000	.016	.064	.135	.275	.177
24.000	0.000	.043	.073	.104	.151	24.000	0.000	.057	.092	.177	.141
28.000	0.000	.031	.076	.127	.148	28.000	0.000	.047	.081	.155	.132
32.000	0.000	0.000	.063	.077	.113	32.000	0.000	.020	.081	.135	.110
36.000	0.000	0.000	.046	.077	.102	36.000	0.000	0.000	.072	.127	.086
40.000	0.000	0.000	.052	.064	.100	40.000	0.000	0.000	.037	.095	.077

Y (CM)	INVERSION, BOT.				
	K-FACTOR				
	X=.5M	X=1M	X=2 M	X=3 M	X=4 M
-20.000	1.419	.771	.473	.302	.205
-16.000	1.478	1.089	.569	.347	.294
-12.000	1.402	1.085	.549	.354	.323
-8.000	1.125	.860	.592	.418	.247
-4.000	1.118	.908	.662	.508	.416
0.000	.887	.759	.598	.484	.424
4.000	.735	.741	.645	.543	.453
8.000	.542	.614	.576	.542	.522
12.000	.162	.463	.370	.362	.307
16.000	.031	.345	.317	.340	.337
20.000	.022	.247	.244	.307	.242
24.000	0.000	.112	.201	.252	.190
28.000	0.000	.072	.166	.225	.229
32.000	0.000	.049	.129	.169	.172
36.000	0.000	0.000	.109	.171	.188
40.000	0.000	0.000	.062	.130	.158

Y (CM)	INVERSION, MID.				
	K-FACTOR				
	X=.5M	X=1M	X=2 M	X=3 M	X=4 M
-20.000	.951	.384	.463	.342	.225
-16.000	1.026	.442	.584	.422	.305
-12.000	1.167	.455	.556	.496	.324
-8.000	1.196	.398	.491	.457	.296
-4.000	1.418	.632	.605	.520	.379
0.000	1.312	.761	.568	.502	.380
4.000	1.351	.781	.663	.604	.488
8.000	1.356	.814	.706	.545	.477
12.000	.742	.580	.595	.488	.335
16.000	.705	.507	.639	.627	.333
20.000	.316	.230	.580	.494	.323
24.000	.120	.066	.486	.412	.276
28.000	.047	0.000	.489	.020	.316
32.000	.039	0.000	.414	.373	.256
36.000	0.000	0.000	.362	.391	.269
40.000	0.000	0.000	.315	.325	.268

Y (CM)	INVERSION, BOT.				
	K-FACTOR				
	X=.5M	X=1 M	X=2 M	X=3 M	X=4 M
-20.000	.761	.649	.443	.305	.190
-16.000	1.133	.644	.554	.369	.292
-12.000	1.206	.669	.579	.358	.277
-8.000	1.159	.702	.526	.347	.263
-4.000	1.544	.945	.655	.442	.318
0.000	1.584	.915	.631	.428	.320
4.000	1.921	1.180	.796	.590	.456
8.000	1.888	1.278	.827	.614	.433
12.000	.859	.976	.725	.451	.396
16.000	.484	.752	.866	.546	.424
20.000	.249	.524	.844	.493	.444
24.000	.103	.401	.714	.412	.381
28.000	.040	.277	.689	.400	.440
32.000	.037	.156	.493	.315	.380
36.000	0.000	.080	.451	.374	.353
40.000	0.000	.023	.427	.316	.340

(Continued)

THETA = 45 INVERSION TOP						THETA = 45 INVERSION MID					
Y (CM)	K-FACTOR					Y (CM)	K-FACTOR				
	X = 5M	X = 1M	X = 2M	X = 3M	X = 4M		X = 5M	X = 1M	X = 2M	X = 3M	X = 4M
-52.	---	---	---	.071	-.044	-52.	---	---	---	.028	---
-48.	---	---	---	.137	.091	-48.	---	---	---	.050	---
-44.	---	---	.164	.175	.119	-44.	---	---	.067	.076	.042
-40.	---	.115	.255	.180	.090	-40.	---	---	.092	.081	.062
-36.	---	.151	.254	.215	.124	-36.	.000	.016	.112	.129	.086
-32.	.031	.234	.280	.224	.171	-32.	.015	.036	.112	.143	.085
-28.	.196	.335	.400	.258	.142	-28.	.052	.064	.214	.183	.101
-24.	.181	.479	.381	.257	.147	-24.	.062	.106	.207	.211	.116
-20.	.322	.732	.437	.300	.215	-20.	.097	.217	.326	.270	.164
-16.	.724	.758	.377	.296	.224	-16.	.230	.228	.314	.306	.158
-12.	.910	.751	.477	.263	.204	-12.	.313	.361	.436	.293	.173
- 8.	1.480	.899	.479	.305	.268	- 8.	.484	.520	.406	.358	.251
- 4.	1.836	.852	.394	.280	.251	- 4.	.644	.678	.428	.308	.247
0.	2.321	.785	.540	.320	.300	0.	.973	.773	.550	.372	.274
4.	1.977	.870	.503	.254	.250	4.	1.037	.708	.514	.343	.246
8.	1.514	.771	.533	.313	.213	8.	1.083	.806	.547	.324	.236
12.	1.346	.768	.517	.315	.274	12.	1.168	.747	.490	.497	.259
16.	.917	.591	.432	.329	.277	16.	.712	.820	.415	.332	.174
20.	.729	.361	.465	.274	.232	20.	.570	.658	.405	.271	.220
24.	.455	.308	.400	.242	.273	24.	.379	.379	.369	.221	.246
28.	.202	.197	.337	.209	.177	28.	.147	.353	.246	.170	.173
32.	.151	.129	.306	.216	.190	32.	.060	.244	.233	.199	.181
36.	.069	.127	.279	.143	.155	36.	.013	.116	.206	.154	.129
40.	.022	.063	.233	.132	.127	40.	.000	.123	.156	.140	.095
44.	.007	.049	.187	.094	.053	44.	---	.080	.128	.131	.020
48.	.000	0.0	.091	.081	---	48.	---	.030	.045	.098	---
52.	---	---	---	---	---	52.	---	.027	---	---	---
56.	---	---	---	---	---	56.	---	---	---	---	---

TABLE OF K FACTOR IN HORIZONTAL PROFILE

THETA = 45 INVERSION BOT

Y (CM)	K-FACTOR				
	X = 5M	X = 1M	X = 2M	X = 3M	X = 4M
-52.	---	---	---	.049	---
-48.	---	---	---	.077	---
-44.	---	---	.063	.072	---
-40.	---	.024	.106	.061	---
-36.	0.000	.052	.154	.108	.043
-32.	.009	.071	.129	.116	.064
-28.	.045	.092	.181	.126	.061
-24.	.058	.200	.183	.155	.108
-20.	.094	.269	.216	.234	.125
-16.	.218	.325	.237	.215	.150
-12.	.305	.441	.356	.237	.150
- 8.	.467	.633	.382	.325	.205
- 5.	.689	.642	.341	.316	.236
0.	.858	.688	.489	.373	.257
4.	1.215	.955	.520	.347	.256
8.	1.353	.954	.570	.319	.286
12.	3.143	1.062	.513	.329	.347
16.	2.866	.972	.459	.362	.337
20.	2.474	.656	.588	.300	.250
24.	1.472	.627	.492	.312	.265
28.	.543	.368	.413	.252	.233
32.	.285	.250	.431	.281	.238
36.	.119	.214	.357	.196	.190
40.	.046	.114	.342	.091	.094
44.	0.000	.087	.246	---	---
48.	---	.052	.104	---	---
52.	---	---	.091	---	---
56.	---	---	---	---	---

THETA = 180 INVERSION BOT

Y (CM)	k-FACTOR				(X = 0.5M)
	Z = 0CM	Z = 5CM	Z = 10CM	Z = 15CM	
0.	1.586	.590	.226	.091	
4.	1.821	.567	.241	.095	
8.	1.888	.674	.221	.064	
12.	.859	1.161	.378	.059	
16.	.484	1.332	.447	0.32	
20.	.249	.967	.484	---	
24.	.103	.891	.488	---	
28.	.040	.593	.264	---	
32.	---	.092	.182	---	
36.	---	.013	.020	---	
40.	---	---	.016	---	
44.	---	---	---	---	
48.	---	---	---	---	

THETA = 0 Inversion Top

Y (CM)	K-FACTOR				(X = 0.5M)
	Z = 0CM	Z = 5CM	Z = 10CM	Z = 15CM	
0.	1.311	.824	1.149	1.250	
4.	.769	.771	.944	1.104	
8.	.667	.472	.579	.782	
12.	.511	.361	.332	.649	
16.	.310	.208	.137	.323	
20.	.105	.094	.045	.190	
24.	---	.042	.000	.102	
28.	---	---	---	.060	
32.	---	---	---	.026	
36.	---	---	---	.009	
40.	---	---	---	---	
44.	---	---	---	---	
48.	---	---	---	---	
52.	---	---	---	---	

THETA = 0 Inversion Mid

Y (CM)	K-FACTOR				(X = 0.5M)
	Z = 0CM	Z = 5CM	Z = 10CM	Z = 15CM	
0.	.934	1.250	1.293	1.076	
4.	1.250	1.104	1.061	.912	
8.	.825	.782	.654	.496	
12.	.707	.649	.458	.286	
16.	.512	.323	.190	.080	
20.	.362	.186	.032	.008	
24.	.283	.102	.012	.029	
28.	---	.060	.000	---	
32.	---	.026	---	---	
36.	---	.009	---	---	
40.	---	---	---	---	
44.	---	---	---	---	
48.	---	---	---	---	

THETA = 0 INVERSION BOT

Y (CM)	K-FACTOR				(X = 0.5M)
	Z = 0CM	Z = 5CM	Z = 10CM	Z = 15CM	
0.	1.419	1.650	.822	.549	
4.	1.534	1.529	.721	.427	
8.	1.402	1.130	.591	.296	
12.	1.125	.994	.545	.215	
16.	.887	.664	.322	.085	
20.	.735	.413	.160	.018	
24.	.542	.226	.042	.012	
28.	.102	.148	---	---	
32.	.031	.127	---	---	
36.	---	.016	---	---	
40.	---	---	---	---	
44.	---	---	---	---	
48.	---	---	---	---	

THETA = 180 INVERSION MID

Y (CM)	K-FACTOR				(X = 0.5M)
	Z = 0CM	Z = 5CM	Z = 10CM	Z = 15CM	
0.	1.312	.935	.451	.203	
4.	1.351	.857	.517	.137	
8.	1.356	.819	.402	.115	
12.	.742	1.116	.462	.118	
16.	.705	.965	.334	.024	
20.	.316	.890	.347	---	
24.	.120	.704	.276	---	
28.	.047	.395	.115	---	
32.	---	.144	.128	---	
36.	---	.038	.046	---	
40.	---	.015	.012	---	
44.	---	---	---	---	
48.	---	---	---	---	
52.	---	---	---	---	

APPENDIX II

FIGURES

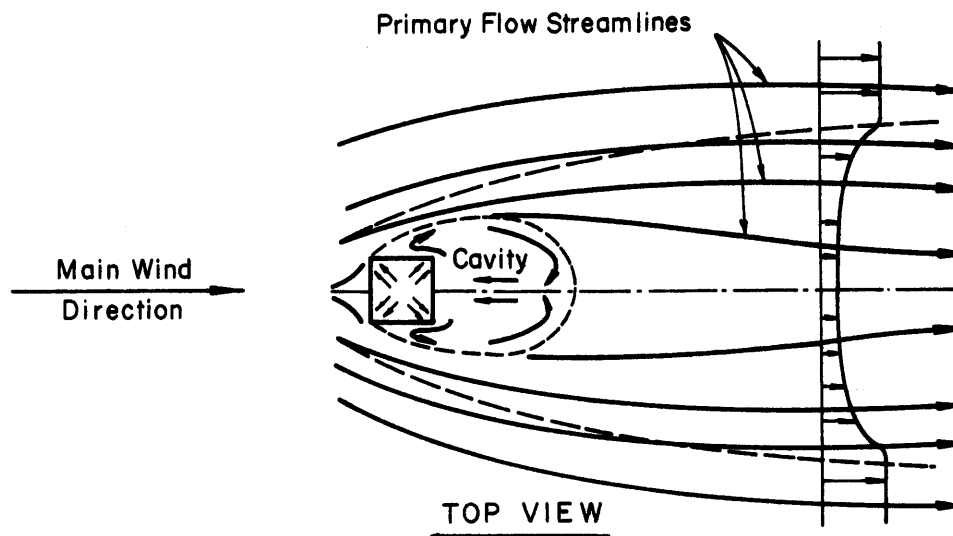
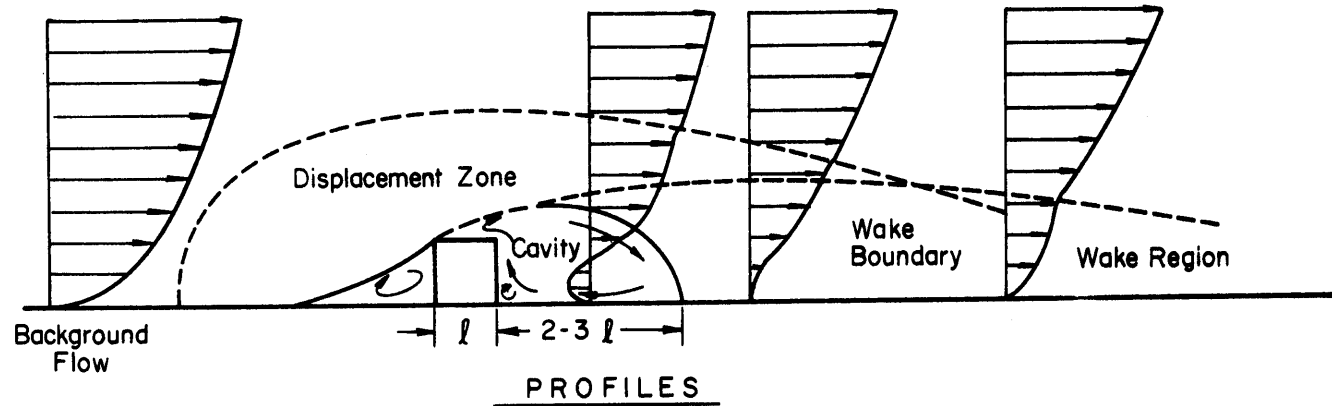


Figure 1 Flow fields about a cube (by Halitsky).

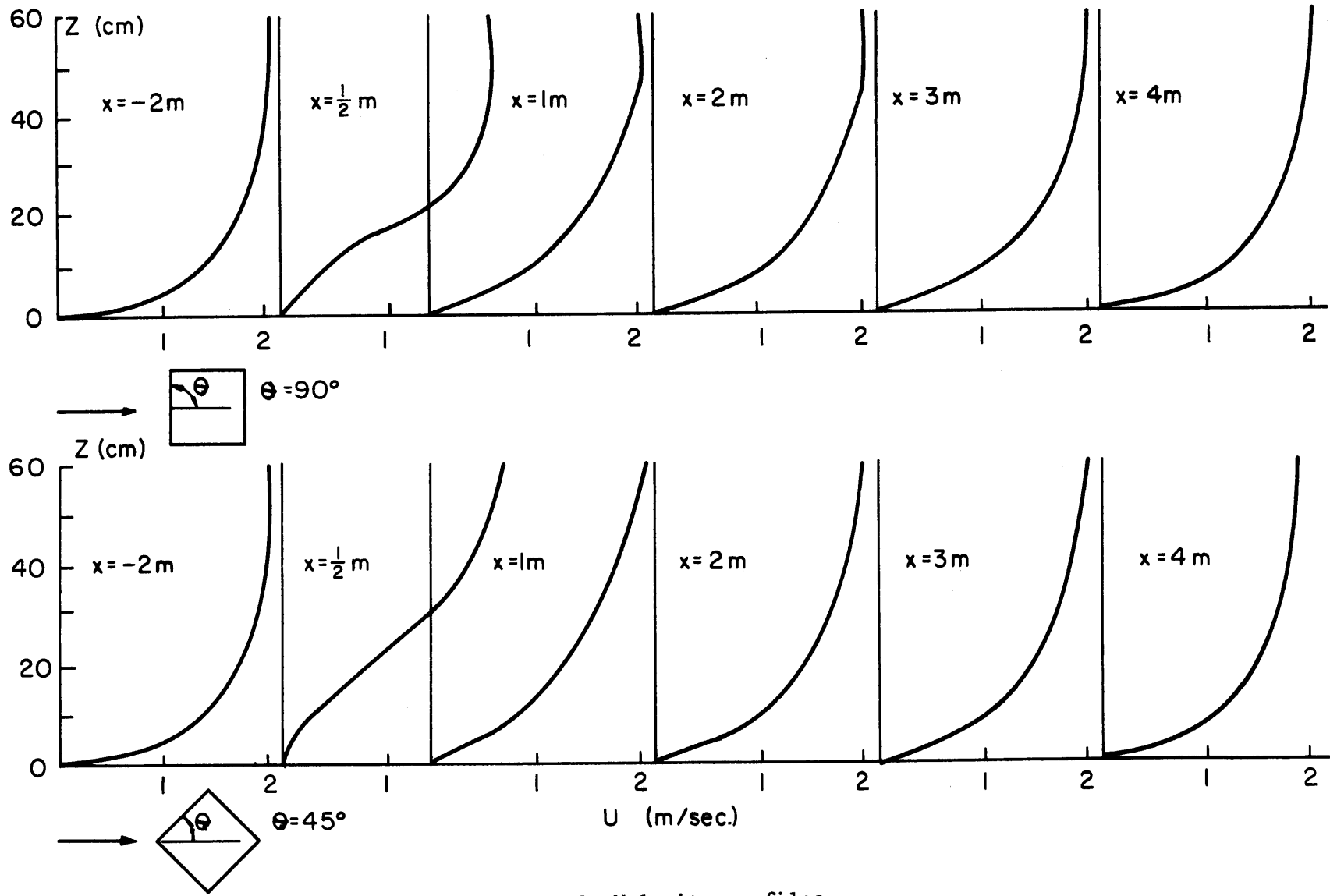


Figure 2 Velocity profiles.

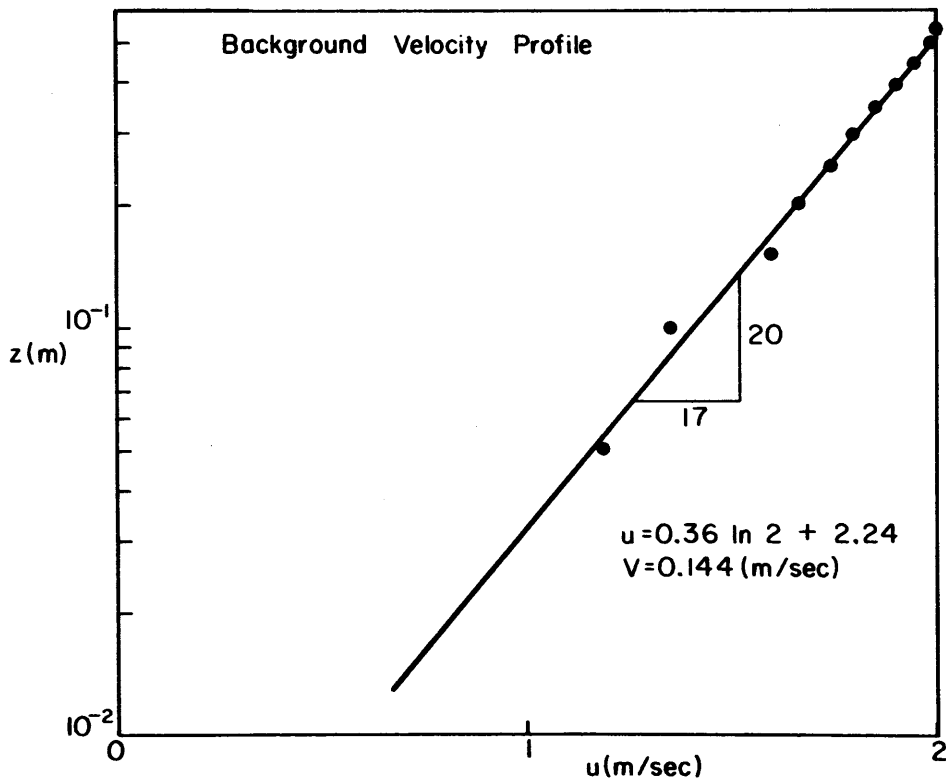
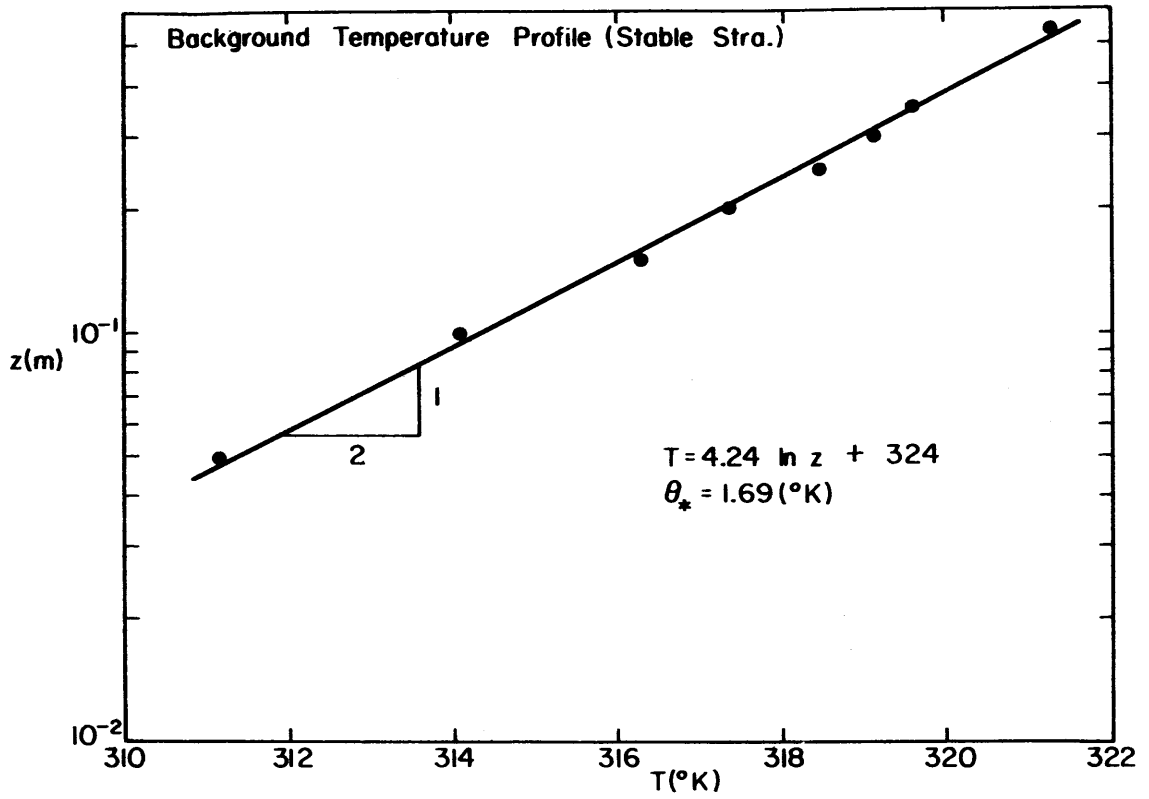


Figure 3. Background temperature and velocity profiles.

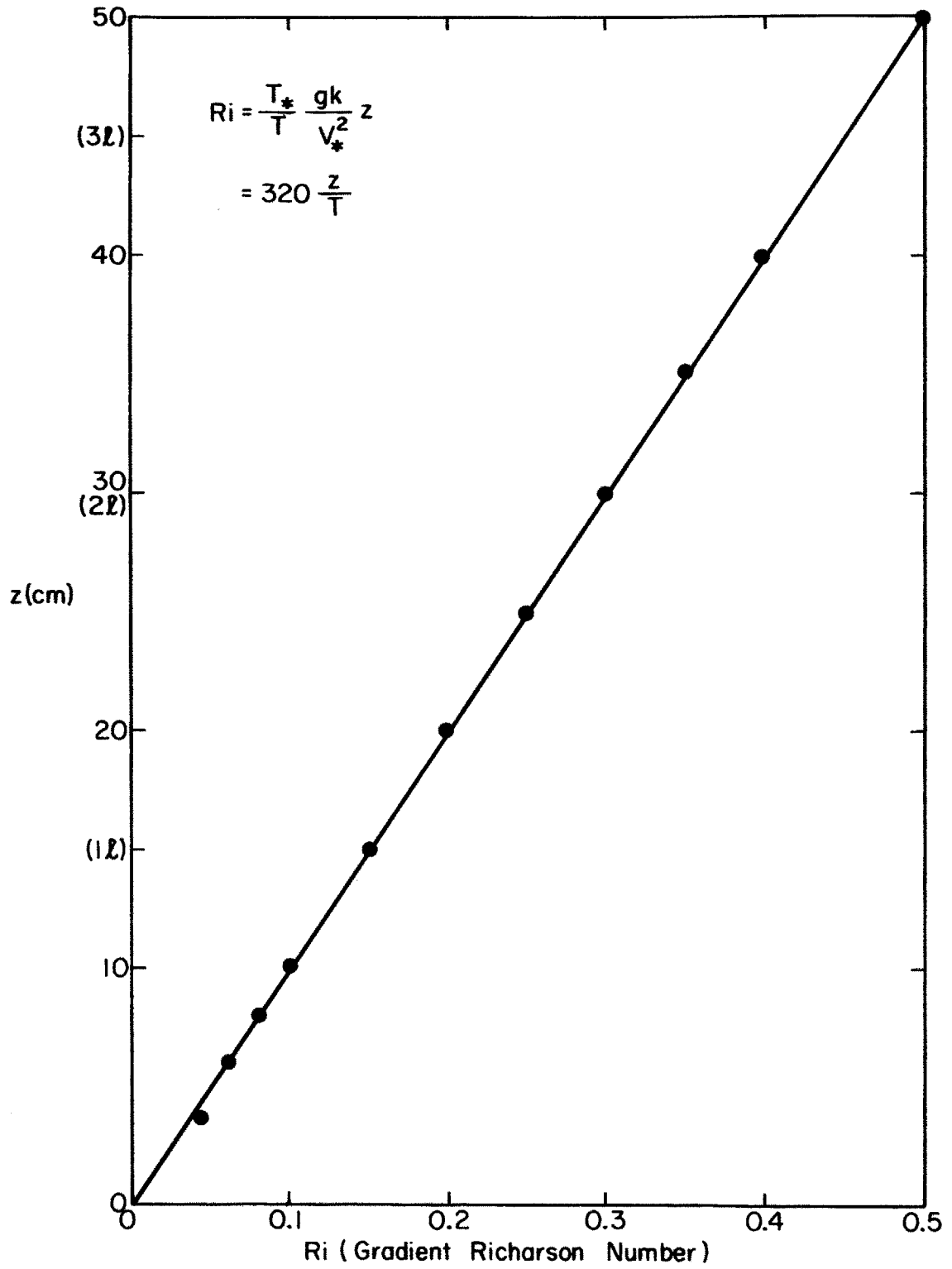


Figure 4 Richardson number profile.

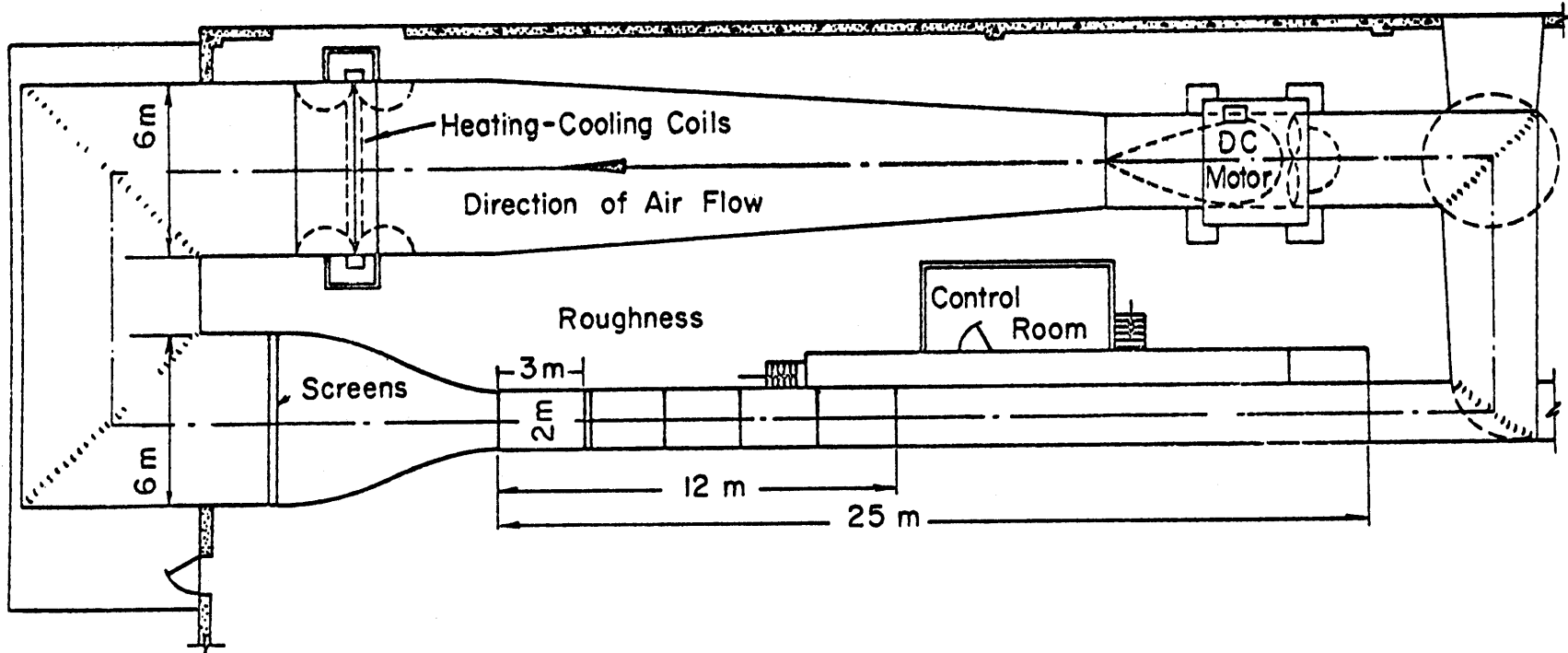


Figure 5 Wind tunnel.

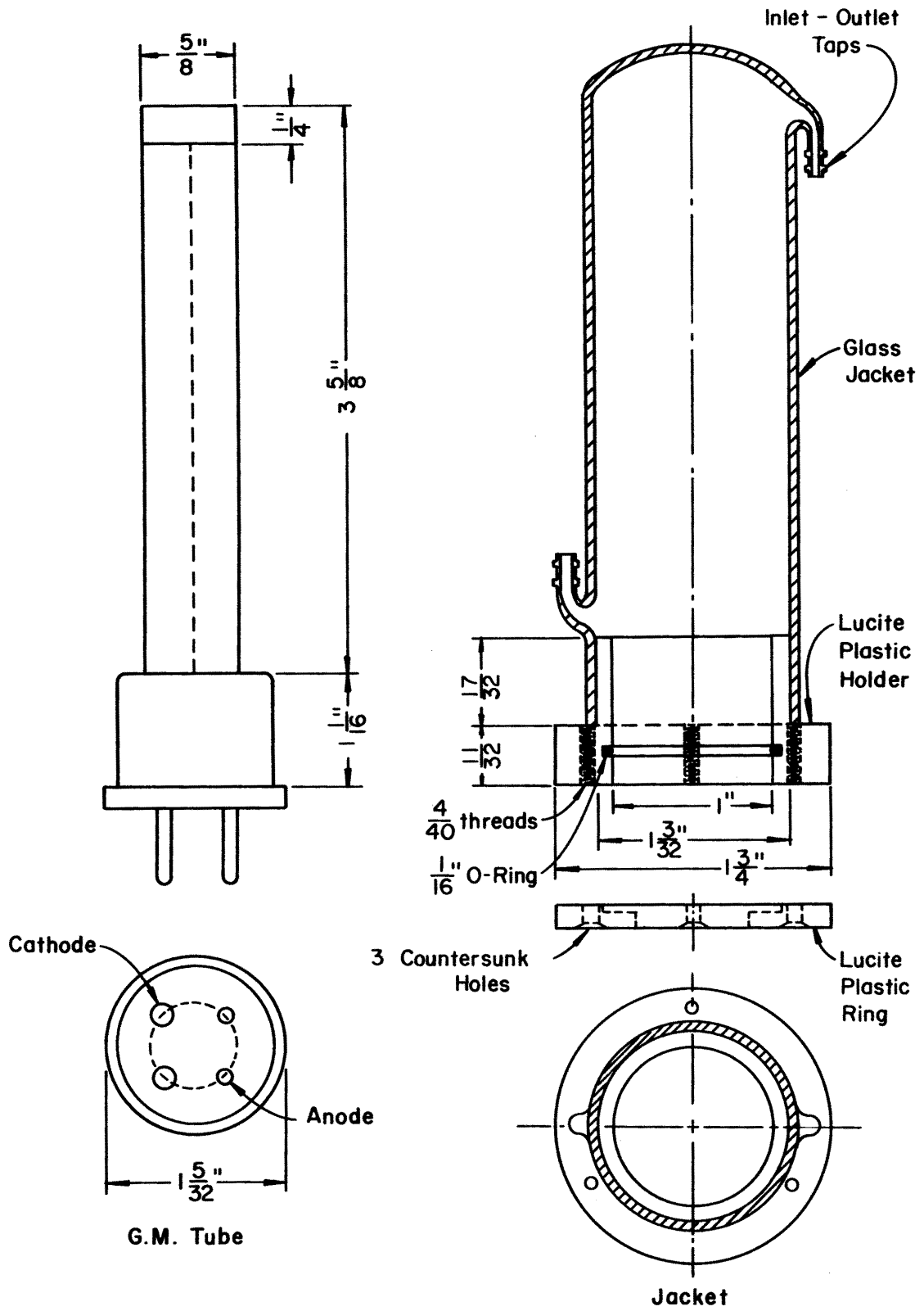


Figure 6 The G-M tube and the glass jacket.

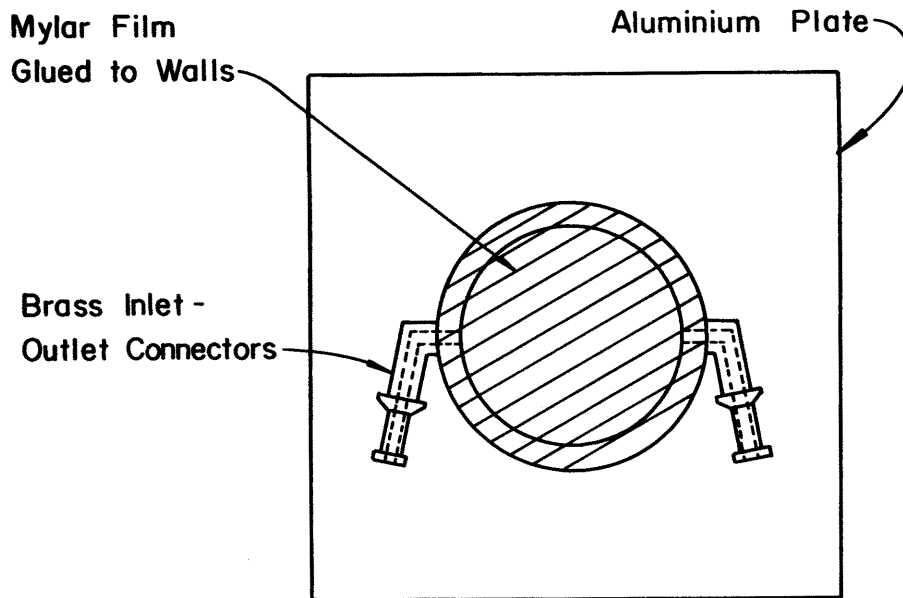
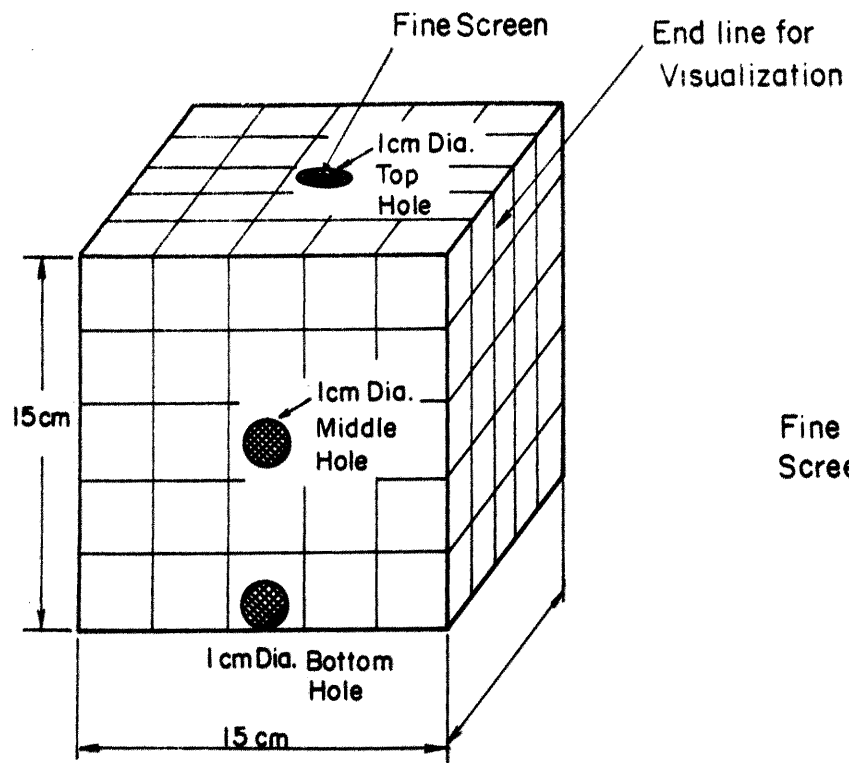


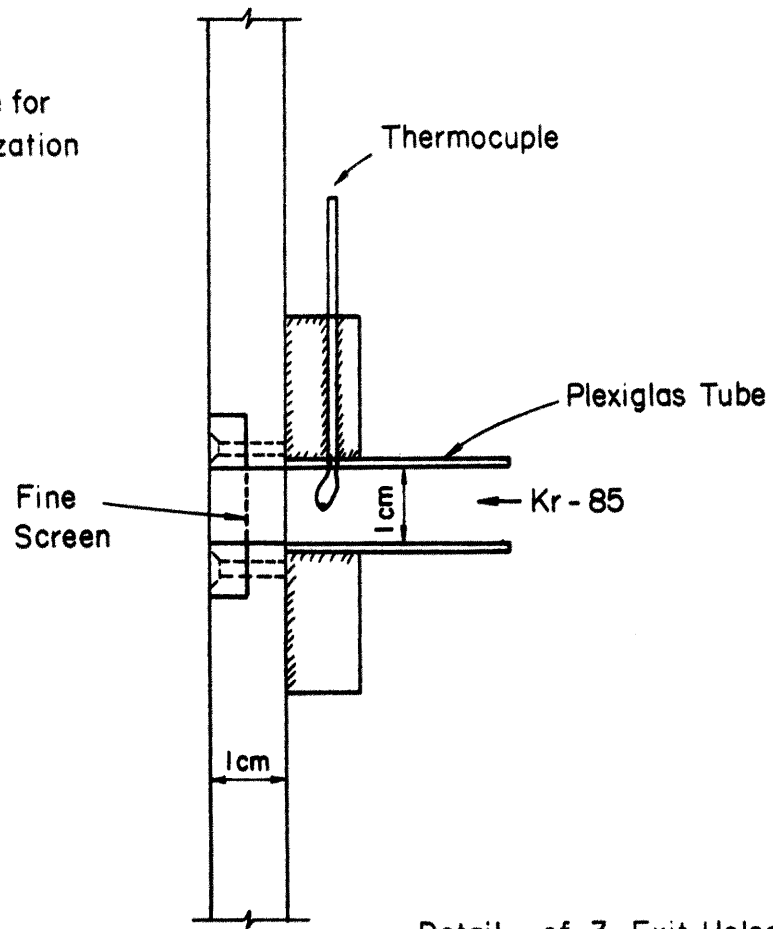
Figure 7 The gas planchet.



Figure 8 Krypton-85 calibration arrangement.



Sketch of the Model



Detail of 3 Exit Holes

Figure 9 Sketch of the model.

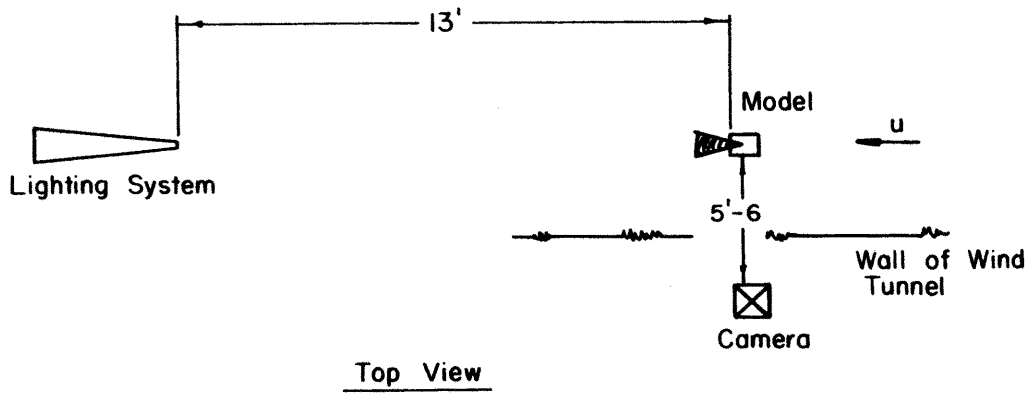
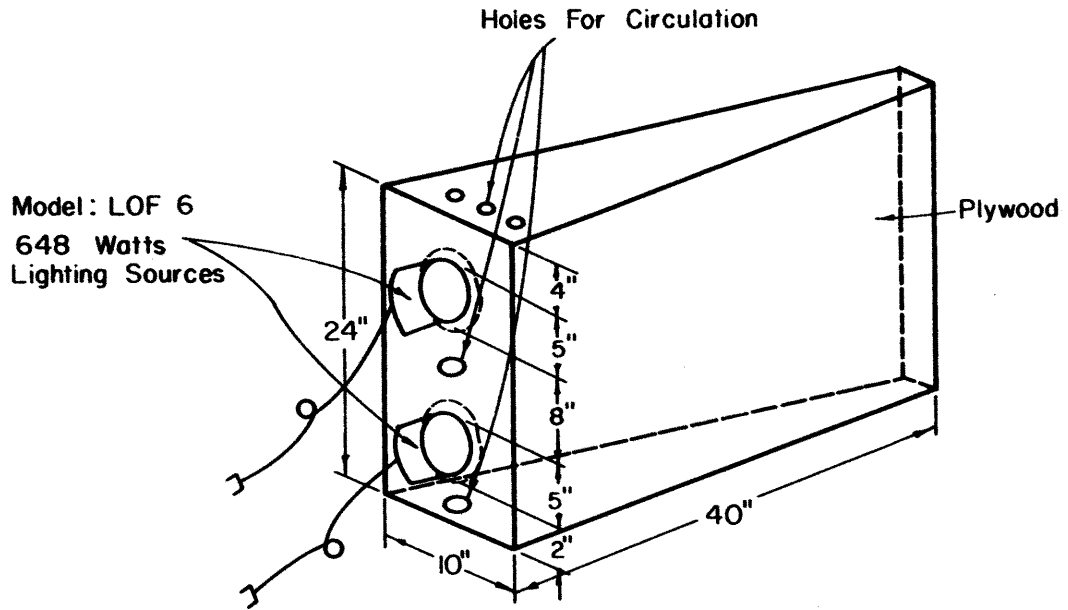


Figure 10 Lighting system.

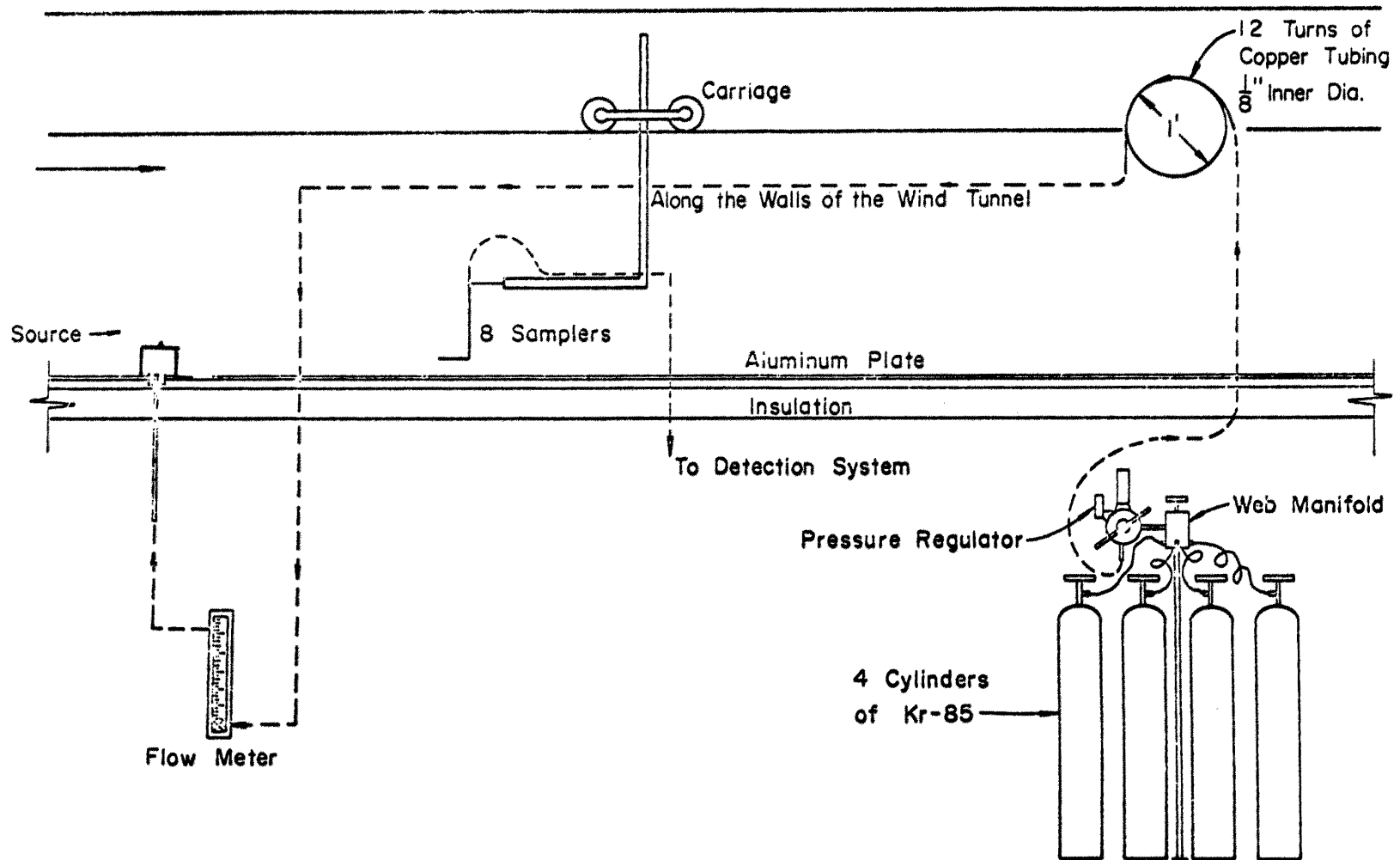


Figure 11 Gas release system.

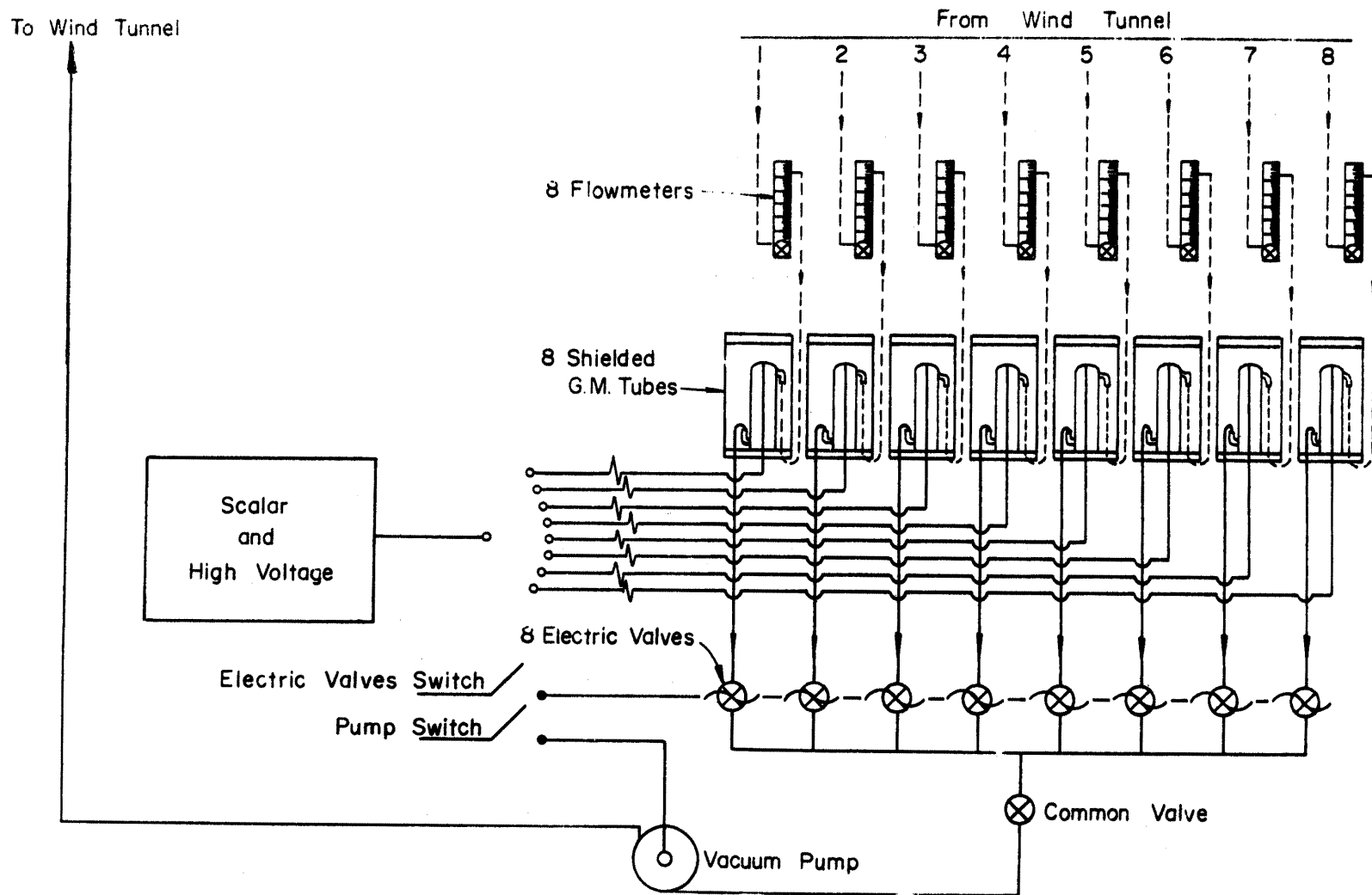


Figure 12 Detection system.

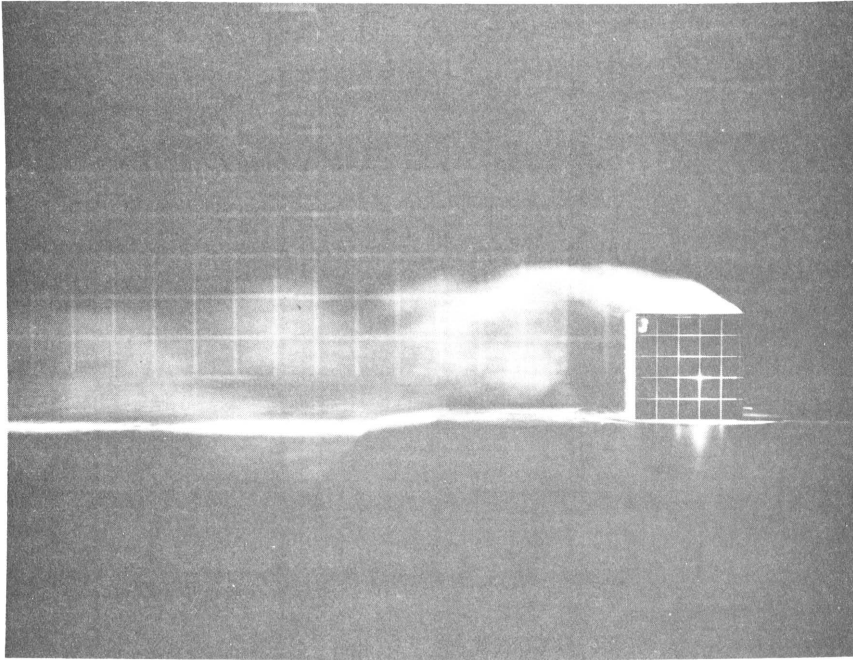


Figure 13  $\theta = 0^\circ, (90^\circ) (180^\circ)$ , top exit port, neutral stratification.

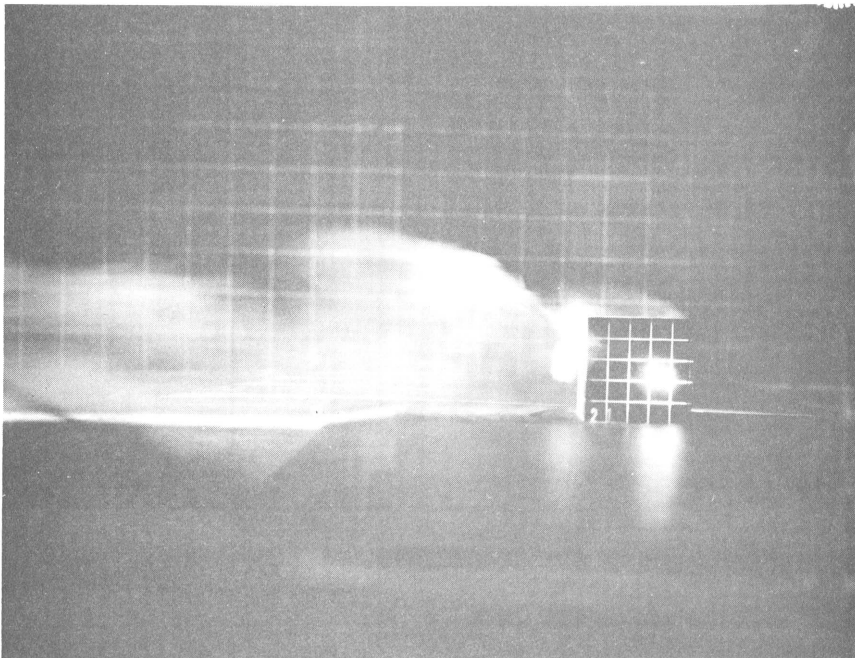


Figure 14  $\theta = 0^\circ$ , middle exit port, neutral stratification.

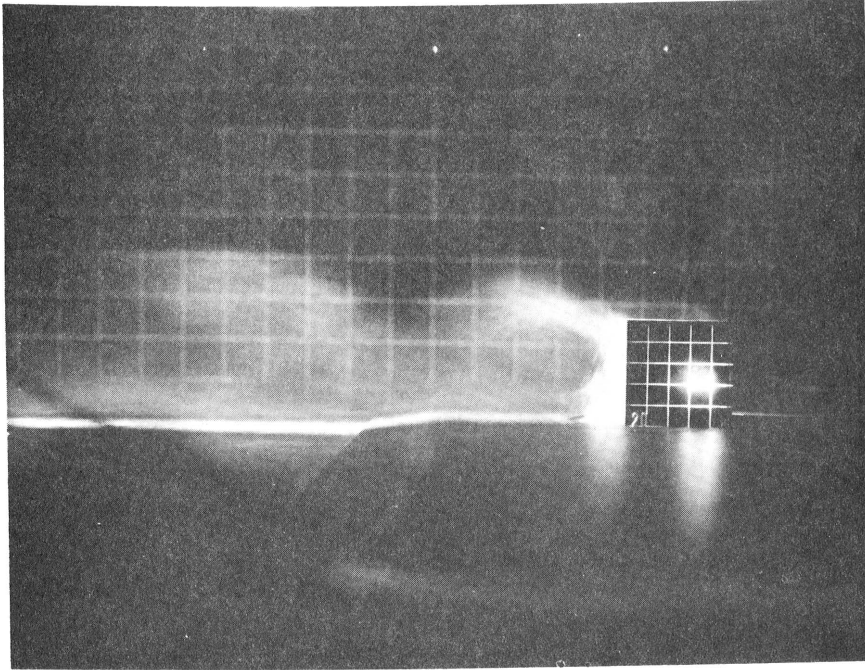


Figure 15  $\theta = 0^\circ$ , bottom exit port, neutral stratification.

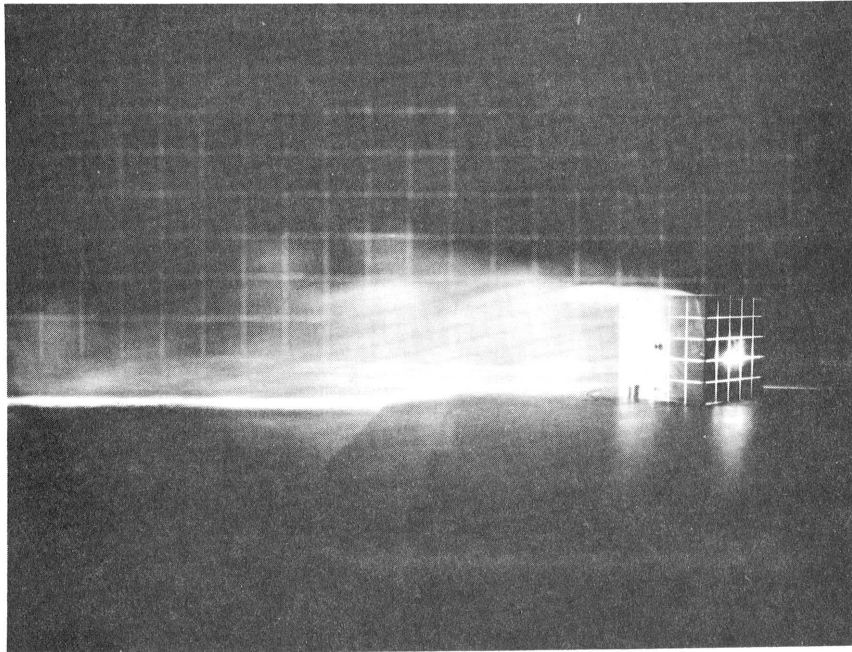


Figure 16  $\theta = 45^\circ$  ( $135^\circ$ ), top exit port neutral stratification.

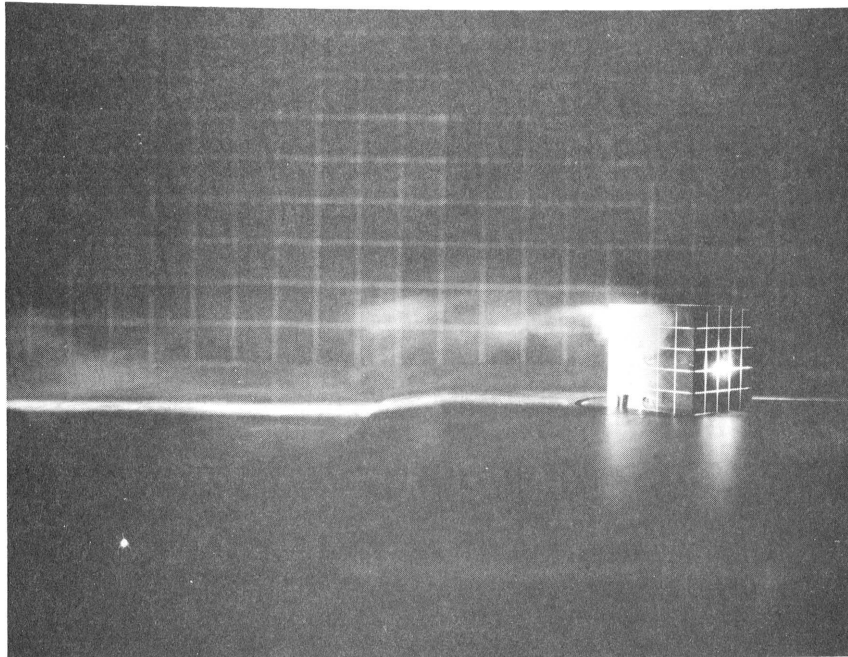


Figure 17  $\theta = 45^\circ$ , Middle exit port, neutral stratification.

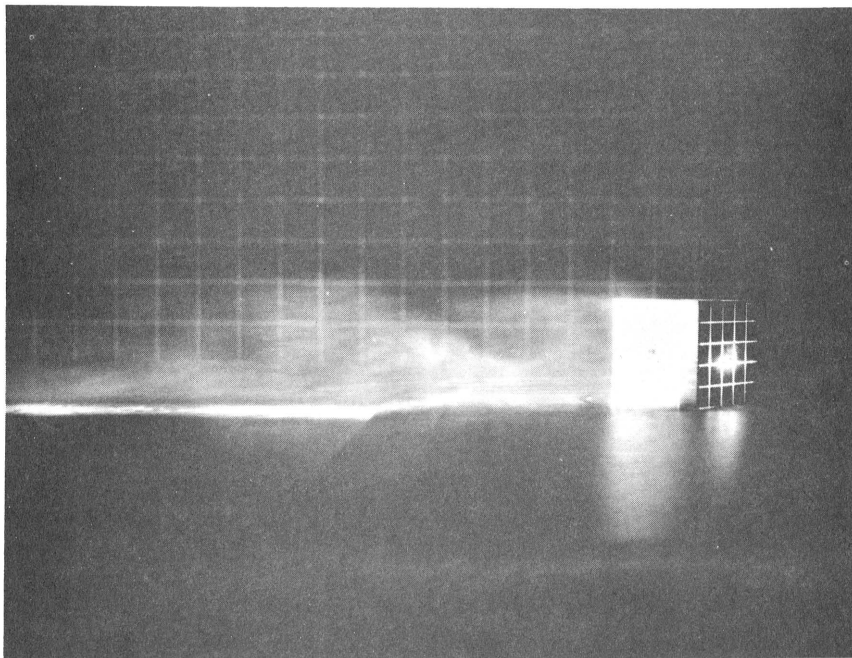


Figure 18  $\theta = 45^\circ$ , bottom exit port, neutral stratification.

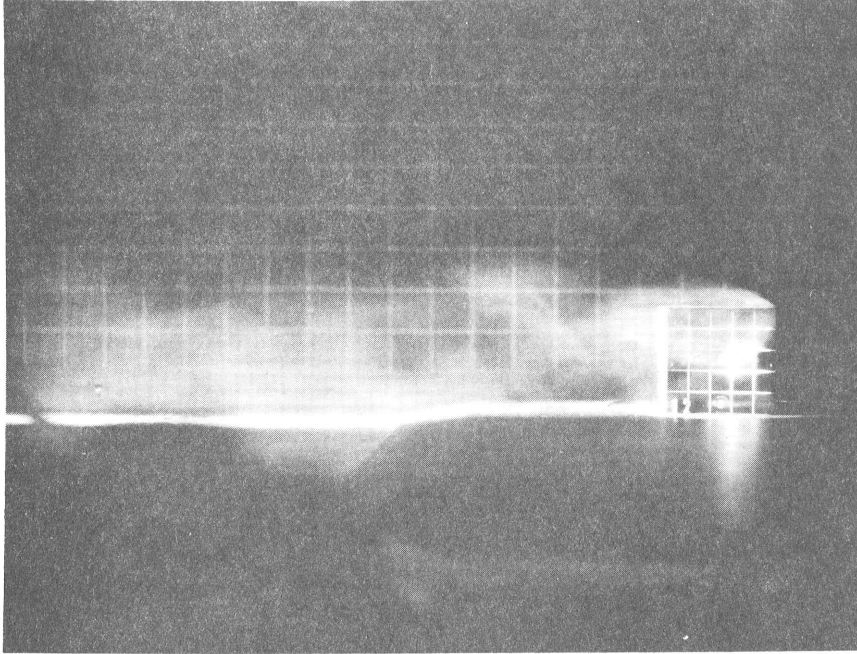


Figure 19  $\theta = 90^\circ$ , middle exit port, neutral stratification.

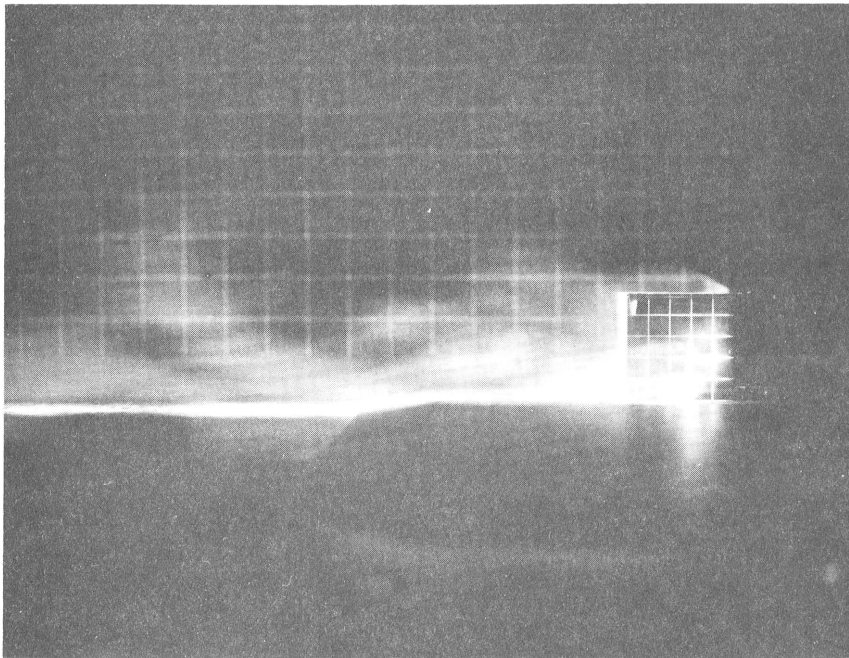


Figure 20  $\theta = 90^\circ$ , bottom exit port, neutral stratification.

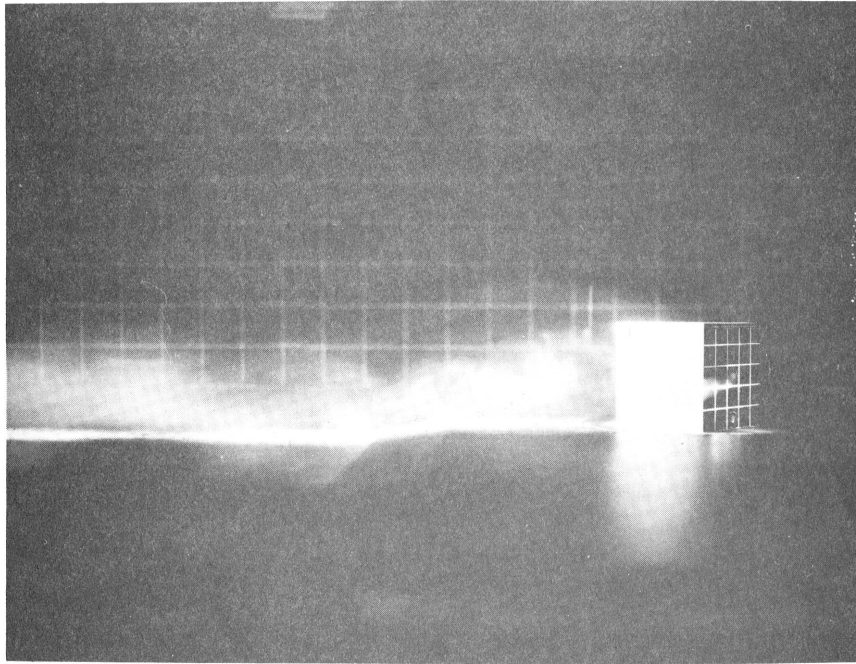


Figure 21  $\theta = 135^{\circ}$ , middle exit port, neutral stratification.

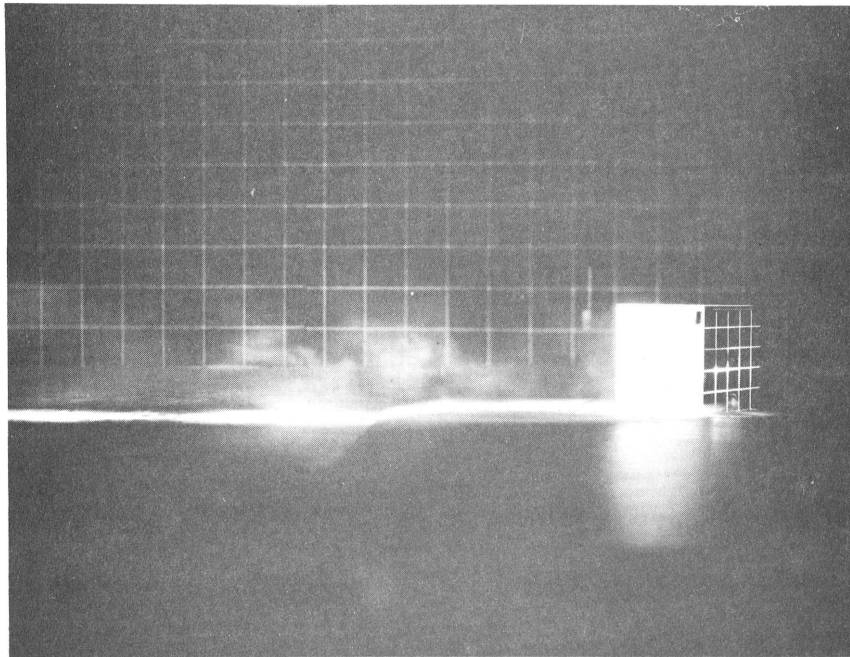


Figure 22  $\theta = 135^{\circ}$ , bottom exit port, neutral stratification.

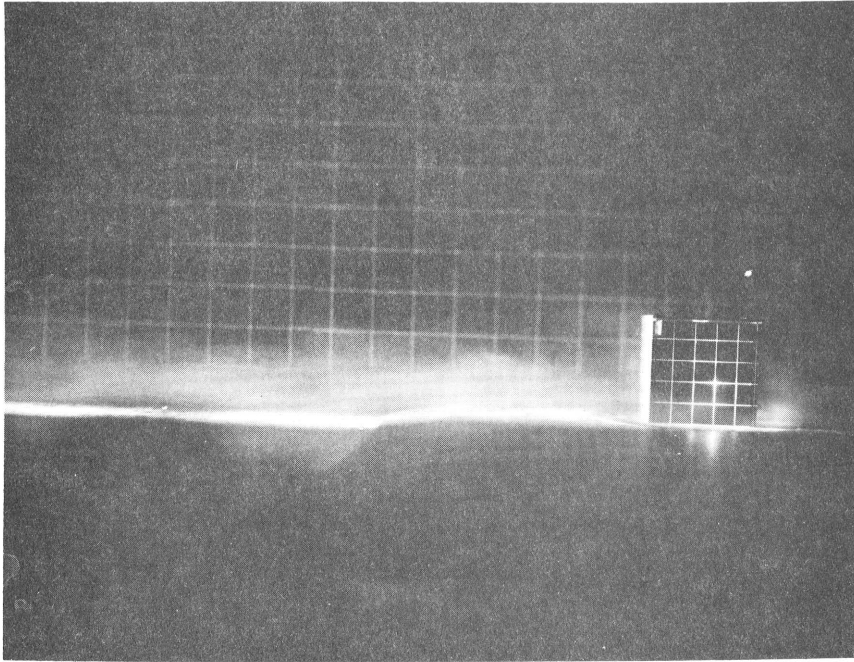


Figure 23  $\theta = 180^\circ$ , middle exit port, neutral stratification.

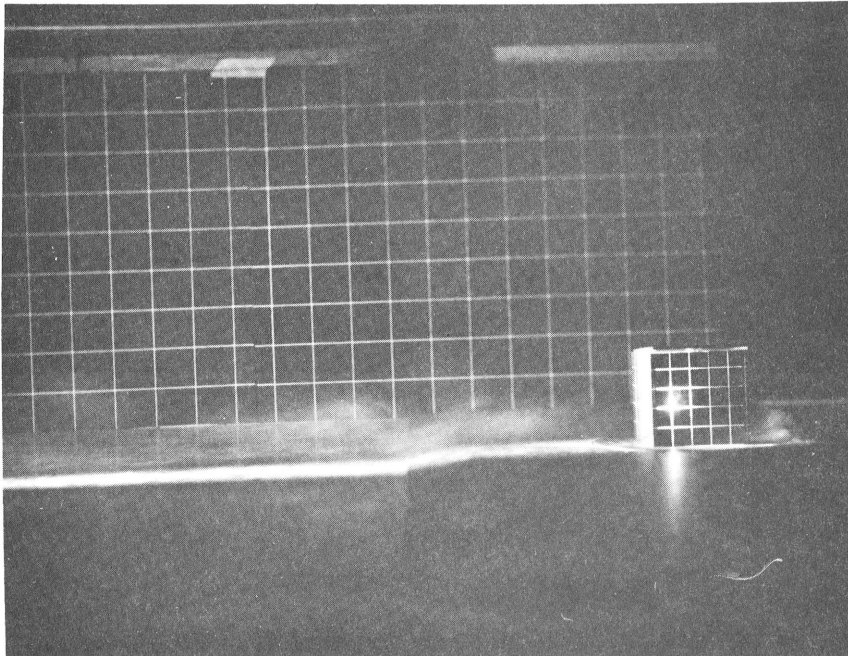


Figure 24  $\theta = 180^\circ$ , bottom exit port, neutral stratification.

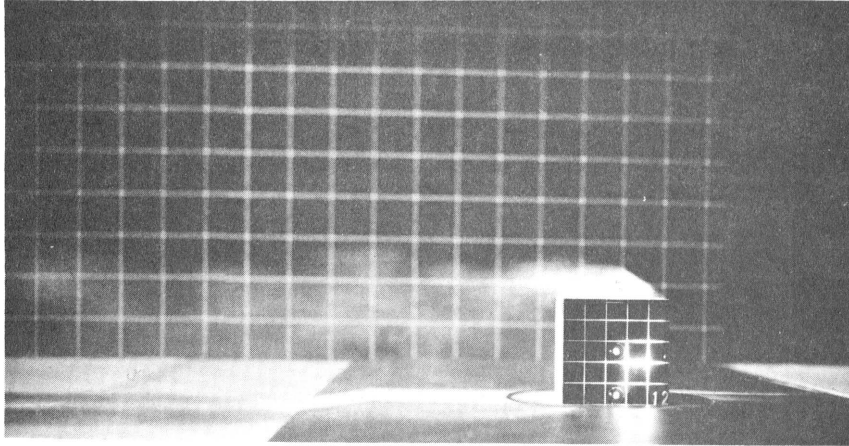


Figure 25  $\theta = 0^\circ, (90^\circ) (180^\circ)$ , top exit port, inversion stratification.

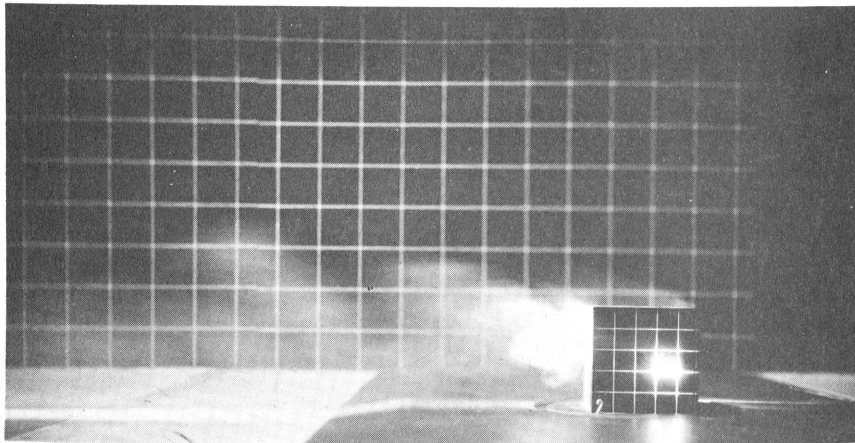


Figure 26  $\theta = 0^\circ$ , middle exit port, inversion stratification.

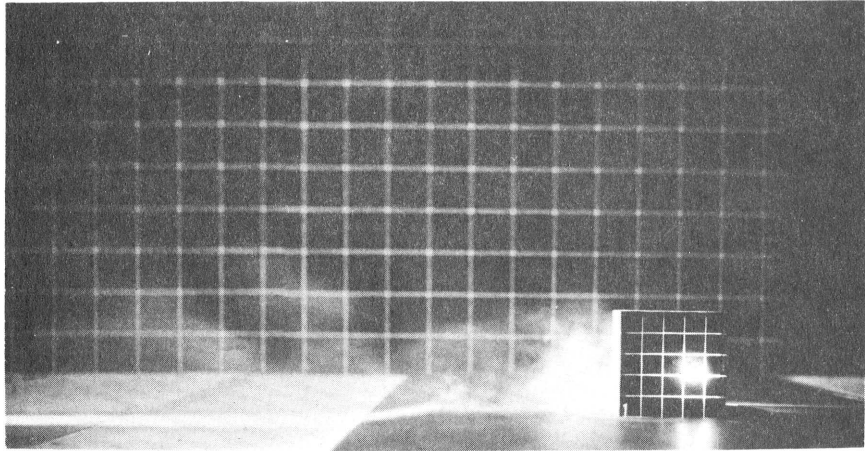


Figure 27  $\theta = 0^\circ$ , bottom exit port, inversion stratification.

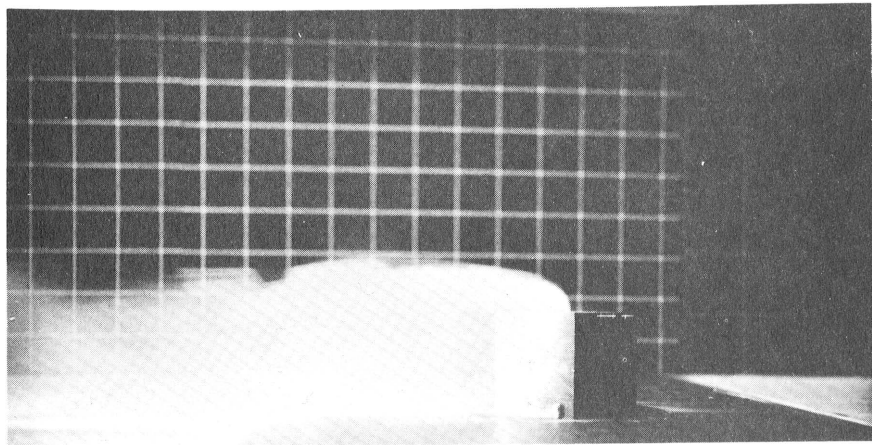


Figure 28  $\theta = 45^\circ$  ( $135^\circ$ ) top exit port, inversion stratification.

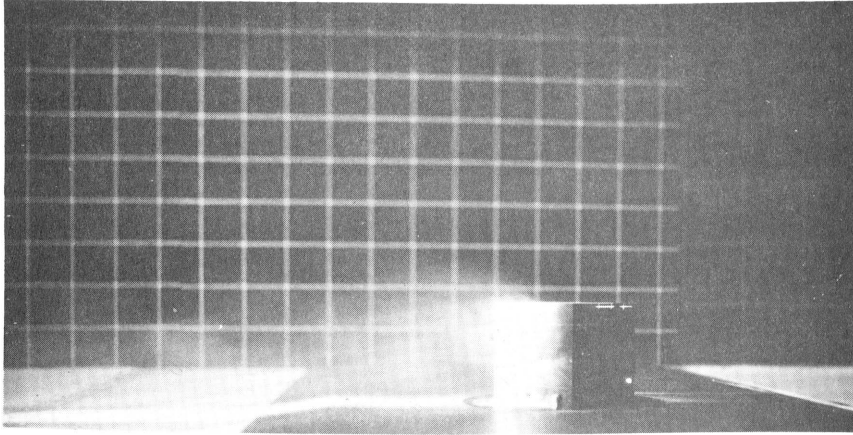


Figure 29  $\theta = 45^\circ$ , middle exit port, inversion stratification.

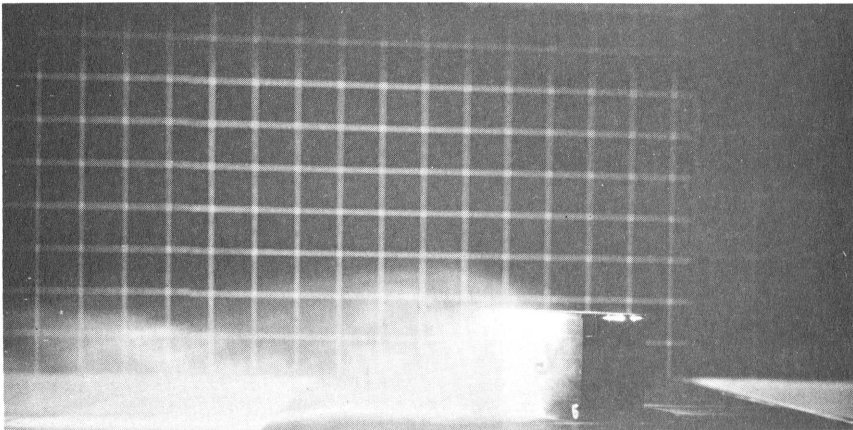


Figure 30  $\theta = 45^\circ$ , bottom exit port, inversion stratification.

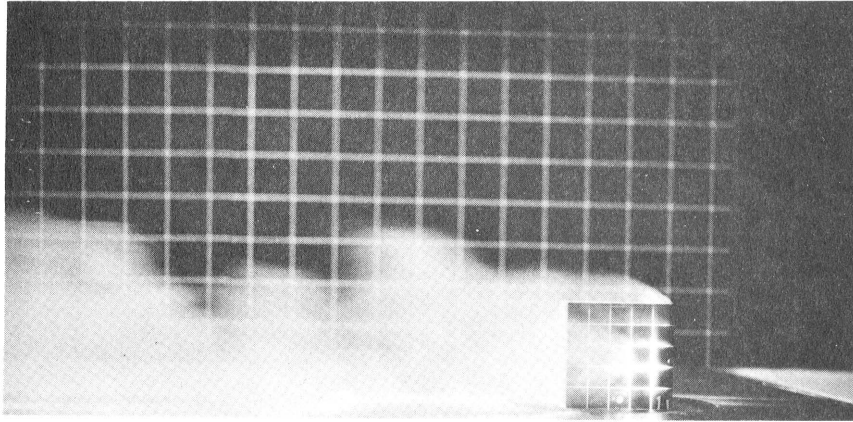


Figure 31  $\theta = 90^\circ$ , middle exit port, inversion stratification.

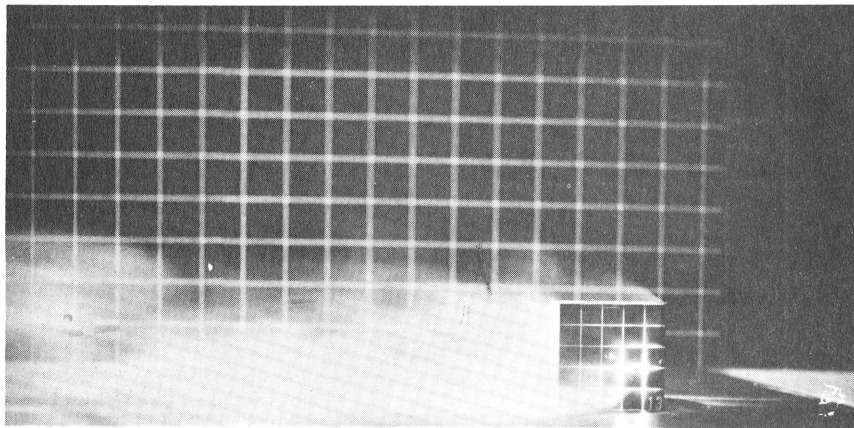


Figure 32  $\theta = 90^\circ$ , bottom exit port, inversion stratification.

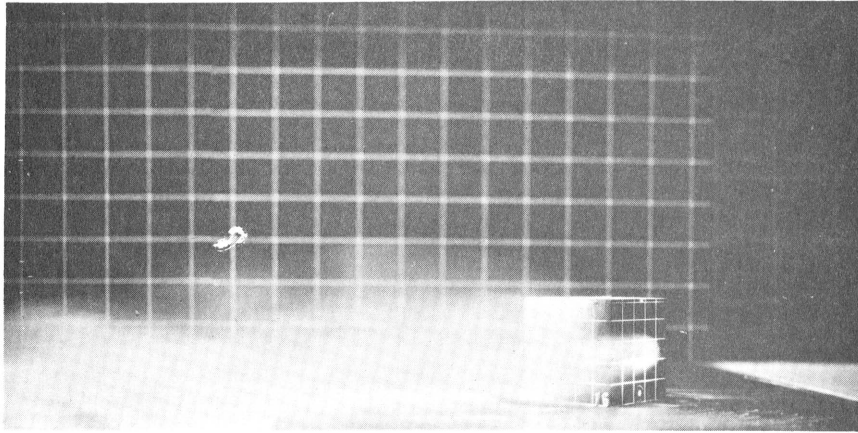


Figure 33  $\theta = 135^\circ$ , middle exit port, inversion stratification.

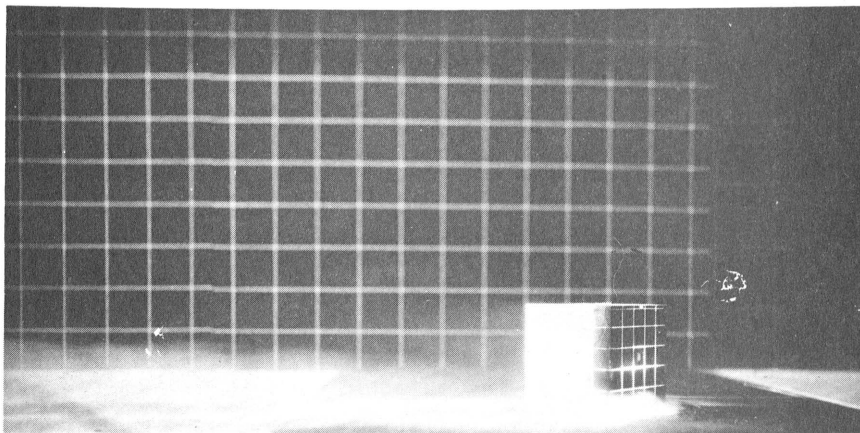


Figure 34  $\theta = 135^\circ$ , bottom exit port, inversion stratification.

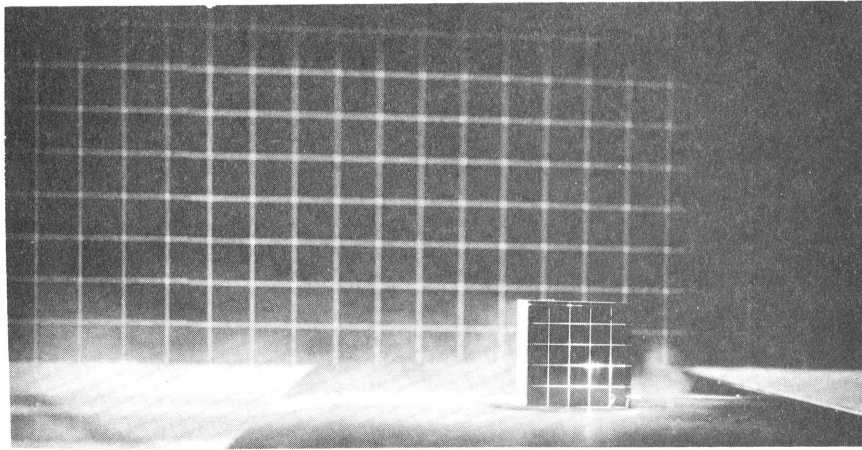


Figure 35  $\theta = 180^\circ$ , middle exit port, inversion stratification.

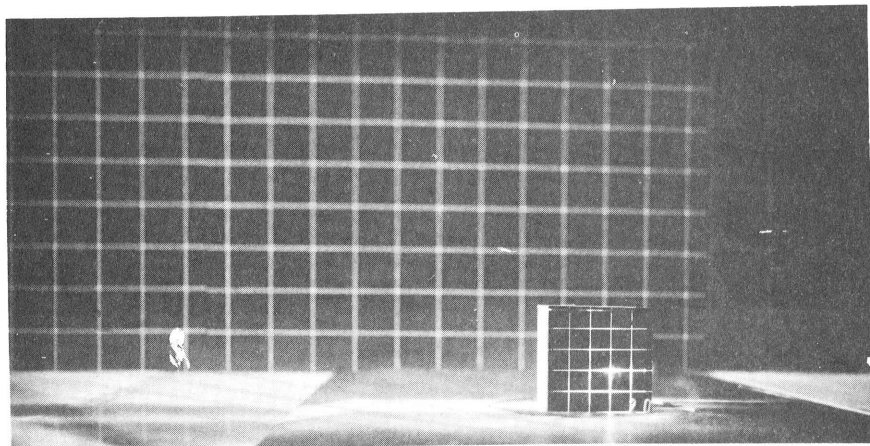


Figure 36  $\theta = 180^\circ$ , bottom exit port, inversion stratification.

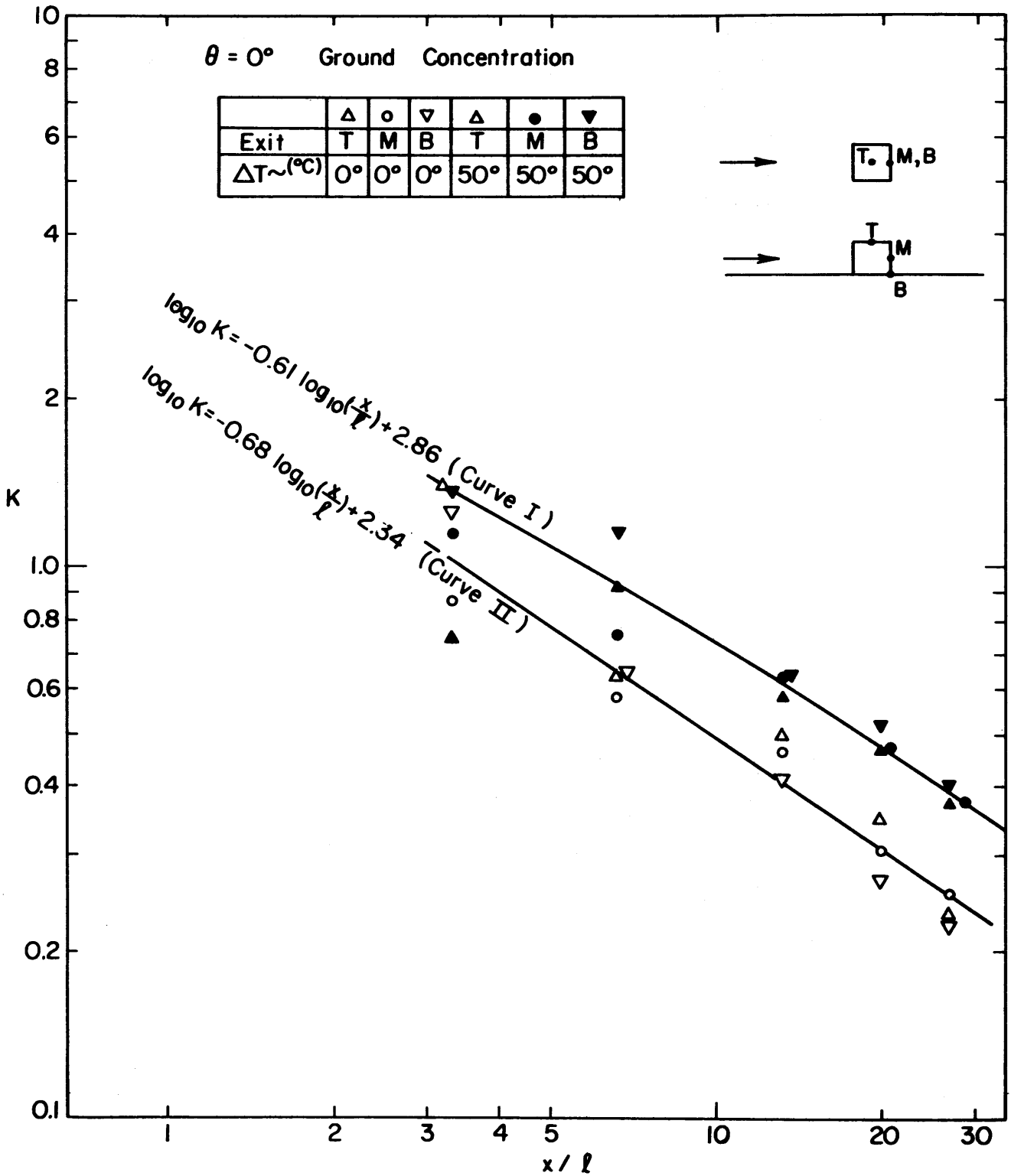


Figure 37 Ground concentration  $\theta = 0^\circ$ .

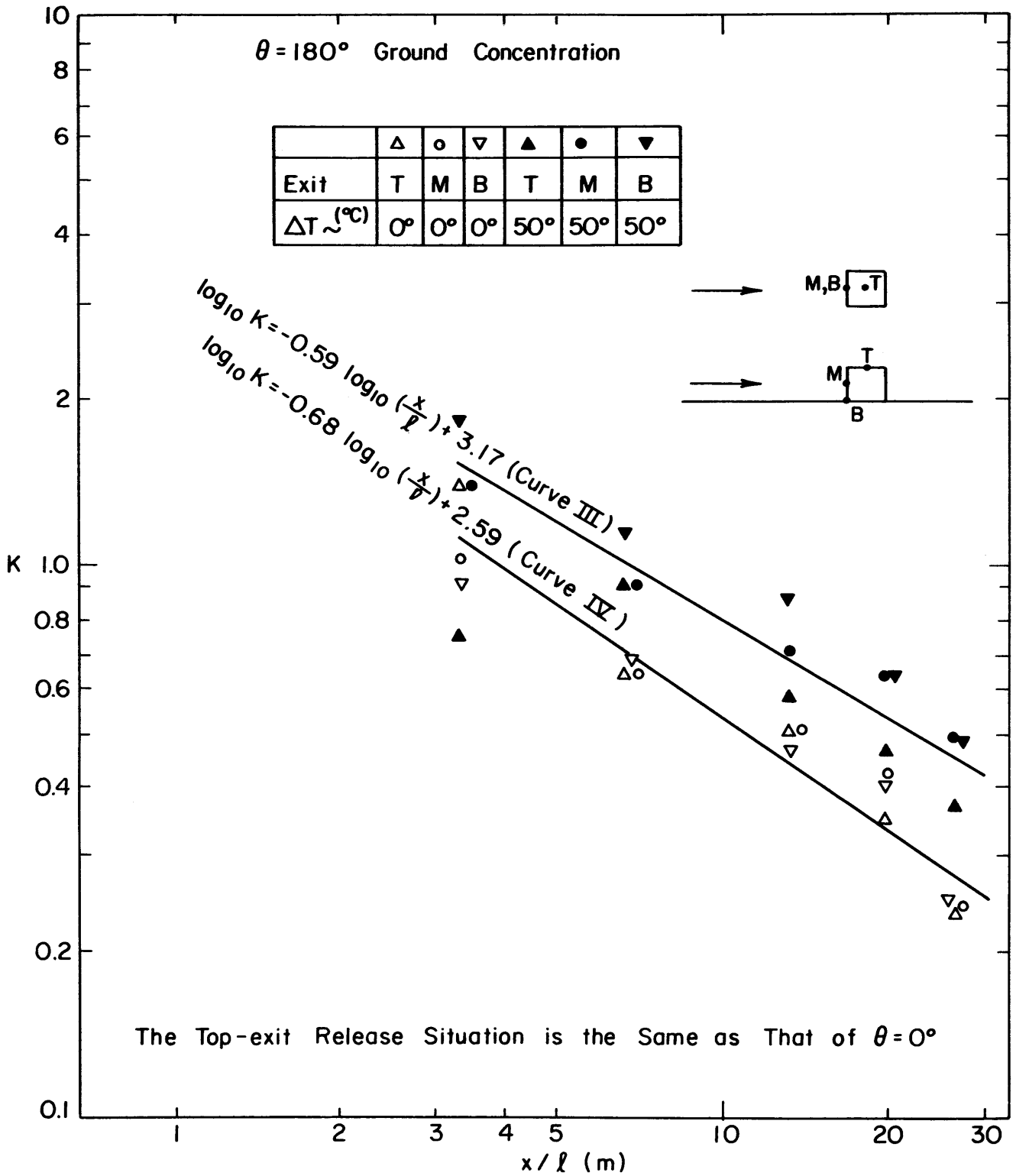


Figure 38 Ground concentration  $\theta = 180^\circ$ .

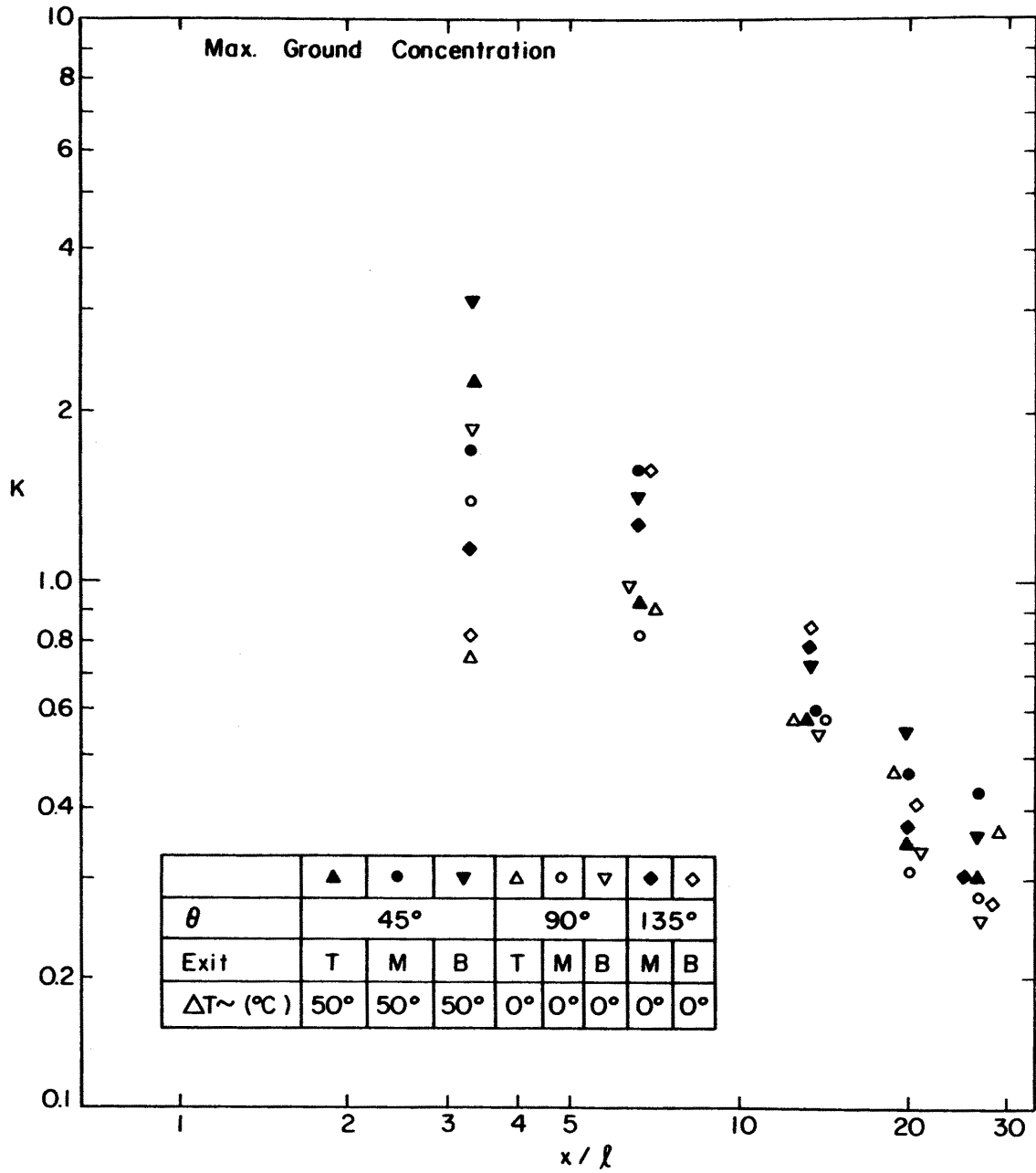


Figure 39 Ground concentration  $\theta = 45^{\circ}, 90^{\circ}, 135^{\circ}$ .

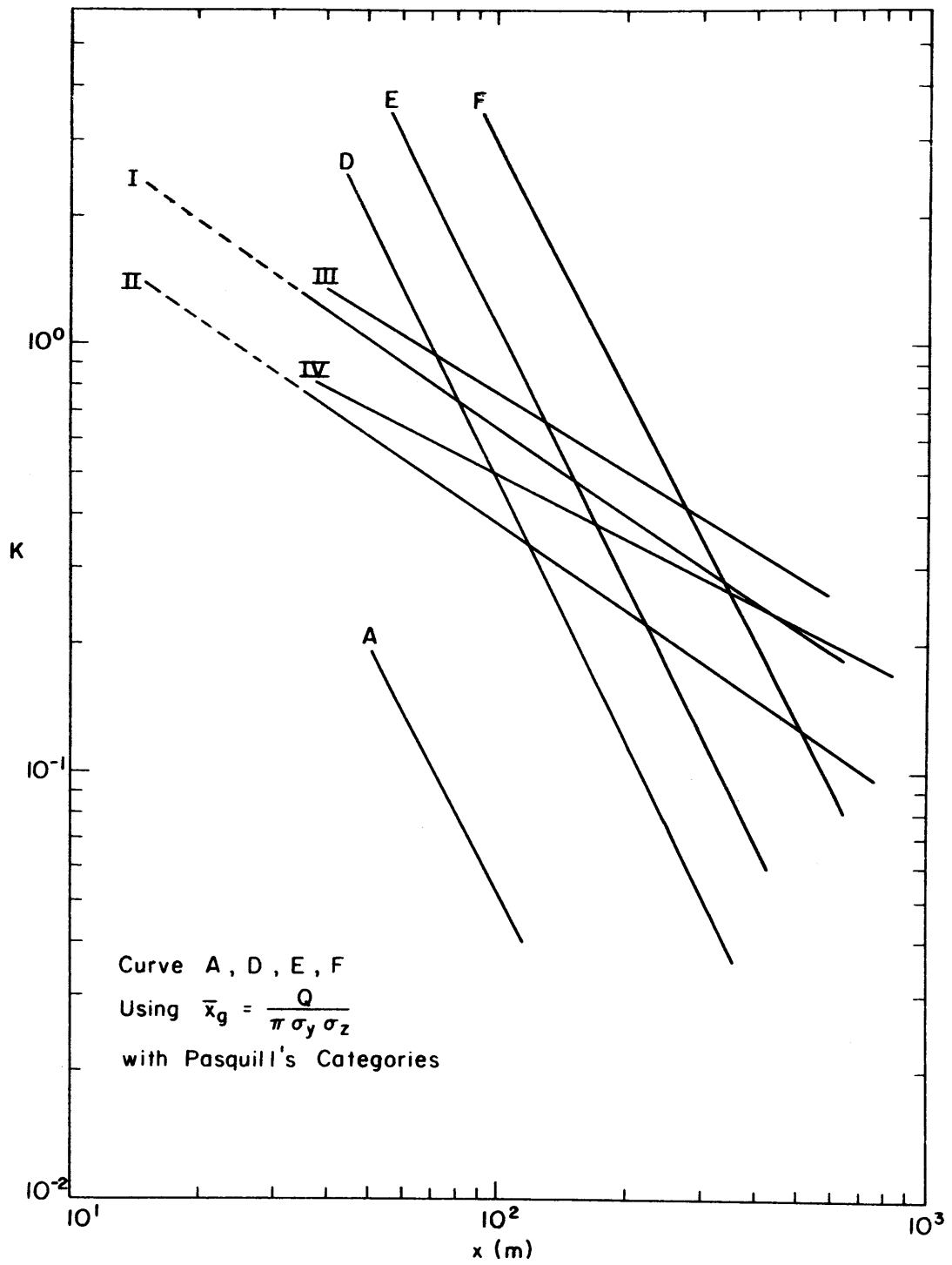


Figure 40 Comparison of ground concentration with Pasquill's categories.

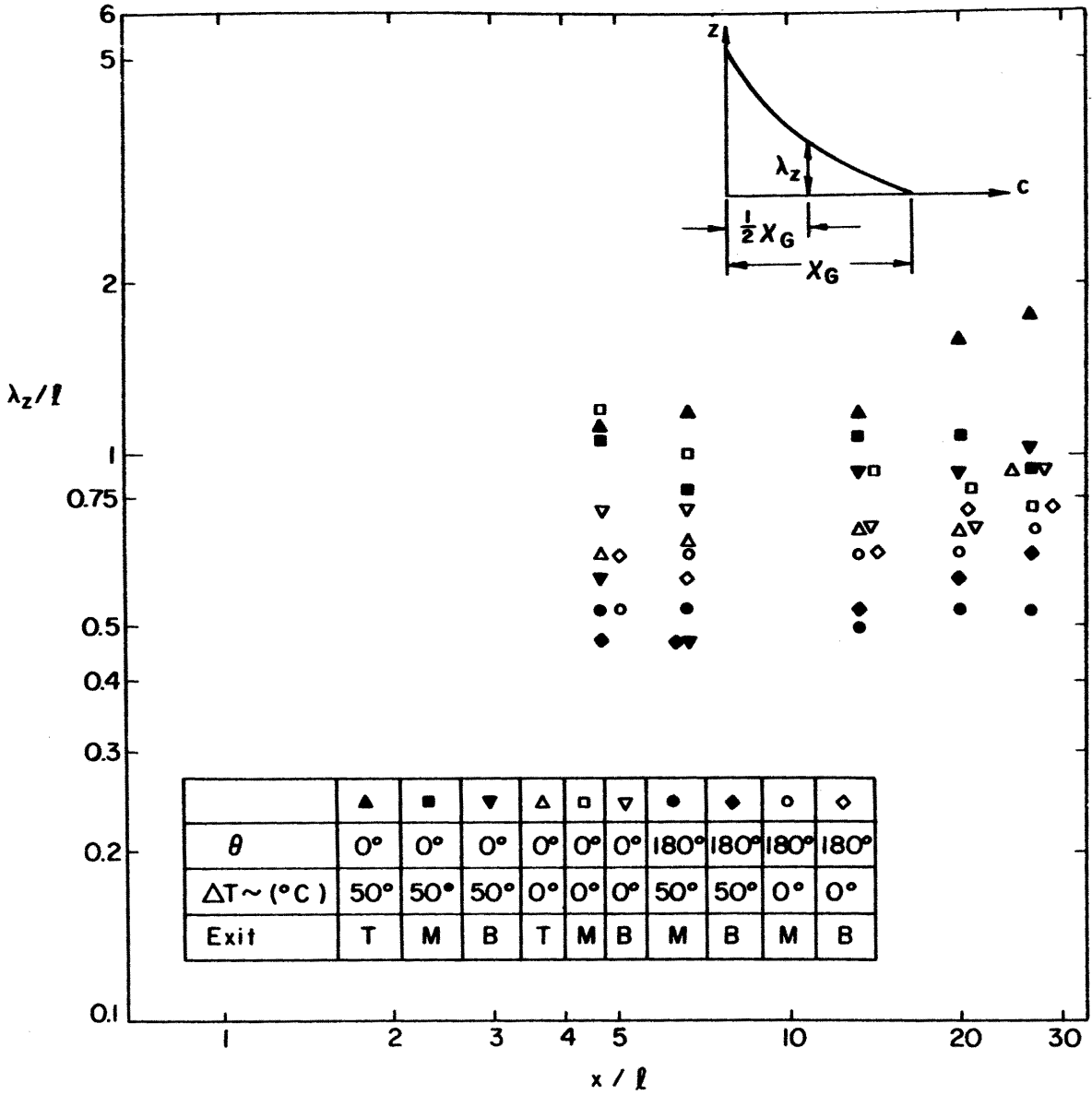


Figure 41 Characteristic plume height  $\lambda_z$ .

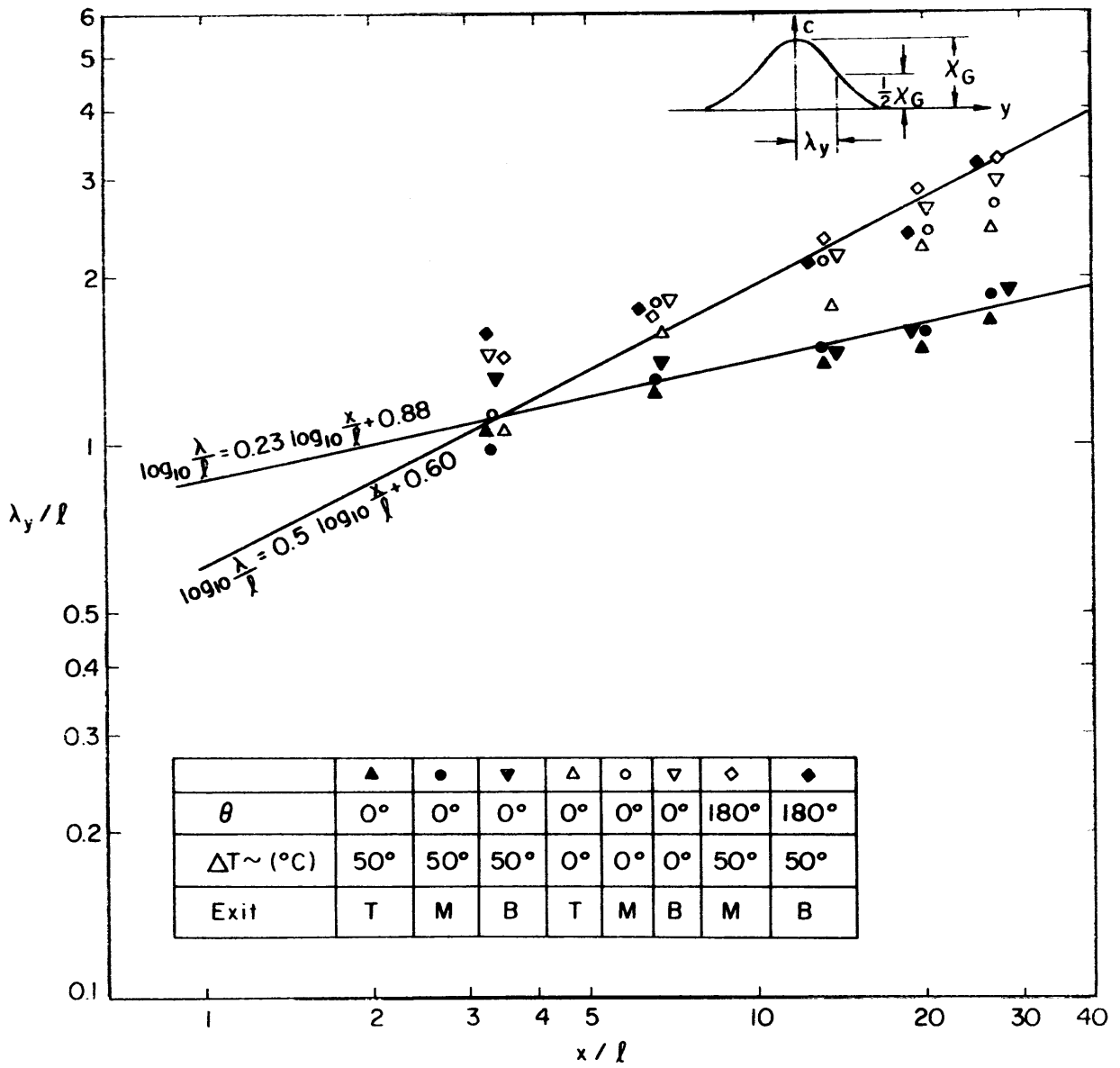


Figure 42 Characteristic plume width  $\lambda_y$ .

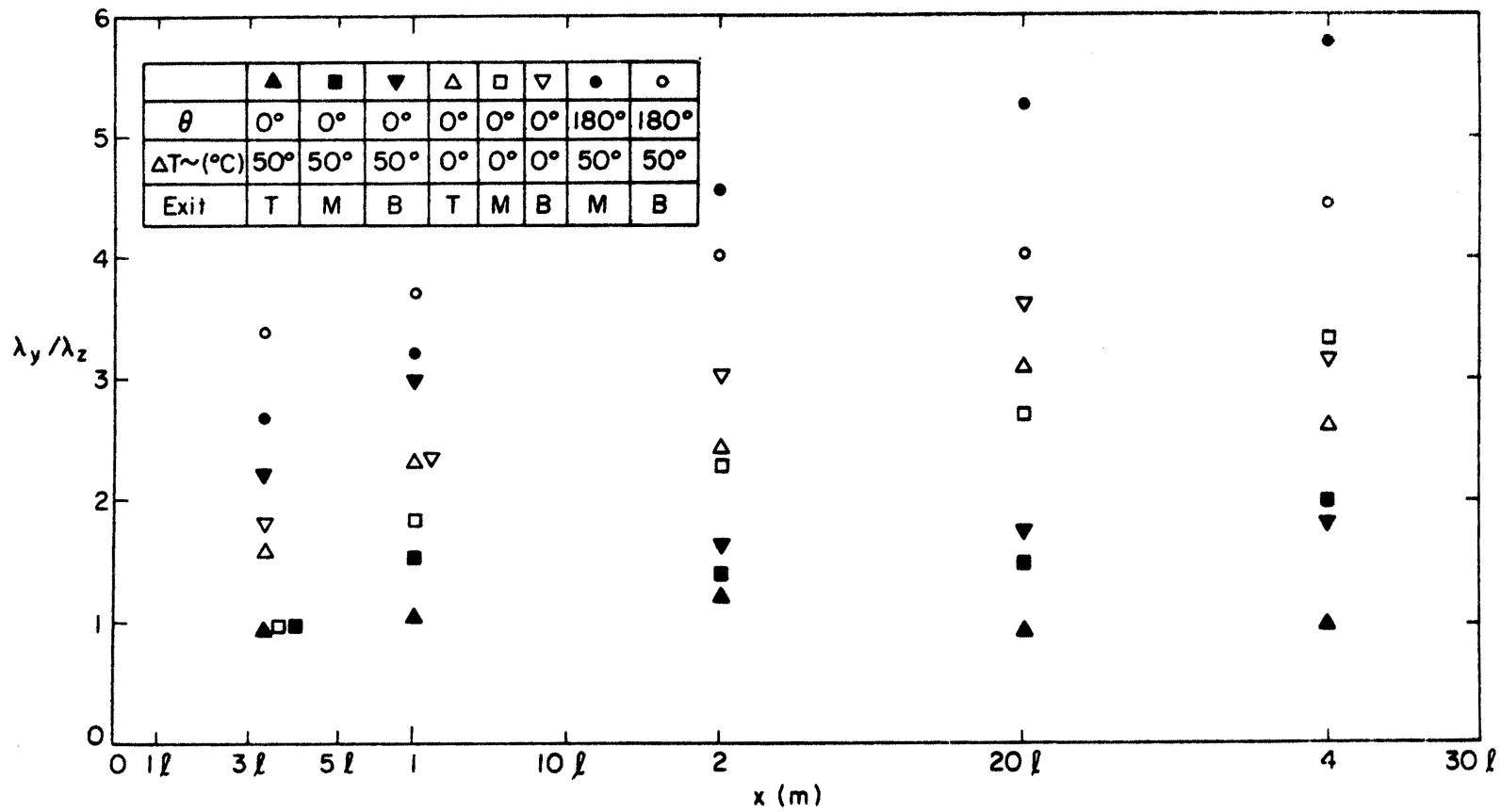


Figure 43  $\lambda_y/\lambda_z$  .

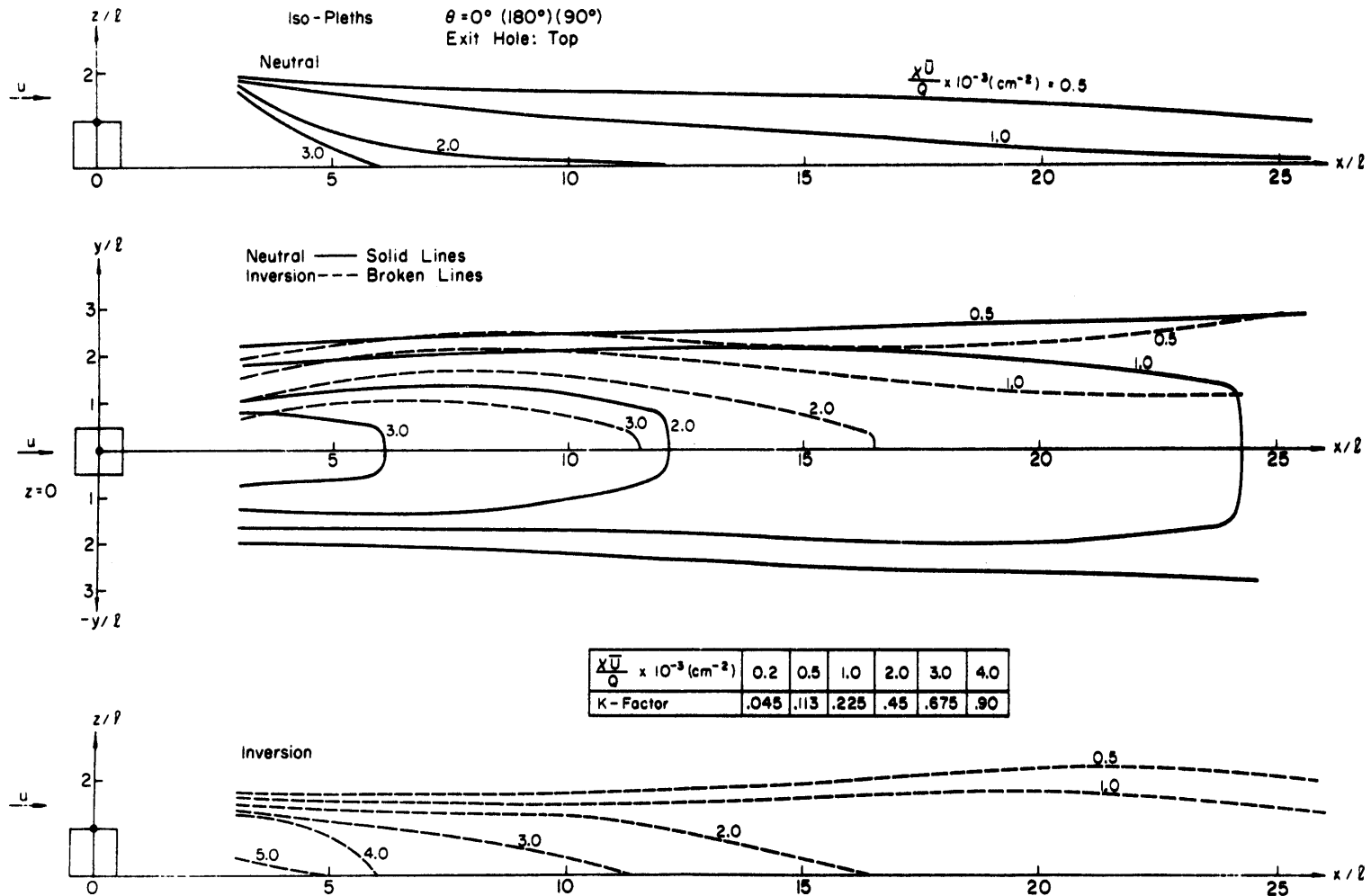


Figure 44 Iso-pleths (a) for  $\theta = 0^\circ, (180^\circ) (90^\circ)$ , top exit port neutral and inversion stratification.

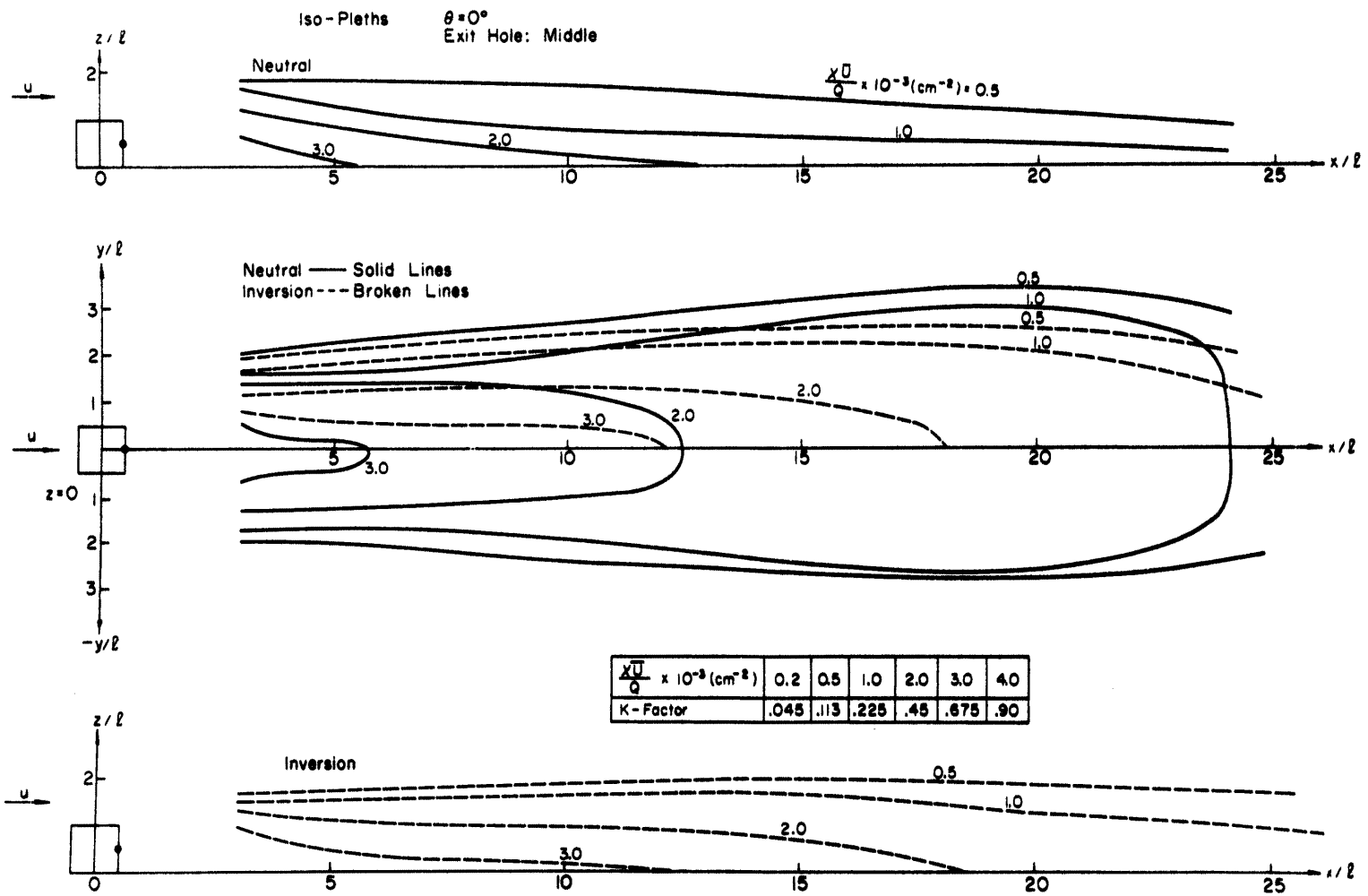


Figure 45 Iso-pleths (b) for  $\theta = 0^\circ$ , middle exit port neutral and inversion stratification.

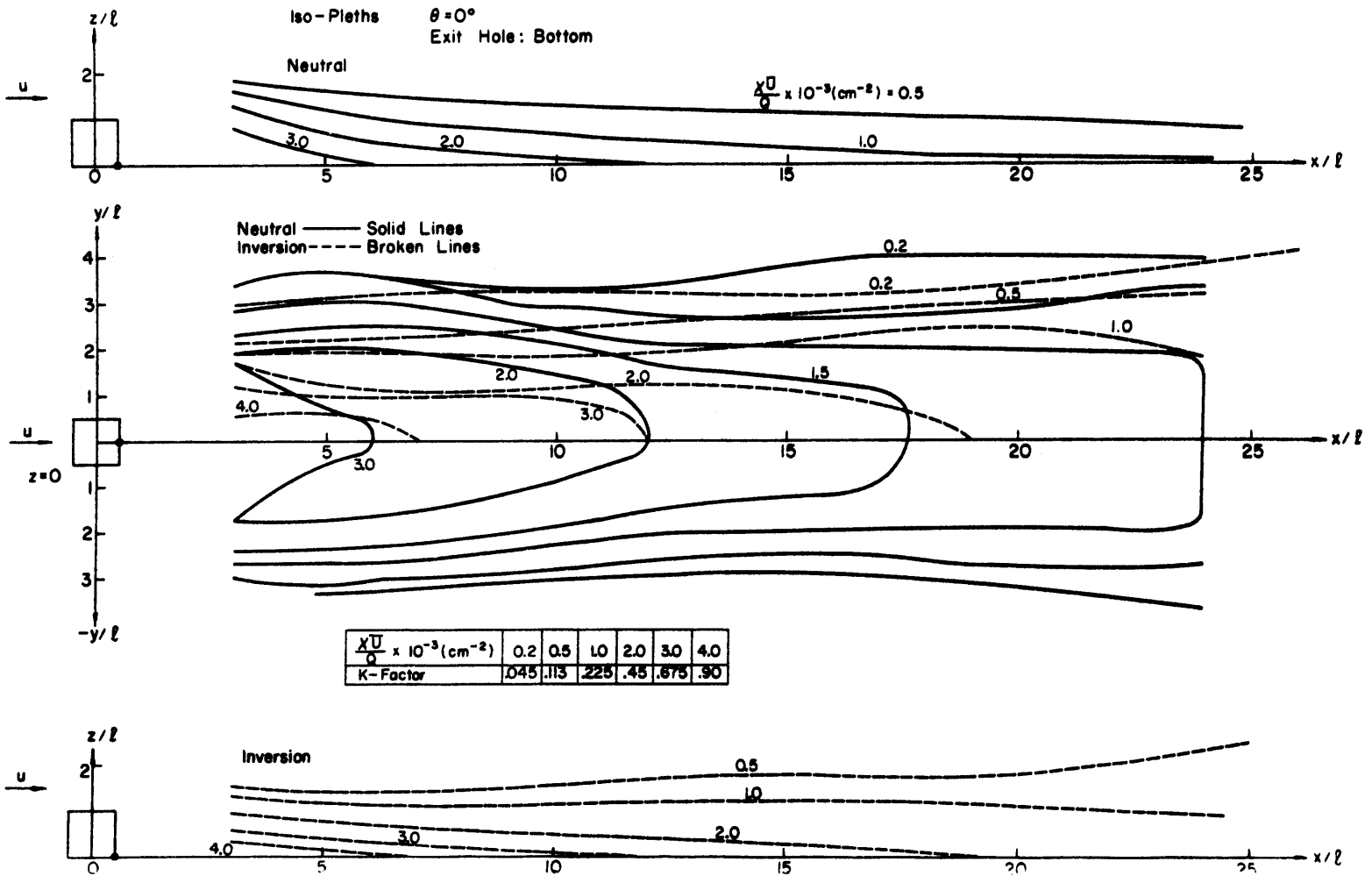


Figure 46 Iso-pleths (c) for  $\theta = 0^\circ$ , bottom exit port, neutral and inversion stratification.

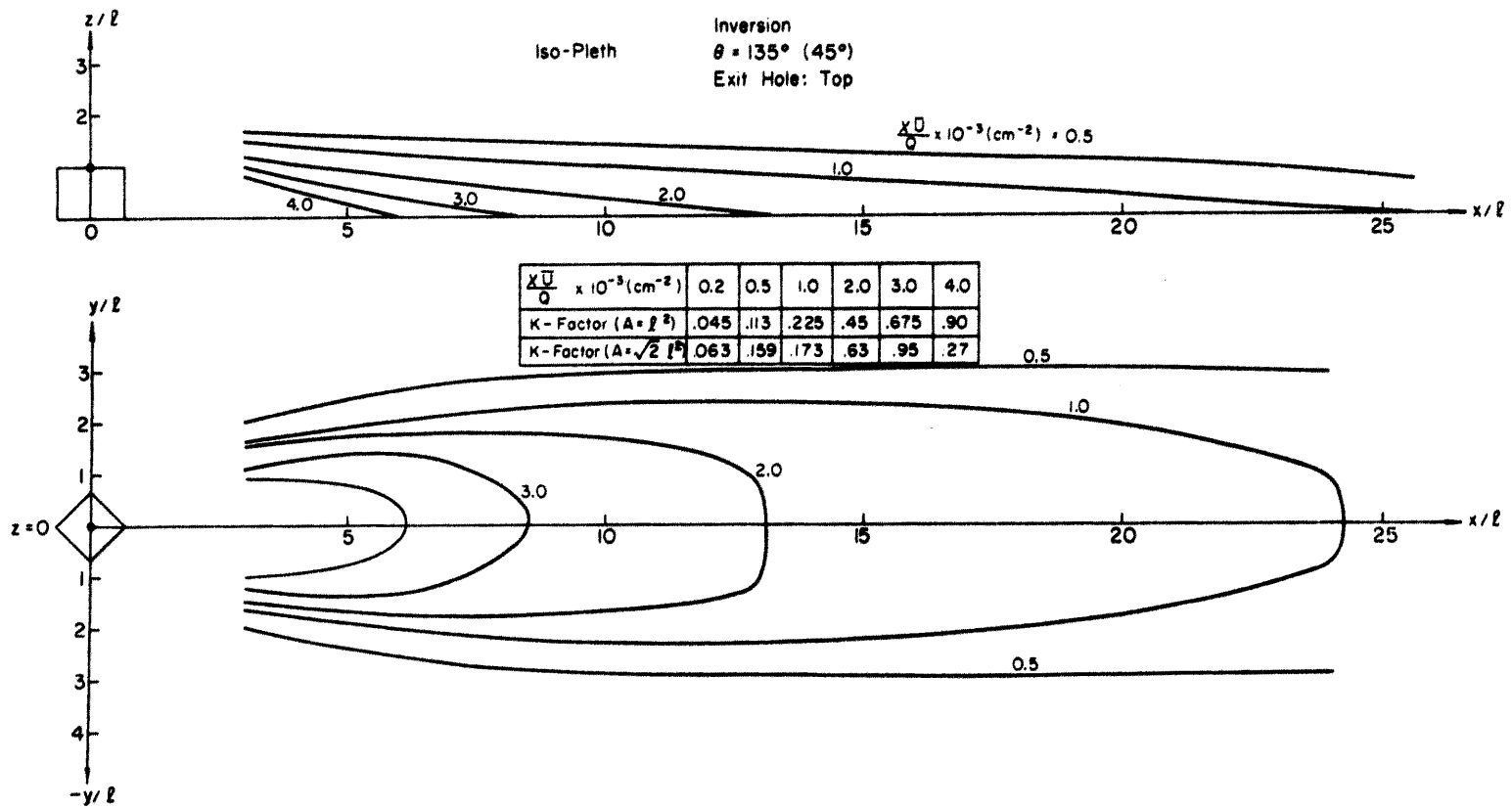


Figure 47 Iso-pleths (d) for  $\theta = 45^\circ (135^\circ)$ , top exit port, inversion stratification.

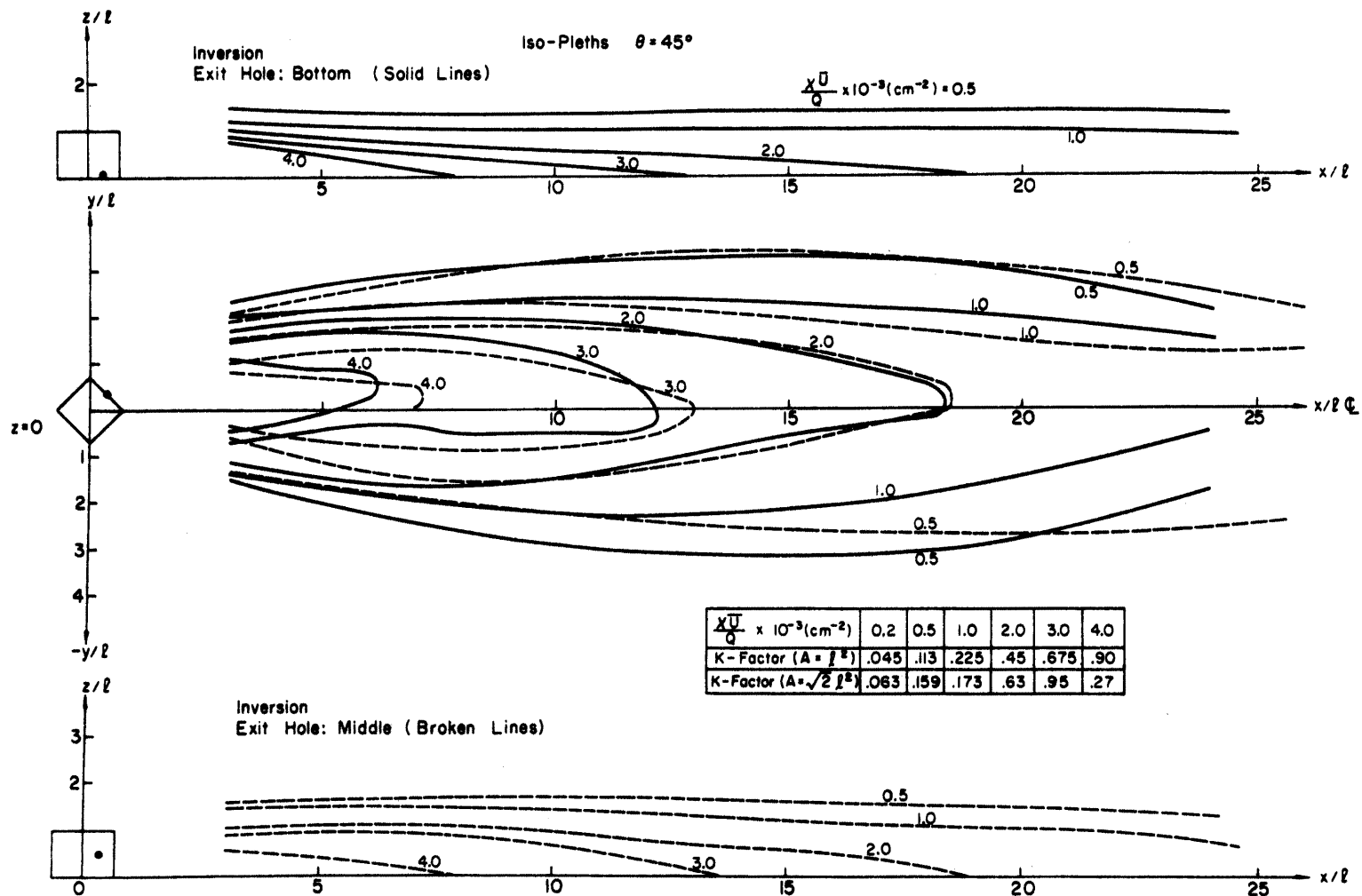


Figure 48 Iso-pleths (e) for  $\theta = 45^\circ$ , middle and bottom exit ports, inversion stratification.

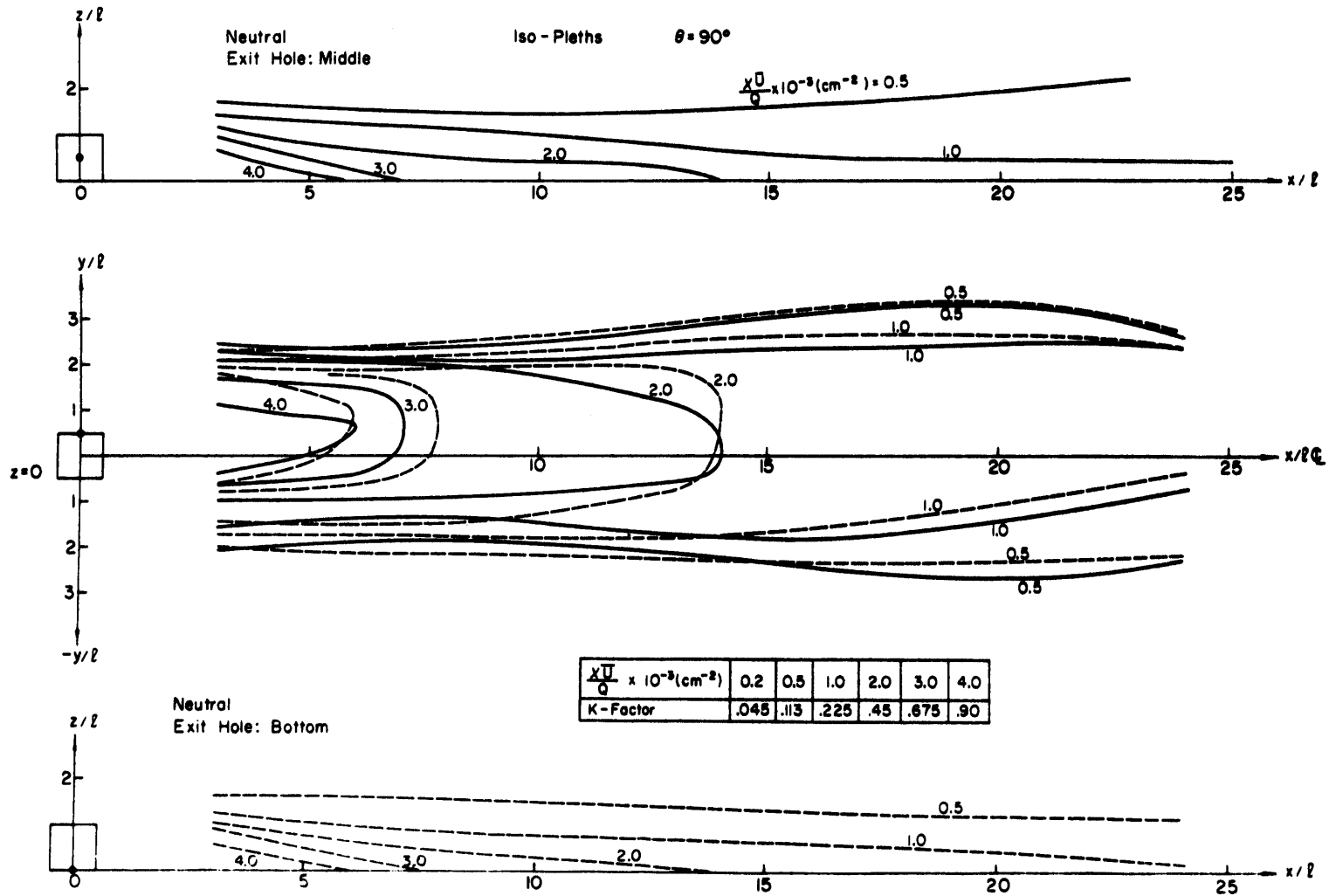
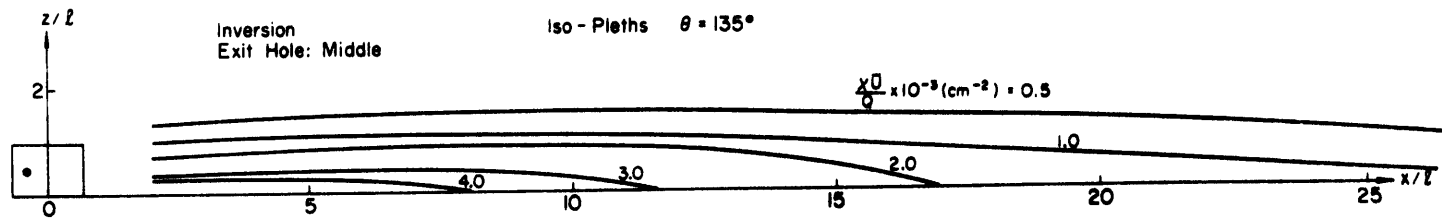


Figure 49 Iso-pleths (f) for  $\theta = 90^\circ$ , middle and bottom exit ports, neutral stratification.



$\frac{\bar{X}}{Q} \times 10^{-3} (\text{cm}^{-2})$	0.2	0.5	1.0	2.0	3.0	4.0
K - Factor ( $A = \beta^2$ )	.045	.113	.225	.45	.675	.90
K - Factor ( $A = \sqrt{2} \beta^2$ )	.063	.159	.173	.63	.95	.27

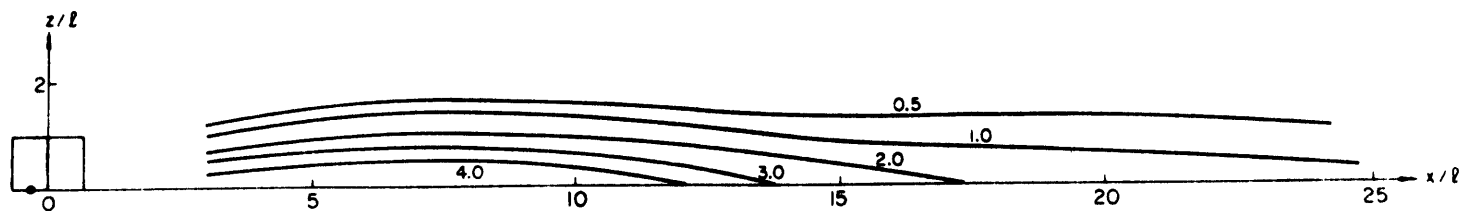


Figure 50 Iso-pleths (g) for  $\theta = 135^\circ$ , middle exit ports, inversion stratification.

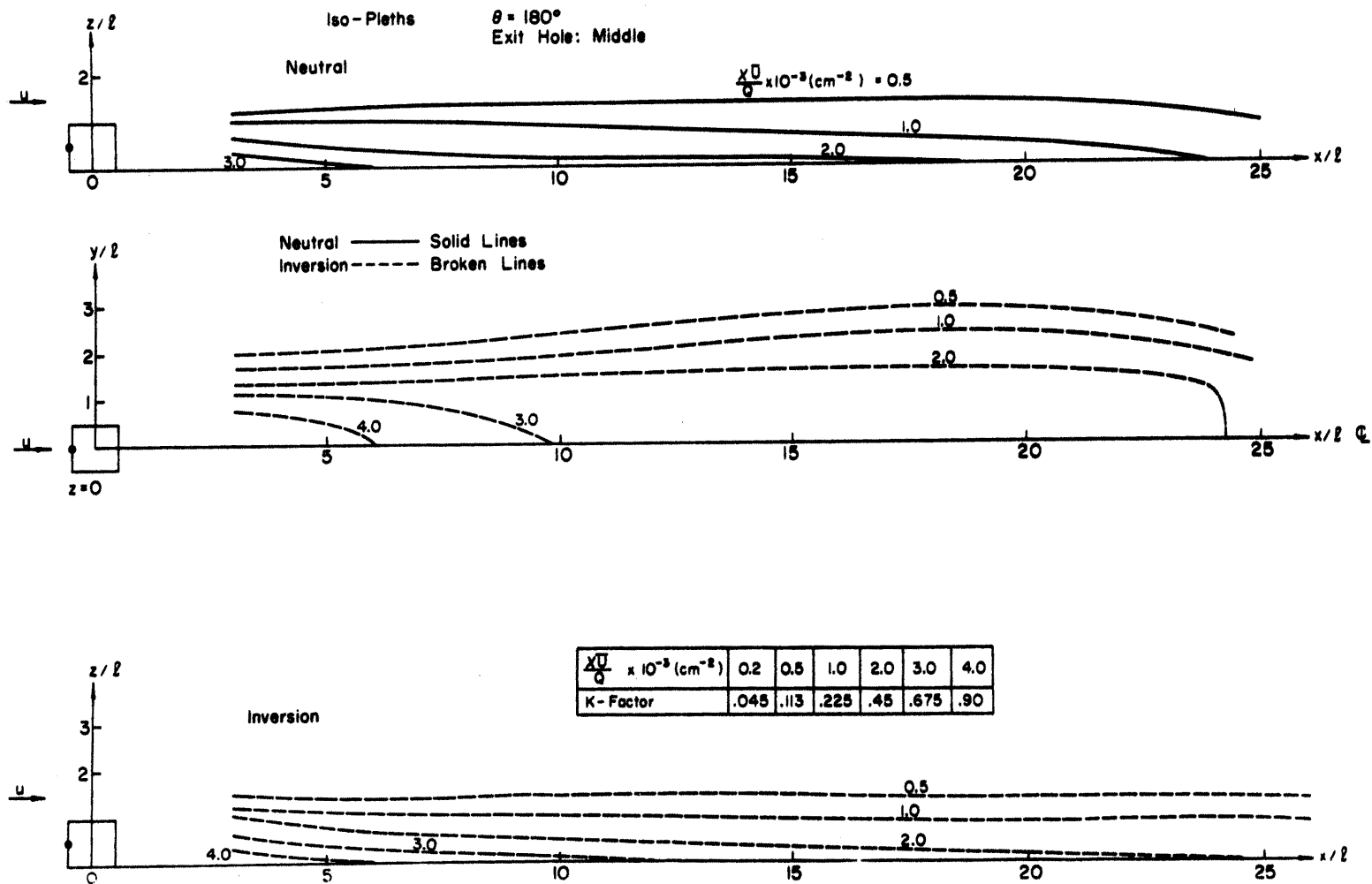
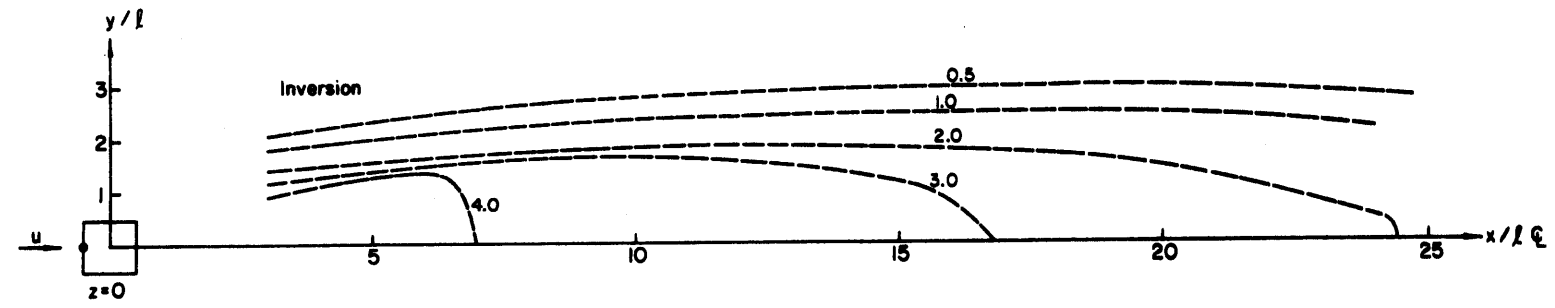
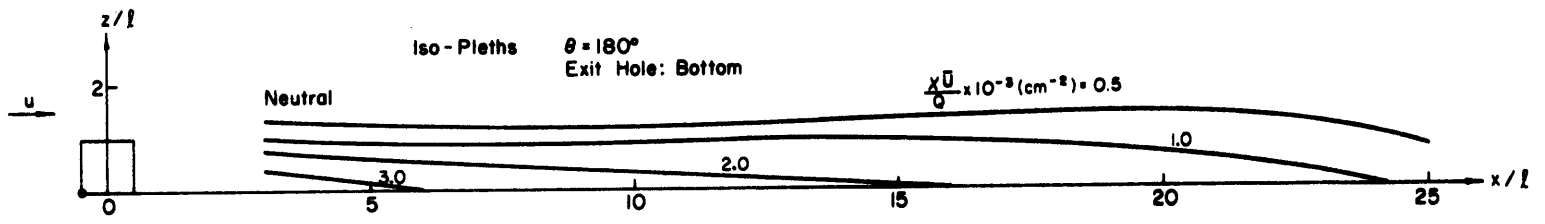


Figure 51 Iso-pleths (h) for  $\theta = 180^\circ$ , middle exit port, neutral and inversion stratifications.



$\frac{\chi \bar{U}}{Q} \times 10^{-3} (\text{cm}^{-2})$	0.2	0.5	1.0	2.0	3.0	4.0
K-Factor	.045	.113	.225	.45	.675	.90

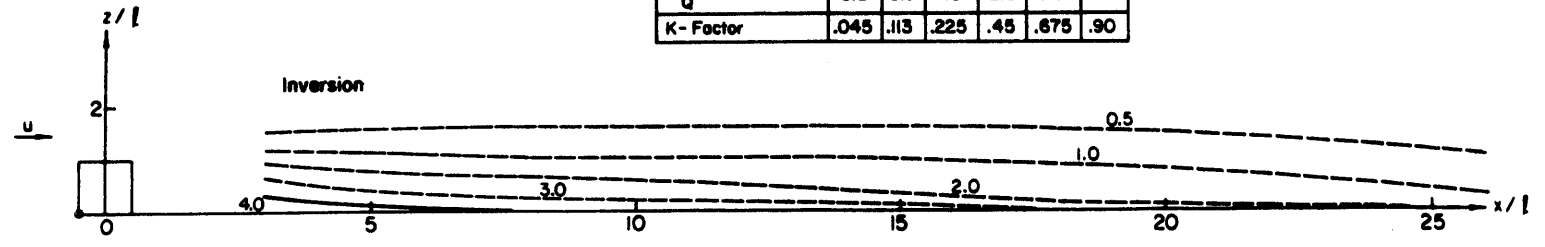


Figure 52 Iso-pleths (i) for  $\theta = 180^\circ$ , bottom exit port, neutral and inversion stratifications.

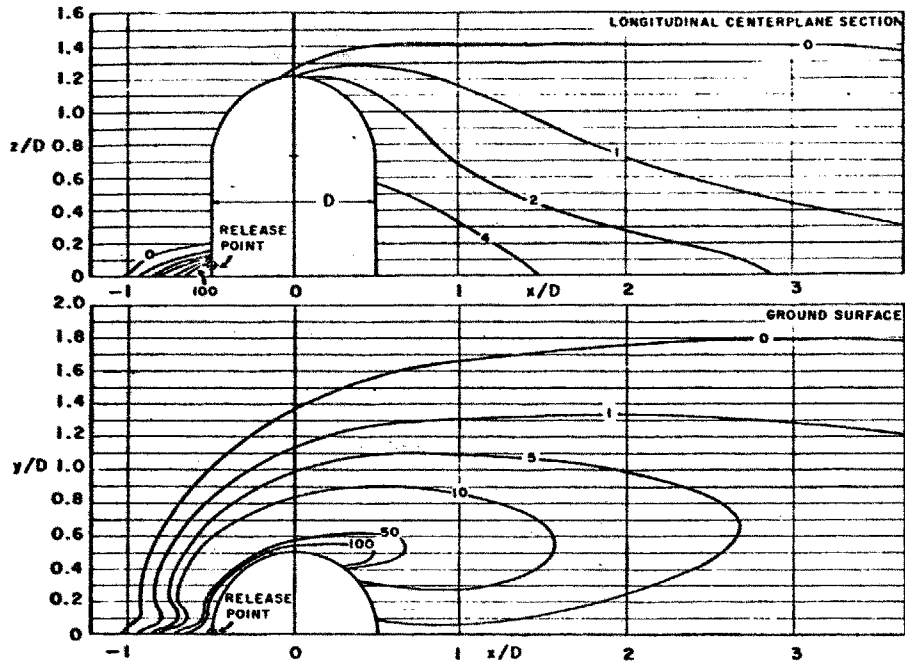


Figure 53 Iso-pleth from the leak of a shell (by Halitsky).

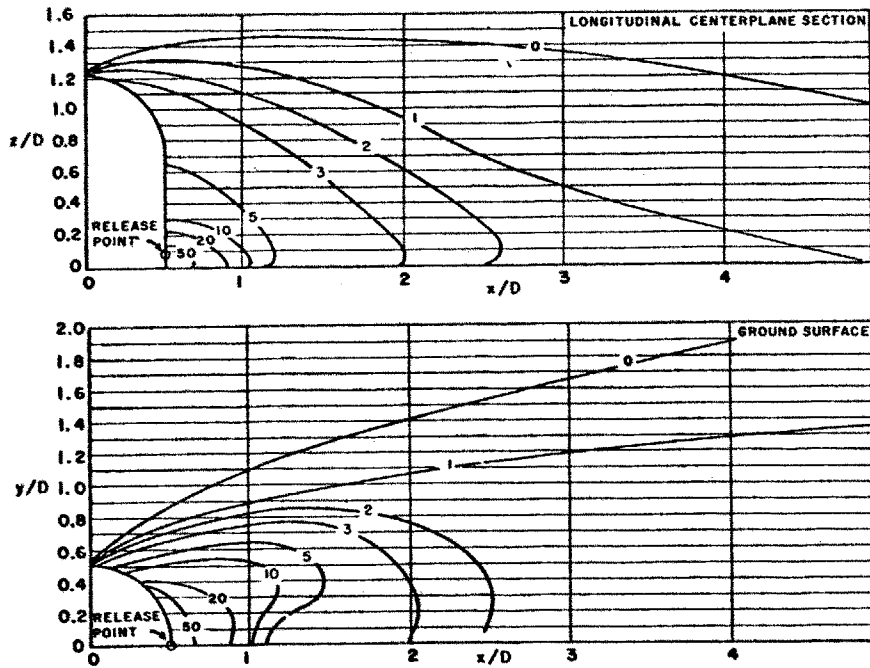


Figure 54 Iso-pleth from the leak of a shell (by Halitsky).

**APPENDIX III**  
**SUPPLEMENTAL FIGURES**

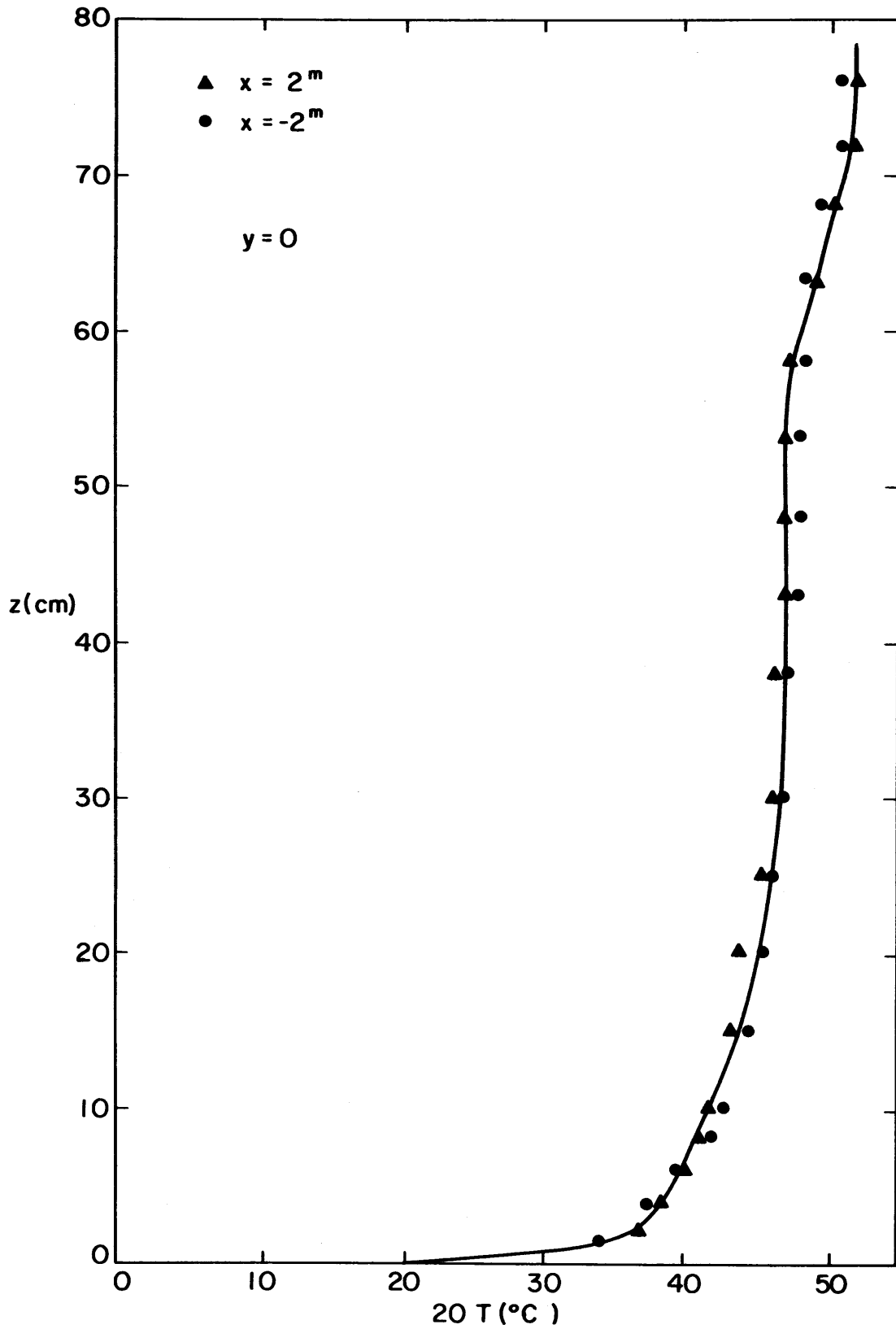


Figure A1 Temperature profiles for  $x = 2^m$  and  $x = -2^m$  at  $y = 0$ .

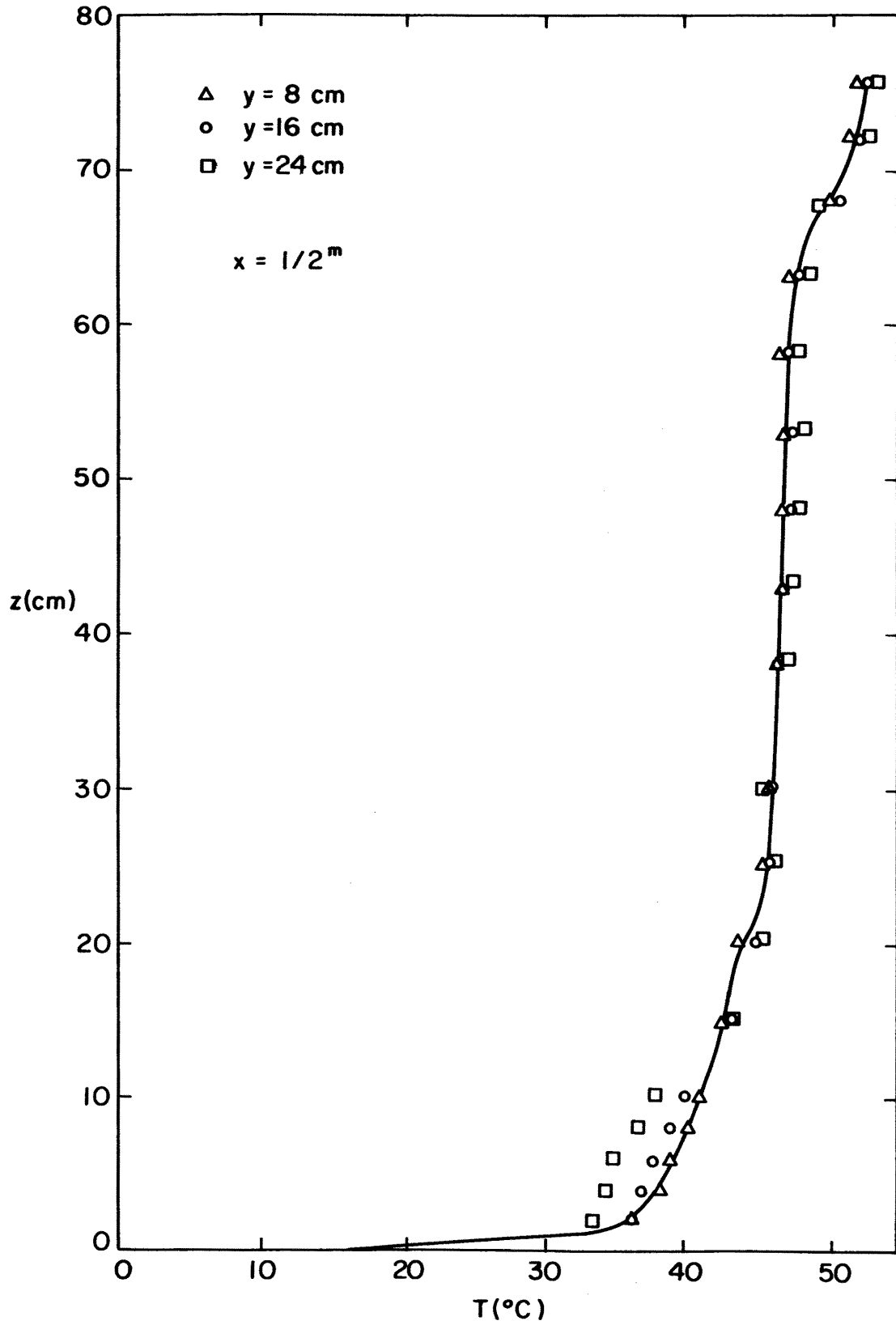


Figure A2 Temperature profiles for  $y = 8^{\text{cm}}$ ,  $16^{\text{cm}}$  and  $24^{\text{cm}}$  at  $x = 1/2^m$ .